Fakultät für Medizin

Promotionsprogramm Experimentelle Medizin

Establishing knockdown strategies to validate therapeutic targets in patients' acute leukemia cells expanding in mice

Jenny Vergalli

Vollständiger Abdruck der von der Fakultät für Medizin der Technischen Universität München zur Erlangung des akademischen Grades eines Doktors der Naturwissenschaften genehmigten Dissertation.

Vorsitzender: Prof. Dr. Jürgen Ruland

Prüfende/-r der Dissertation:

1. Prof. Dr. Marc Schmidt-Supprian

2. Prof. Dr. Wolfgang Wurst

Die Dissertation wurde am 14.11.2018 bei der Technischen Universität München eingereicht und durch die Fakultät für Medizin am 05.11.2019 angenommen.

Considerate la vostra semenza: fatti non foste a viver come bruti, ma per seguir virtute e canoscenza

Consider ye the seed from which ye sprang: ye were not made to live like unto brutes, but for pursuit of virtue and of knowledge

(Dante Alighieri. Divina Commedia. Inferno XXVI vv.118-120 – translated by H.W.Longfellow)

Table of contents

1A. Zusammenfassung

Die akute Leukämie (AL) ist ein hämatopoetischer Tumor mit schlechter Prognose, vor allem bei Erwachsenen und im Rezidiv, und bedarf dringend neuer therapeutischer Optionen. So ist es von höchster Wichtigkeit, Strukturen in Leukämie-Zellen zu identifizieren und zu validieren, die eine essentielle Funktion für den Tumor besitzen und als neue therapeutische Zielstrukturen dienen können, vor allen in individuellen Zellen einzelner Patienten und in der *in vivo* Situation.

Hier setzen wir uns das Ziel, neue Techniken zu etablieren, die es ermöglichen, einen Knockdown von Zielgenen in Patient-abgeleiteten Xenograft (PDX) AL Zellen durchzuführen, während diese in Mäusen wachsen. Dies stellt eine große Herausforderung dar, weil PDX AL Zellen nicht *in vitro* wachsen und sich ausgesprochen schlecht transfizieren lassen.

Um die Expression der shRNA direkt mit der Expression eines Reporter-Proteins unter dem gleichen Promotor zu verknüpfen, wählten wir einen mikro RNA 30 (miR-30) Hintergrund. Um sehr seneitive und zuverlässige Experimente durchführen zu können, entschieden wir uns für einen Fluorochrom-markierten kompetitiven Ansatz. Unsere neu etablierte Knockdown Strategie ermöglichte eine starke und stabile Reduktion des anti-apoptotischen Proteins XIAP zu mehr als 90%. Die Reduktion der XIAP Expression führte zu einem Wachstums-Nachteil sowohl von ALL Zellinien, als auch von PDX AL Zellen *in vivo*, was erstmalig nahelegt, dass XIAP eine essentielle Funktion für das Wachstum von PDX AL Zellen in der Maus besitzt.

Um unsere Analysen auf stark essentielle Zielstrukturen auszuweiten, die keine Herstellung von PDX AL Zellen mit stabilem Knockdown erlauben würden, entwarfen wir ein System des induzierbaren Knockdowns. Hierzu exprimierten wir eine induzierbare Form der Cre Rekombinase und setzten die miR-30 Kassette zwischen zwei unterschiedlichen Paare von loxP Stellen, so dass die miR-30 Kassette erst durch Zugabe von Tamoxifen exprimiert wurde. Mit Hilfe dieses neuen Ansatzes konnten wir zeigen, dass ein Verlust der Funktion des anti-apoptotischen Proteins Mcl-1 die Proliferation von PDX AL Zellen in Mäusen verhindert, so dass Mcl-1 eine attraktives therapeutisches Zielstruktur für die AL darstellt.

Zusammen genommen etablierten wir neue molekulare Techniken, die grundsätzlich die Expression jedes interessierenden Gene in PDX AL Zellen *in vitro* und *in vivo* ermöglicht und damit erlaubt, therapeutische Zielstrukturen zu identifizieren und zu validieren, was zu neuen therapeutischen Ansätzen für die AL in der Zukunft führen sollte.

1B. Abstract

Acute leukemia (AL) is a hematopoietic malignancy with unsatisfactory prognosis, particularly in adults and upon relapse. Thus, novel options for treatment are intensively required. Towards this aim, it is of major importance to identify and validate structures within tumor cells which harbor an essential function and might serve as therapeutic targets, especially in patients' individual tumor cells and in an *in vivo* setting.

Here, we aimed at establishing novel techniques enabling to knockdown target genes in patient-derived xenograft (PDX) AL cells expanding in mice. This task is challenging as PDX AL cells are reluctant to proliferate *in vitro* and belong to the most difficult type to transfect.

We selected a microRNA (miR-30) backbone to directly couple the shRNA transcription to the expression of a reporter gene under the control of a single promoter. For highly sensitive and reliable experiments, we decided for a competitive approach monitored by fluorochrome markers. Our newly established knockdown strategy induced a strong and stable reduction of the anti-apoptotic protein XIAP by well more than 90%. The inhibition of XIAP induced a proliferative disadvantage in both AL cell lines and PDX AL cells *in vivo*, indicating for the first time that XIAP harbors an essential function for PDX AL cells expanding in mice.

To extend our analyses to strongly essential targets which would not allow the production of PDX AL cells with a stable knockdown, we designed a system for inducible knockdown. Here, we expressed an inducible form of the Cre recombinase $CreER^{T2}$ and flanked the miR-30 cassette with two different pairs of loxP sites to enable their recombination by Tamoxifen. Using this novel technique, we could show that the loss-of-function of the anti-apoptotic protein Mcl-1 is responsible for proliferation disadvantage of PDX AL cells expanding in mice, proving Mcl-1 as important putative therapeutic target in AL.

Taken together, we established innovative molecular techniques, enabling silencing any desired gene both *in vitro* and *in vivo* in PDX AL cells in order to identify and validate therapeutic targets and leading to novel treatment approaches for AL in the future.

2. Introduction

The identification of relevant targets for the treatment of acute leukemia remains a major challenge. Here, I aimed at the development of advanced molecular techniques in the individualized preclinical model of acute leukemia for the precise evaluation of the role of single proteins for acute leukemias' cells proliferation and viability.

2.1 Acute leukemia

Acute leukemia is a progressive hematopoietic malignancy characterized by the diffused replacement of the normal bone marrow with accumulating immature, non-functional white blood cells. These neoplastic diseases are classified according to the predominant proliferating cell type: in acute lymphoblastic leukemia (ALL) there is an abnormal amount of lymphocytes, whereas in acute myeloid leukemia (AML) there is an increased number of myeloblasts (Esparza and Sakamoto 2005; Estey 2014). The more common symptoms associated with these diseases are fever, fatigue, headache, sore throat, pallor, weight loss, bleeding from the mucous surfaces, and eventually the enlargement of spleen, lymph nodes and liver. Acute leukemias may be appreciated via peripheral blood smears; however, the diagnosis requires the confirmation via the analysis of bone marrow biopsy and aspiration. Acute leukemia arises from a combination of exogenous and endogenous perturbing sources, genetic susceptibility and bad chance (Inaba, Greaves, and Mullighan 2013). ALL occurs in both children and adults, but its peak of incidence is during childhood between two and five years of age, accounting for 30% of all cancers in children, and for about the 75% of all pediatric acute leukemias (Pui and Evans 2013). On the contrary, AML are less frequent malignancies in children with an incidence strongly related to age, accounting for less than 3% of all cancers and approximately 20% of all leukemias (Deschler and Lubbert 2006). The immunophenotyping provided the possibility to distinguish different subtypes of ALL and AML: ALL can be mainly classified in B-ALL or T-ALL based on the lymphoid compartment from which the disease has origin, while AML is characterized by many different subtypes due to the complexity of the myeloid lineage.

2.1.1 Prognosis and treatment of patients with acute leukemia

Improved therapeutic strategies have markedly increased the cure rates of pediatric ALL from only 20% in the 1960s to above 90% nowadays (reviewed in Pui and Evans 2013). However, infants and adult patients still have a poor prognosis with a 5-years survival rate of only 40 to 50%. Most of the drugs used for the treatment of ALL patients were developed before 1970, but their dosage and schedule have been optimized on the basis of biological features, response to treatment, pharmacodynamics and pharmacogenomics, resulting in a higher survival rate (Inaba, Greaves, and Mullighan 2013). The standard remission induction therapy aims to eradicate the initial leukemic cell burden and restore the normal hematopoiesis, and generally includes glucocorticoids, vincristine, and asparaginase, with or without anthracycline (Bassan and Hoelzer 2011). The consolidation therapy is given to eradicate the residual leukemic cells, and often includes high doses of methotrexate and mercaptopurine (Pui, Robison, and Look 2008). Additionally, some patients can benefit from treatment with tyrosine-kinase inhibitors, for instance those with a BCR-ABL1 positive disease (Ravandi et al. 2010; Schultz et al. 2009). The allogenic hematopoietic stem cell transplantation (HSCT) has become an option for ALL patients with high risk or persistent disease (Balduzzi et al. 2005). Nevertheless, the treatment of patients with relapsed ALL has a sub-optimal re-induction remission rate and consequent very poor long-term overall survival rate, especially in adults (50% in children) (Chessells et al. 2003). Further intensifications of the available regimens are unlikely to substantially improve the survival but would rather increase the adverse effects.

Adult patients suffering from AML have an age-dependent 5-years survival rate of only 30 to 40% (65% for children). Recent introduction of high-resolution profiling techniques for the detection of genetic alteration and consequent advances of the knowledge about the molecular biology and the genetic landscape of AML have led to an increasing number of distinct AML subsets. However, the current management of AML patients has remained disappointingly uniform, and still relies on intensive chemotherapy and allogenic HSCT, which allowed to achieve a durable remission in a large proportion of younger patients who can tolerate such intensive treatment regimen (Dombret and Gardin 2016). The current front-line induction therapy for AML involves the use of cytarabine and anthracycline. More recent randomized studies have refined the therapies with the possible addition of a third agent depending on different parameters such as doses, age, AML biology and response to treatment. However, these aggressive drugs and intensive regimens of treatment are associated with severe side effects, which contribute to an increased mortality (Estey and

Dohner 2006). The post-remission therapy may involve allogenic HSCT or the administration of several intensive cycles of chemotherapy (Koreth et al. 2009; Mayer et al. 1994). Nevertheless, the occurrence of relapse remains associated with unsatisfactory outcome (Breems et al. 2005). The analysis of the genetic profile of AML allowed a more detailed risk-stratification; however, trials with novel drugs and targeted therapies are still disappointing.

2.1.2 Adverse characteristics of tumor cells

Chemotherapeutic drugs can be classified into several groups depending on their mechanism of action or chemical structure, but all aim at the induction of cell death of tumor blasts. Many patients respond to the conventional initial treatments and the chemotherapeutic agents can eradicate most of the tumor cells. However, some leukemic blasts may survive, persist in the patient and become the source of relapse. The biological conditions of the relapse remain partially elusive and it is still unclear if the relapse-inducing cells already exist at the diagnosis or develop as a consequence of therapy, and whether other cell characteristics influence poor outcome. The hallmarks of cancer are defined as different but complementary biological capabilities acquired by the tumor cells during the carcinogenesis process, and together they provide a logical framework for understanding the complex diversity of the human neoplastic diseases (Hanahan and Weinberg 2000, 2011). The pinnacle of these traits is the ability of cancer cells to sustain chronic proliferation, regardless of the homeostasis of the cell number, tissue architecture and function. The second hallmark of cancer cells is the ability to circumvent the cellular programs that depend on the activity of tumor suppressor genes. Additionally, cancer cells have the ability to resist to cell death via evolving a variety of strategies to limit this process. The fourth characteristic is the capability of unlimited replicative potential; therefore, the eventual immortalization of rare subpopulations of cells confers to the tumor the ability to indefinitely generate and re-generate tumor cells. The other features of cancer also involve the micro-environment in which the tumor has origin, the ability to escape the immune system destruction and the capability of reprogramming energy metabolism.

2.2 Apoptosis: pathways and regulation

Apoptosis is a highly regulated and remarkably conserved process for programmed cell death characterized by a specific unstoppable sequence of biochemical events and morphological changes (Wyllie, Kerr, and Currie 1980; Kroemer et al. 2009). Apoptosis plays a crucial role during multicellular organisms' lifecycle for sculpting the body's structures throughout the embryonic development, deleting structures that are no longer required, adjusting the cells number to maintain tissue homeostasis, shaping the immune-repertoire, and eliminating dangerous or injured cells. The distinctive morphological changes of an apoptotic cell are defined by cell shrinkage, the appearance of highly condensed chromatin, dynamic membrane blebbing with loss of adhesion to surrounding cells or extracellular matrix, and eventual fragmentation into multiple small apoptotic bodies easily recognized and engulfed by phagocytes (Green 2005; Taylor, Cullen, and Martin 2008). The highly complex and sophisticated molecular machinery which leads to cell death can be triggered by one of the two main biochemical routes: (1) the extrinsic or (2) the intrinsic pathway (also known as mitochondrial pathway). The extrinsic pathway begins on the cell surface involving transmembrane receptor-mediated interactions, and the sequence of events that defines it is best characterized with the FasL/FasR and TNF-α/TNFR1 models (reviewed in Curtin and Cotter 2003): upon ligand binding, adapter proteins are recruited together with procaspases-8 on the cytoplasmic portion of the transmembrane receptor, forming a death-inducing signaling complex. Within this complex, procaspases are in close proximity of one another facilitating their auto-catalytic activation and release in the cytoplasm, where they initiate the caspases cascade (reviewed in Elmore 2007). On the other hand, the intrinsic pathway involves a spectrum of negative or positive non-receptor-mediated stimuli within the cell, such as the absence of cytokines or growth factor starvation, presence of toxins, viral infections, hypoxia, DNA damage, temperature changes, defective cell cycle or other types of severe cell stress (Adams et al. 1999; Strasser 2005). All these stimuli converge on the mitochondria causing changes to its outer membrane permeability with consequent release into the cytosol of pro-apoptotic proteins (reviewed in Saelens et al. 2004). Additionally, the proteolytic activity of the activated caspase-8 leads to mitochondrial damage, creating a cross-talk between the intrinsic and extrinsic pathways (reviewed in Igney and Krammer 2002). Both pathways lead to the final stage of apoptosis, which starts with the activation of the downstream effector caspases that are responsible for the irreversible activation of cytoplasmic endonucleases and proteases that perform the proteolytic cleavage of nuclear material and cytoskeletal proteins (Figure 1).

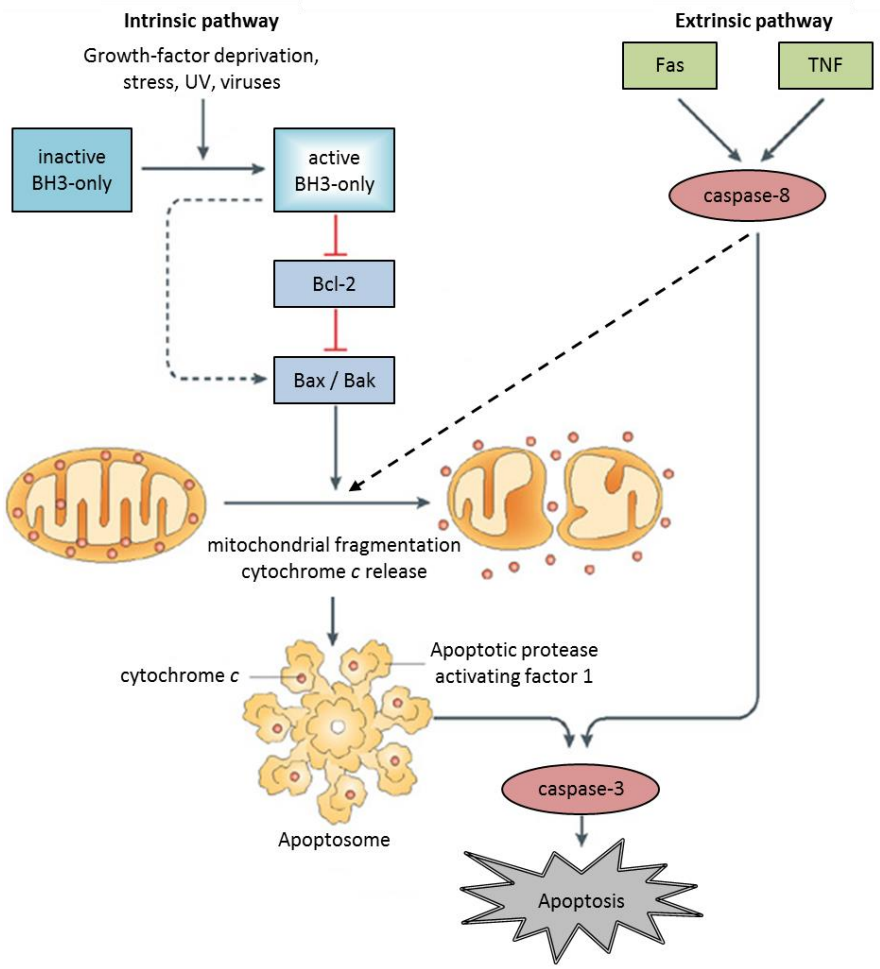

Figure 1. Scheme of the intrinsic and extrinsic pathways of apoptosis.
Intrinsic (left) and extrinsic (right) pathways induce apoptosis upon the integration of different signals coming from the inside or the outside of the cell and throughout a sequence of biochemical events. The model summarizes the steps that lead to the activation of effector caspases and shows the connection between the two pathways (adapted figure from Youle and Strasser 2008).

2.2.1 Regulator of apoptosis proteins

Because of the importance of the apoptotic process, the activation of caspases is under the tight control of several activator and inhibitor proteins, which in turn are subject to many layers of regulation. The benefits of the redundancy in the mechanisms that regulate apoptosis relay on the necessity to compensate the possible loss or deregulation of specific proteins because of genetic mutations. Therefore, the presence of multiple pathways serves to ensure the execution of the apoptotic program even when some proteins are lost. Proteins of the Bcl-2 family and inhibitor of apoptosis proteins (IAP) are among the main intracellular regulators of apoptosis, and the existence of numerous family members in each

class of the apoptotic regulators with redundant and compensatory function adds complexity to the apoptosis machinery.

The proteins of the Bcl-2 family (Figure 2) are all small, globular proteins that have a crucial role in the regulation of procaspases activation. All members of this family of proteins contain one to four BCL-2 homology (BH) domains. The BH3 domain is common to all members of the superfamily and it is the most important conserved region for the dimerization and/or activation of these proteins. Most members also contain a transmembrane (TM) domain that typically associates them with membranes. Based on the structure and functional characteristics of its members, the Bcl-2 family can be divided in three subfamilies (reviewed in Adams and Cory 1998). The anti-apoptotic multi-domain proteins are generally found on the outer mitochondrial membrane, where they act as inhibitors of the pro-apoptotic Bcl-2 proteins. The pro-apoptotic Bcl-2 subfamily can be divided in the groups of multi-domain effectors and BH3-only proteins. The multi-domain pro-apoptotic proteins promote the mitochondrial outer membrane polarization by oligomerizing to form pores (Mikhailov et al. 2003). The BH3-only proteins act either as direct activators of the pro-apoptotic members Bax and Bak, or as de-repressors of the anti-apoptotic Bcl-2 and Bcl-X_L (Letai et al. 2002).

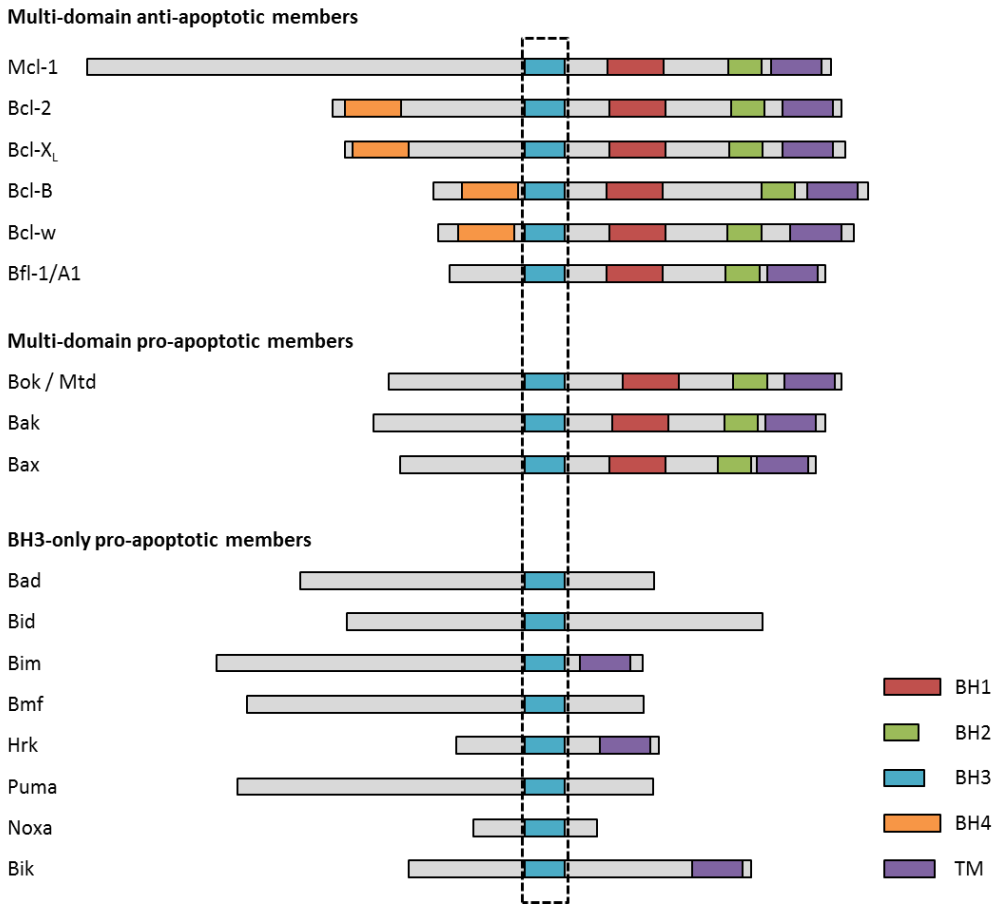

Figure 2. Bcl-2 family of proteins.
The comparison of domain structures of the different family members shows that all proteins contain at least one BH domain (the BH3). Most of the anti-apoptotic proteins present four BH domains and the TM domain. Members of the pro-apoptotic Bax-like subfamily lack the BH4 domain. The BH3-only subfamily is a structural diverse group of proteins with pro-apoptotic function that only display homology within the BH3 motif.

Another important category of intracellular apoptosis regulators is the IAP family of proteins (Figure 3), and it consists of eight members divided in three classes depending on their structure. The proteins of this family are characterized by the presence of one to three baculovirus IAP repeats (BIR) domains at the N-terminal end that supports the protein-protein interactions. Most members exhibit also a really interesting new gene (RING) zinc-finger domain at the C-terminal end (Salvesen and Duckett 2002). The presence of the RING domain can mediate ubiquitination of substrates, thus leading to the alteration of their signaling properties or proteasomal degradation (Vucic, Dixit, and Wertz 2011). The IAP family members control apoptosis induced by a variety of stimuli through several mechanisms, but the best understood is the caspase inhibition. Indeed, the specific activity of the IAP proteins is the inhibition of the effector caspase-3, -7 and -9 to prevent apoptosis (Fulda and Vucic 2012). These proteins can also regulate other processes such as cell division, cell cycle progression and cell migration.

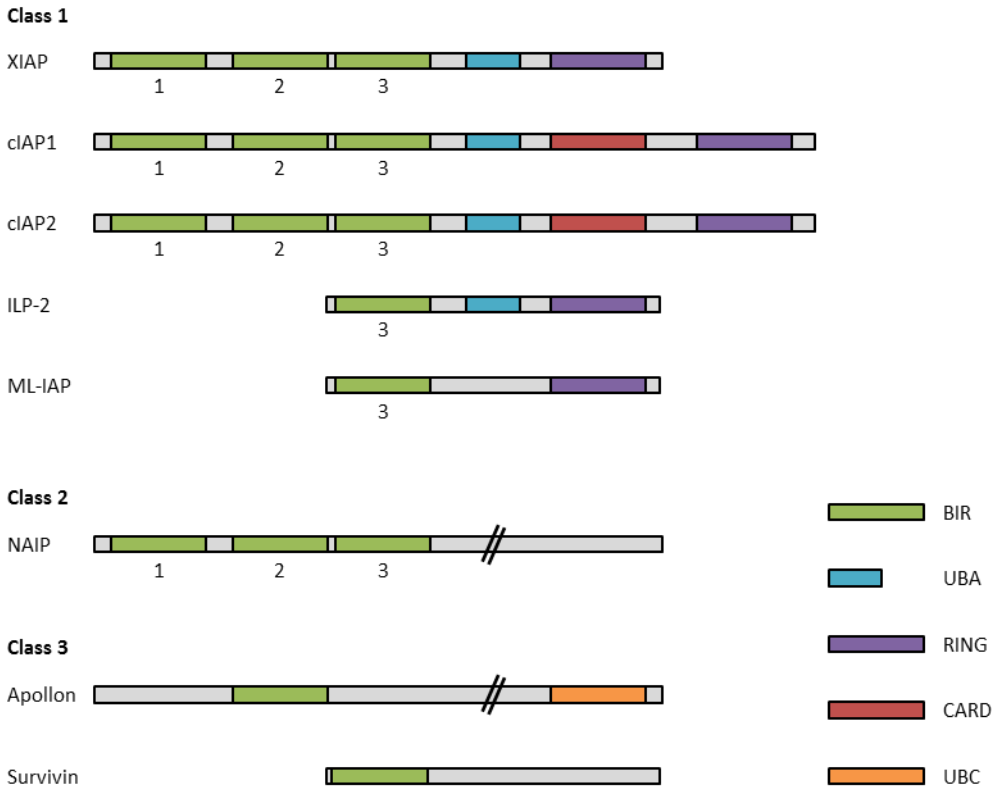

Figure 3. IAP family of proteins.
Here is shown the schematic structure of the eight members and their functional domains. These proteins all share the BIR domain(s) and those of the class 1 present also a RING finger domain for the E3-ubiquitin ligase activity. Other structures present on some IAP family members are the caspase activation recruitment (CARD) domain, the ubiquitin-conjugating (UBC) and ubiquitin-associated (UBA) domains.

2.2.1.1 E3 ubiquitin-protein ligase XIAP

The E3 ubiquitin-protein ligase XIAP gene (also known as X-linked inhibitor of apoptosis protein) maps on chromosome X (Xq25) and comprises nine exons all of which contribute to the two different splice variants. The first variant represents the shortest transcript and the second variant differs from it in the 5' UTR. Nevertheless, both variants encode for the same protein of 497 amino-acid (aa) residues (Figure 4). Also, the XIAP gene encodes for a third non-coding transcript variant which lacks a large portion of the coding region including the translational start codon. The XIAP protein contains three BIR domains (BIR1-3) in its N-terminal half, which are responsible for the interaction with proteins that modulate the NF-kB signaling pathway (BIR1) (Lu et al. 2007) and are critical for the interaction with caspases (BIR2-3) (Huang et al. 2001; Srinivasula et al. 2001). The C-terminal end presents an ubiquitin-associated (UBA) domain for ubiquitin binding and a RING domain with E3-ubiquitin ligase activity and responsible for the stability of XIAP itself (reviewed in Joazeiro and Weissman 2000).

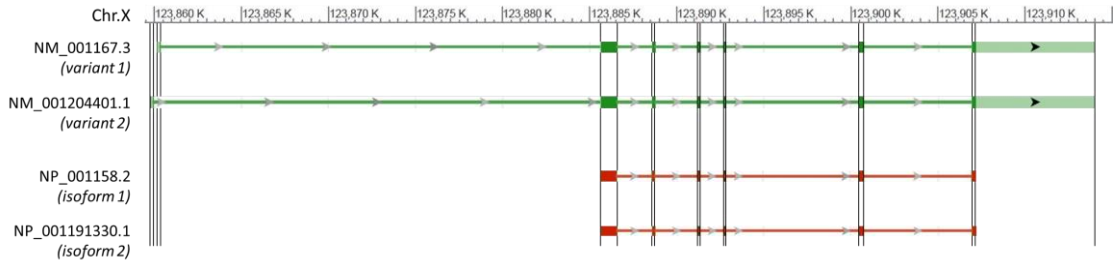

Figure 4. Genomic and protein structure of XIAP.
Schematic representation of the two coding transcript variants of the XIAP gene (in green) which encode for the same protein (in red). Dark green blocks indicate the exons, while light green blocks and green connecting lines represent the non-coding sequences and introns respectively. Dark red blocks represent the translated sequences that form the final protein structure. The third non-coding transcript variant is not shown.

XIAP is the best characterized multi-functional member of the IAP family of protein and inhibits apoptosis via direct interaction with both initiator and effector caspases (reviewed in Eckelman, Salvesen, and Scott 2006). It is considered the most potent caspase-binding protein and inhibitor of both intrinsic and extrinsic pathways of apoptosis (reviewed in Chaudhary et al. 2016). More precisely, XIAP binds with the BIR2 domain directly to the active site pocket of caspase-3 and caspase-7 preventing the entry of caspase-activating substrates, and it catalyzes their ubiquitination for recognition and degradation proteasome-dependent thanks to the RING domain. Also, it inactivates caspase-9 by keeping it in a monomeric state via the binding with the BIR3 domain. Thus, although XIAP does not interact with caspase-8, it is responsible for inhibiting the apoptotic pathway (Figure 5). Additionally, it regulates the NF-kB signaling pathway controlling cell survival and proliferation (Salvesen and Duckett 2002).

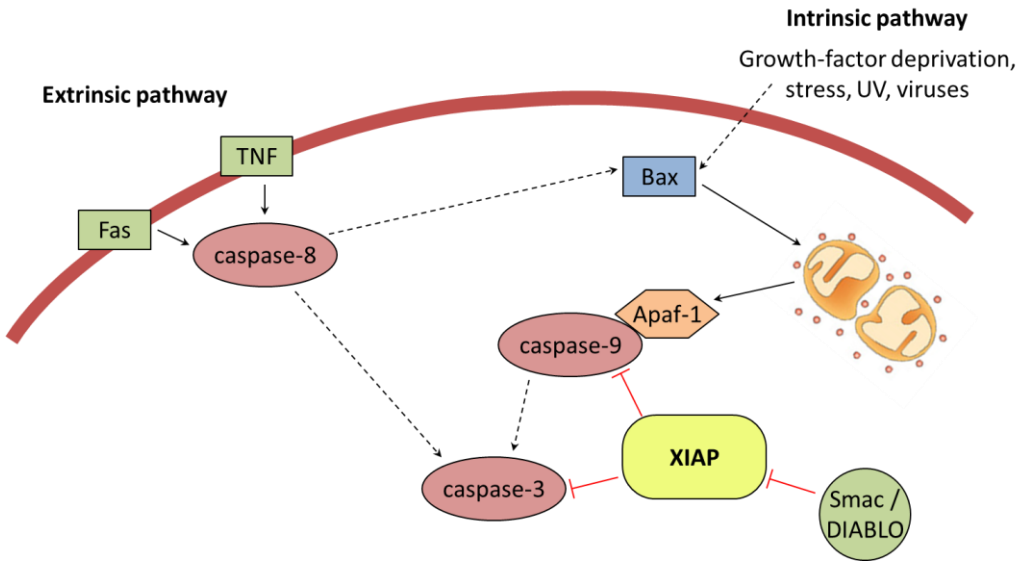

Figure 5. Overview of the XIAP mechanism of action.
XIAP interferes with the apoptotic cell death via inhibiting the activation of caspase-9 and selectively binding and inhibiting the caspase-3 (and caspase-7). The inhibition of XIAP is mediated by Smac/DIABLO, a mitochondrial protein released into the cytoplasm of the cell as consequence of the permeabilization of the outer mitochondrial membrane.

Given the key role of XIAP in influencing cell survival and apoptosis, multiple transcriptional, translational and post-translational mechanisms are involved to regulate its expression. For instance, it has been shown that the stress-activated NF-kB transcription factor induces XIAP transcription (Stehlik et al. 1998). Moreover, XIAP mRNA presents protein-binding regions targeted by a variety of different regulators, for example the Smac/DIABLO protein (Salvesen

and Duckett 2002). Additionally, XIAP function and stability are regulated by post-transcriptional modification, as ubiquitination (reviewed in Galban and Duckett 2010). Thus, the functions of XIAP make it a potential oncogene: its overexpression in cancer cells is well described as mechanism of resistance to chemotherapy and targeted therapy, and it is associated with aggressiveness and poor clinical outcome in different tumor types (Schimmer et al. 2006), including also hematological malignancies. In certain types of solid tumors, therapeutic strategies targeting XIAP were successful especially as sensitizers of the conventional chemotherapy (Ehrenschwender et al. 2014; Hu et al. 2003) and, more recently, also for enhancing immunotherapy (Evans et al. 2016). Nevertheless, despite the important role in regulating apoptosis, it has been demonstrated that the deletion of XIAP is not toxic for normal cells (Harlin et al. 2001).

2.2.1.2 Induced myeloid leukemia cell differentiation protein Mcl-1

The induced myeloid leukemia cell differentiation protein Mcl-1 gene (also known as myeloid cell leukemia 1) was originally identified by Kozopas et al. in 1993 (Kozopas et al. 1993). The gene maps on chromosome 1 (1q21.2) and comprises four exons all of which contribute to the three different splice variants. The longest and more abundant mRNA variant encodes for the prototypical Mcl-1 protein of 350 aa residues. The second and third variants encode for a 271 and a 197 aa residues protein respectively (Figure 6). Mcl-1 contains three BH domains (BH1-3) but lacks the BH4 domain. It presents a TM domain at the C-terminal end that serves for the localization of the protein to the outer mitochondrial membrane (Yang, Kozopas, and Craig 1995). The N-terminal end contains two PEST (proline, glutamic acid, serine and threonine rich peptide sequence) domains, common feature of proteins with a high turnover. The Mcl-1 protein has a short half-life (one to a few hours), and its major route of degradation is proteasome-dependent (Nijhawan et al. 2003).

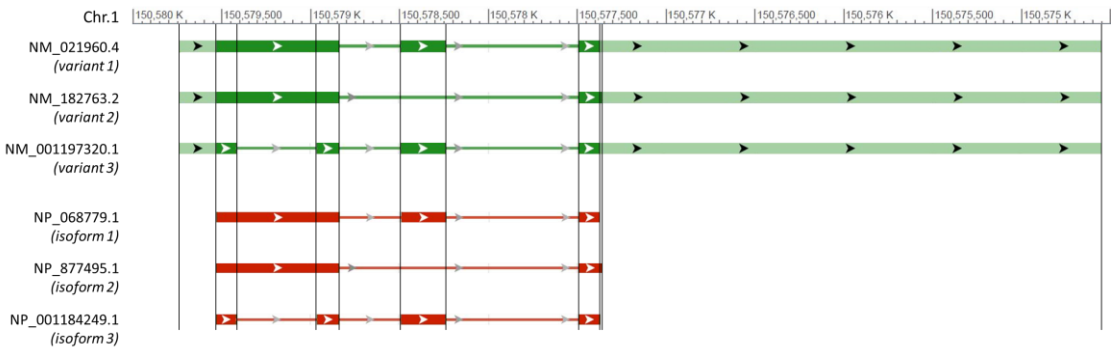

Figure 6. Genomic and protein structure of Mcl-1.
Schematic representation of the three transcript variants of the MCL-1 gene (in green) which encode for the three different isoforms (in red). Dark green blocks indicate the exons, while light green blocks and green connecting lines represent the non-coding sequences and introns respectively. Dark red blocks represent the translated sequences that form the final protein structure.

Mcl-1 is a pro-survival member of the Bcl-2 family of proteins, and its molecular function is to block the progression of apoptosis via binding the pro-apoptotic proteins Bak and Bax, which would otherwise form pores on the outer mitochondrial membrane allowing the release of the cytochrome *c* into the cytoplasm of the cell with consequent activation of the caspases cascade (Akgul, Moulding, et al. 2000). Mcl-1 also binds a subset of BH3-only pro-apoptotic proteins that would induce and help the polymerization of Bak and Bax (Figure 7).

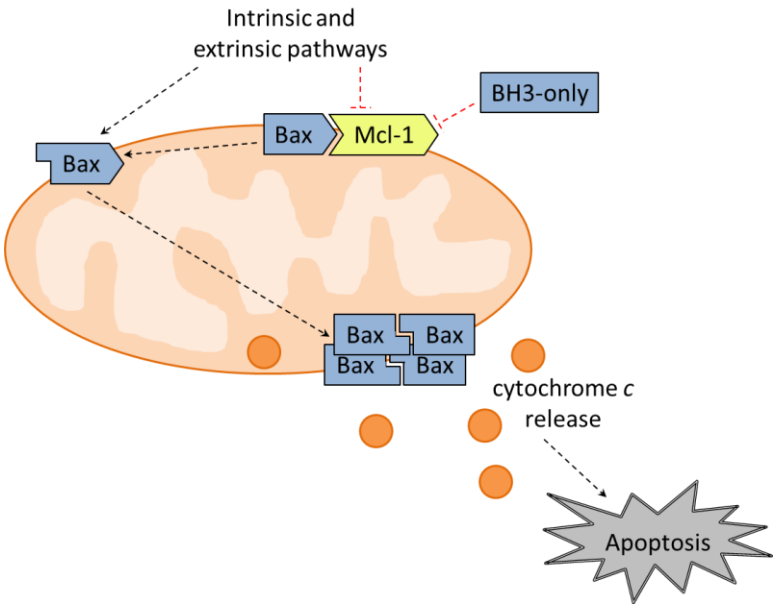

Figure 7. Overview of Mcl-1 implication in the apoptotic process.
The anti-apoptotic Mcl-1 protein interacts with Bax (and Bak) inhibiting their polymerization. The interaction of Mcl-1 with BH3-only pro-apoptotic members of the Bcl-2 family induces the dissociation of Mcl-1 from Bak and Bax, which can in turn interact with each other and promote the construction of pores on the outer mitochondrial membrane allowing the release of apoptotic proteins, including the cytochrome *c*.

Mcl-1 turnover varies between cell type, it may be significantly shortened or lengthened depending on the cellular conditions and can be influenced by numerous factors. An increasing number of studies demonstrated the dependency of Mcl-1 expression on the

presence of growth factors (reviewed in Thomas, Lam, and Edwards 2010), hypothesis supported by the characterization of Mcl-1 promoter region which contains an array of binding sites for transcription factors (Akgul, Turner, et al. 2000). In addition to the transcriptional regulation, Mcl-1 is also subject to post-transcriptional and translational controls, for instance by the binding of the microRNA 29b (Mott et al. 2007) or RNA binding proteins (Subramaniam et al. 2008). In addition to its role in the apoptotic process, and thanks to its connection to many signaling networks (Craig 2002), Mcl-1 is implicated in the regulation of cell cycle progression and check-points and widely distributed in many tissues (Fujise et al. 2000; Jamil et al. 2005). Moreover, Mcl-1 is an immediate-early gene that contributes both to cell viability and regulation of cell proliferation, with demonstrated essential expression for embryogenesis (Rinkenberger et al. 2000) and for the development of several cell lineages including neutrophils (Dzhagalov, St John, and He 2007), both B and T lymphocytes in animals (Opferman et al. 2003) and hematopoietic stem cells (Opferman et al. 2005). Additionally, Mcl-1 is highly overexpressed in a variety of human cancers as trigger of tumor cells to evade cell death: the dysregulation of Mcl-1 is an important genomic change on which cancer cells often depends for survival and resistance to chemotherapy. Also, it has been shown that Mcl-1 is important for leukemic cell survival and its overexpression in hematopoietic stem and progenitor cells promotes the malignant transformation (Campbell et al. 2010).

2.2.2 Implication of apoptotic pathways and regulators in cancer

The deregulation of programmed cell death is a process observed in many human conditions including degenerative diseases (Parkinson's disease, Alzheimer's disease, Huntington's disease, and Amyotrophic Lateral Sclerosis), ischemia, AIDS, autoimmune diseases and many types of cancer. As mentioned in paragraph 2.1.2, the ability of the cells to suppress the apoptotic program during carcinogenesis plays a central role for the development and progression of cancer (Kerr, Winterford, and Harmon 1994). Since the apoptotic process is a gene-directed program, there is an extend variety of strategies that can be used to limit or escape apoptosis, some of which are common to a number of different cancers and other that are specific to a particular tumor type. The alteration of the balance between the Bcl-2 family members, by overexpressing anti-apoptotic proteins and/or decreasing the pro-apoptotic ones, can prevent the activation of caspases. In addition, many cancers exhibit

alterations in the expression of the IAP proteins, which sometimes lead to circumvent apoptosis through other signaling pathways.

2.2.3 Targeting apoptosis in cancer treatment

The ability to interact and modulate the fate of a cell is recognized for its immense therapeutic potential. Given the crucial role of the members of the Bcl-2 family in regulating cell death, a substantial effort is devoted to develop drugs with the ability of mimic the BH3 domain with the aim to prevent the binding of pro-apoptotic proteins by their pro-survival counterparts. Several preclinical studies and clinical trials using BH3 mimetics have shown promising results, as the ABT-737 compound and its oral derivative ABT-263 that target BCL-2, BCL-X_L and BCL-W, or the newer ABT-199 compound that specifically targets BCL-2 (Oltersdorf et al. 2005; Souers et al. 2013; Tse et al. 2008). However, other effective BH3 mimetics targeting Mcl-1 have been less successful and therefore the research remains ongoing (reviewed in Czabotar et al. 2014).

Smac proteins are also part of the cell death machinery via inhibiting the activity of IAP proteins; therefore, several small molecules that mimic Smac proteins have been developed for anticancer therapy. Several studies have shown that the use of Smac mimetics in cancer therapy synergizes with other compounds to reduce the tumor burden, as the LBW242 in combination with the protein kinase inhibitor PKC412 for the treatment of FLT3-mutated AML (Weisberg et al. 2007), or the BV6 in combination with either glucocorticoids or demethylating agents for the treatment of either childhood ALL or AML respectively (Belz et al. 2014; Steinhart, Belz, and Fulda 2013; Varfolomeev et al. 2007). Because of these promising results, there is much interest in the possibility of adding more Smac mimetics to the conventional anti-cancer therapies.

2.3 Gene silencing and genome editing

To provide answers to specific questions with an exquisite precision, the parallel development of different approaches of genetic engineering, as for instance gene silencing and genome editing, is essential. Gene silencing techniques have been widely used to study the importance of the expression of specific genes in association with a given disorder, including human malignancies. Another common approach to modify the genetic landscape of cells is the ability to modify specific DNA sequences with the aim to correct or replace defective genes associated with a certain disease.

2.3.1 Regulation of gene expression by RNA interference

The discovery by Lee et al. in 1993 that genes can be turned off post-transcriptionally by RNA interference (RNAi) (Lee, Feinbaum, and Ambros 1993) has facilitated reverse genetic experiments, making the RNAi an useful genetic technique for effective and stable knockdown of desired target genes, thus allowing loss-of-function studies and the regulation of the expression of specific genes, and in the future, perhaps, used as therapy.

2.3.1.1 RNAi: the natural pathway

Eukaryotic cells have many different sophisticated ways to regulate gene expression. RNAi is an important pathway to control gene silencing and it involves two important types of non-coding RNA molecules: (1) microRNA (miRNA) and (2) small interfering RNA (siRNA). Most of the miRNAs are generated by gene clusters found in regions of the genome quite distant from known genes, suggesting that they derive from the processing of multi-cistronic primary transcripts of independent transcription units. About a quarter of human miRNA genes are located in the introns of pre-mRNAs (preferentially in the same orientation as the predicted mRNA, but also within exons and in the antisense transcript) implying that they are not under the control of own promoters, but they take advantage of a convenient mechanism for their coordinated expression with proteins (reviewed in Bartel 2004). Because of the differential distribution of the miRNA genes in the genome, their transcriptional units and regulation vary with the gene loci (Rodriguez et al. 2004). The synthesis of miRNAs is predominantly done by the RNA polymerase II (pol-II) (Lee et al. 2004) but can also be performed by the RNA polymerase III (pol-III) (Borchert, Lanier, and Davidson

2006), and they can be expressed in a tissue- or developmental- specific manner (reviewed in Bartel 2004). The primary miRNA (pri-miRNA) transcribed by either pol-II or pol-III goes through a two-steps maturation process, with a first nuclear and then a cytoplasmic cleavage performed by two endonucleases. The process begins with the nuclear cleavage of the long stem-loop pri-miRNA by the class II RNase III endonuclease Drosha as part of a protein complex (microprocessor complex), which cuts the stem at around 22 nucleotides (nt) away from the terminal loop with subsequent release of a shorter miRNA hairpin precursor (pre-miRNA) of around 65 nt. Drosha cleavage defines the characteristic 2-nt 3' overhang-ending of the future mature miRNA. The pre-miRNA is incorporated into another complex with nucleocytoplasmic transporter proteins which prevents the nuclear degradation and facilitates the translocation of the pre-miRNA to the cytoplasm. Here, the pre-miRNA is bound at the 2-nt 3' overhang-ending by the class II RNase III endonuclease Dicer which cleaves around 22 nt away from the base of the pre-miRNA hairpin removing the terminal loop and leaving another 2-nt 3' overhang-ending. Double stranded miRNAs are generally transient duplex molecules consisting of a sense-passenger strand and an antisense-guide strand, which presents a seed sequence on the 2-8 nt at the 5' end. The duplex is then unwound and the antisense-guide strand is the mature miRNA molecule that is loaded into the RNA induced silencing complex (RISC). The activated RISC binds the 3' UTR of the target mRNA through base-pairing: the recognition relies on the match between the seed sequence of the miRNA guide and the sequence on the 3' UTR of the target mRNA (reviewed in Fellmann and Lowe 2014) (Figure 8).

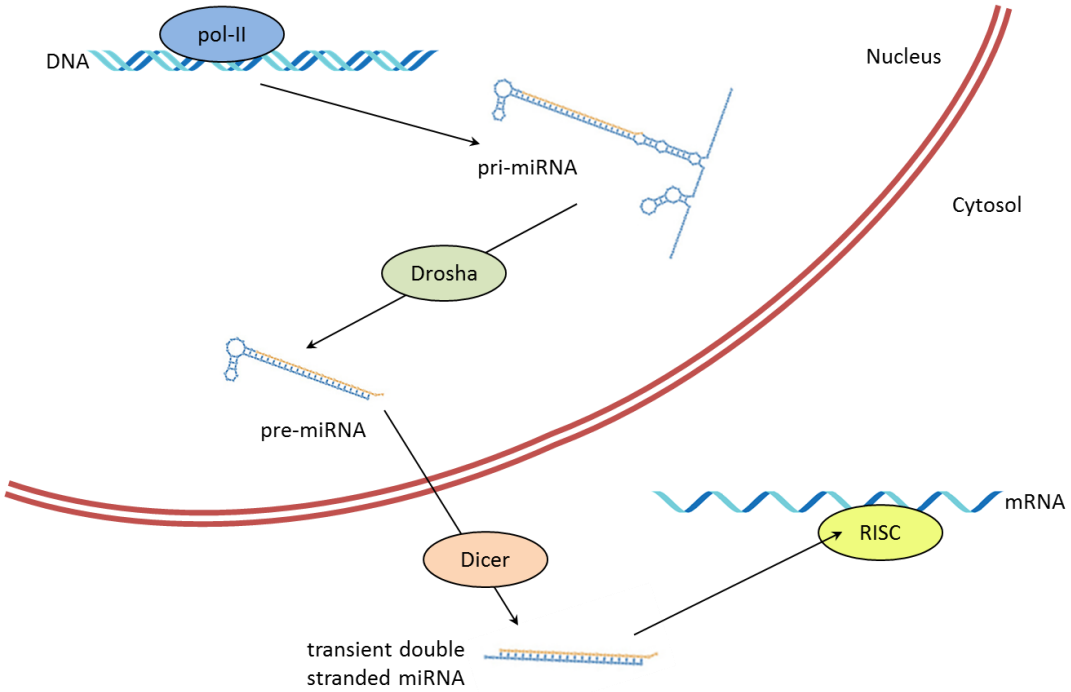

Figure 8. miRNA biogenesis pathway in vertebrate cells.
In the canonical miRNA biogenesis pathway, the pri-miRNAs are transcribed by pol-II and cut by the enzyme Drosha inside the nucleus. The resulting pre-miRNA translocates to the cytoplasm where it is further cut by the enzyme Dicer. The mature miRNA is loaded into the effector complex RISC to direct the translational repression of the target mRNA.

siRNAs are a class of double-stranded RNA molecules of 21-25 base pair (bp) which belong as well to the RNAi pathway. siRNAs can be products of foreign nucleic acids introduced directly into the cell cytoplasm or taken up from the environment and involved in the natural role of genome defense, as observed during transgene- and virus- induced silencing. Recently, also a number of endogenous sources of siRNAs have been identified (reviewed in Golden, Gerbasi, and Sontheimer 2008). miRNAs and endogenous siRNAs share the same biogenesis and have interchangeable function, therefore they cannot be distinguished by their chemical composition or mechanism of action. However, important distinctions can be made in regard to their origin, evolutionary conservation and the type of genes that they silence (Bartel and Bartel 2003). Regardless of the differences between miRNAs and siRNAs, the exposure to these RNA molecules leads to the down-regulation of gene expression as result of multiple levels of suppression: the degree and nature of complementarity between the guide and the target mRNA determines the mechanism of gene silencing (Hutvagner and Zamore 2002). Thus, the regulation of gene expression can occur at transcriptional level as RISC cleaves the target mRNA in the middle of the complementary region (Elbashir, Lendeckel, and Tuschl 2001) and the subsequent presence of ATP enhances the efficiency of degradation through multiple rounds of cleavage preventing the protein production (Hutvagner and Zamore 2002). Another mechanism of miRNA-guided gene regulation takes place at the translational level: the target mRNA contains several binding sites for the miRNAs in its 3' UTR in association with polyribosomes, suggesting that the miRNA blocks the elongation or termination of the translation rather than its initiation, thus reducing the protein synthesis but not affecting the mRNA abundance (reviewed in Bartel 2004).

2.3.1.2 Triggering the RNAi machinery

As recapitulated in the preceding paragraph, the miRNA biogenesis pathway includes three distinct double-stranded RNA intermediates that can be replaced by artificial RNA molecules to engage the RNAi machinery at different entry points and efficiently suppress the expression of a desired target gene (reviewed in Fellmann and Lowe 2014). One of these

approaches relies on the transfection of the target cell with synthetic short interfering RNAs that can suppress endogenous or heterologous gene expression. However, this method has the disadvantages to have a transient effect and to be limited to cells amenable of transfection. To overcome these problems, it is possible to use vectors integrated into the genome and stably expressing stem-loop short hairpin RNAs (shRNAs) that mimic the pre-miRNA. Although such stem-loop shRNAs provide a robust, continuous and heritable source of RNAi triggers, they are expressed by pol-III promoters, and therefore they are not suitable for spatial or temporal control. Additionally, they skip the early steps of the miRNA biogenesis with consequent saturation of the endogenous RNAi processing factors which in turn leads to cell toxicity. The more advanced approach consists in embedding the shRNA sequence into an endogenous miRNA backbone with a configuration recognized as a natural substrate of the RNAi pathway. This enables stable expression of the miRNA by pol-II promoters, ensuring an efficient production of mature small RNA duplex without interfering with the natural pathway, and thus reducing toxicity and enhancing the efficiency of the whole process. In principle, the above described tools can be used to suppress the expression of any gene. However, due to the uncomplete understanding of the RNAi biogenesis and target inhibition, these approaches are sometimes still unpredictable and often not efficient as desired. For instance, not all the sequences are target-specific as the seed sequence that ultimately drives the knockdown is relatively short. Indeed, the primary concern when interpreting RNAi results is the potential off-targets effect due to the homology of the sequence with non-target transcripts, or due to an aberrant processing of the miRNAs, or the general perturbation of the cell state derived by the presence of exogenous RNA molecules (reviewed in Kaelin 2012). Moreover, shRNA sequences able to induce a potent knockdown of the target are rare and need to be identified among many other possible sequences (Fellmann et al. 2011). Nevertheless, to identify effective RNAi triggers and minimize the undesired effects, many rules and algorithms based on empirical and systematic analysis using conventional and machine learning-based approaches have been designed and developed (reviewed in Fellmann and Lowe 2014).

2.3.1.3 microRNA 30

As mentioned in the previous paragraph, via embedding a synthetic shRNA sequence into the context of endogenous miRNAs backbone, it is possible to generate shRNAmir structures which can serve as natural substrates of the miRNA biogenesis pathway and trigger a potent

knockdown of the desired target, as it has been demonstrated for a number of miRNA backbones, including the microRNA 30 (miR-30) (Zeng, Wagner, and Cullen 2002) (Figure 9).

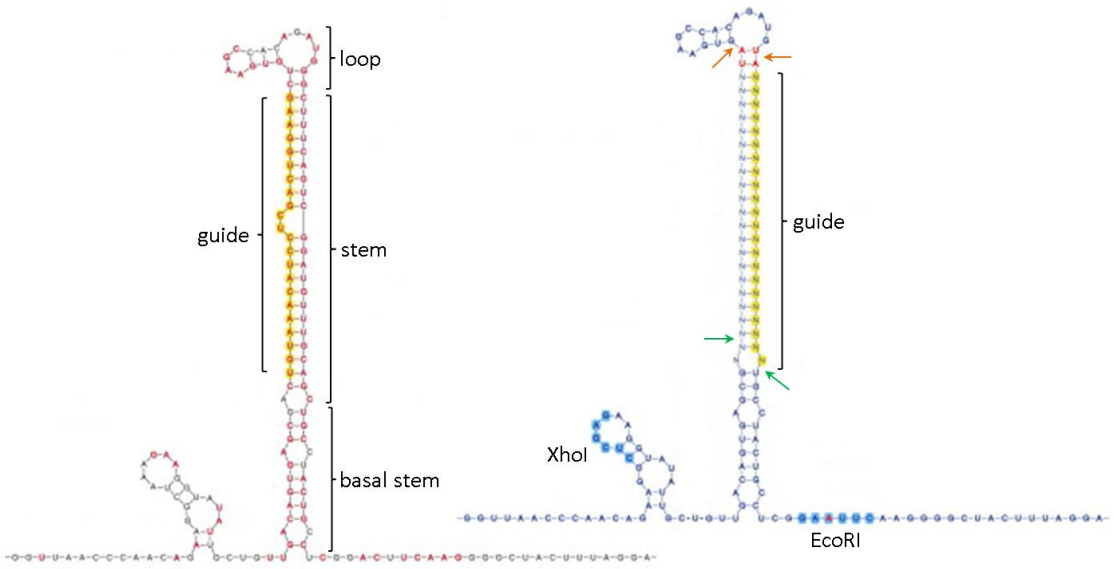

Figure 9. Comparison of the sequences and structures of the endogenous human MIR30A and the experimental miR-30 backbone.
In the endogenous MIR30A (left), the conserved nucleotides are depicted in dark red, and the guide strand is highlighted in yellow. In the experimental miR-30 (right), the "N" in the stem represents the variable nucleotides of the target, the guide strand is highlighted in yellow, the restriction sites used for the shRNA sequences cloning are highlighted in blue, and all the nucleotides that are altered compared to the endogenous MIR30A are in red. The arrows indicate the canonical Drosha (green) and Dicer (orange) cutting sites. In comparison to the natural human MIR30A, the synthetic common miR-30 backbone differs in three relevant features: the miR-30 stem has no bulge and harbors the intended guide on the opposite strand, two bp flanking the loop were changed to design the 3' overhang-ending, and the XhoI/EcoRI restriction sites were introduces in highly conserved regions of the basal stem in order to allow the cloning of artificial shRNA sequences (adapted figure from Fellmann et al. 2013).

This shRNAmir-based system offers several advantages, as for instance the already mentioned expression from pol-II promoters, thus minimizing toxicity for not interfering with the endogenous miRNA pathway. Also, the loop configuration ensures a more precise Dicer cleavage and therefore reduces off-targets effects. Moreover, the expression of the shRNAmir can be directly monitored when placed in the 3' UTR of a reporter (reviewed in Fellmann and Lowe 2014). Therefore, the miR-30 backbone is a well-established and commonly used system that has proved its effectiveness and versatility for RNAi triggering.

2.3.2 Genome tailoring by Cre recombinase

The Cre-loxP recombination was first described by Sternberg and Hamilton in 1981 (Sternberg and Hamilton 1981), and it still provides one of the best experimental tool for the manipulation of a variety of organisms in order to control gene expression, delete undesired DNA sequences and modify chromosome architecture. By allowing high-fidelity spatiotemporally controlled DNA modification, this system helped the understanding on gene function, genetic relationships and diseases.

2.3.2.1 Cre recombinase: activity, efficiency and toxicity

The Cre (Cyclization recombination) recombinase is an enzyme that belongs to the integrase family of site-specific recombinases derived from the Enterobacteria phage P1, and it catalyzes the site-specific recombination between two DNA recognition sites called loxP sites (locus of X(cross)-ingover of P1) (Hamilton and Abremski 1984). The DNA segment flanked by two loxP sites is said to be floxed. A loxP site is a 34 bp consensus sequence composed by an asymmetric 8 bp core spacer sequence that determines the orientation of the loxP site, and flanked by two 13 bp palindromic sequences. Each palindromic sequence is bound by a single Cre recombinase which then form a tetramer of enzymes that bring together two loxP sites (Voziyanov, Pathania, and Jayaram 1999). The recombination occurs within the core spacer area of the loxP sites where the DNA strands are cut and subsequently rejoined. Since the loxP sequences are directional, there are three different possibilities of recombination depending on the location and orientation of the loxP sites: if the loxP sites are placed in a *cis* arrangement, Cre recombinase can mediate (1) an excision when the loxP sites are oriented in the same direction, or (2) an inversion when the loxP sites are oriented in opposite direction; if the loxP sites are placed in a *trans* arrangement, the Cre recombinase mediates (3) a translocation (Figure 10).

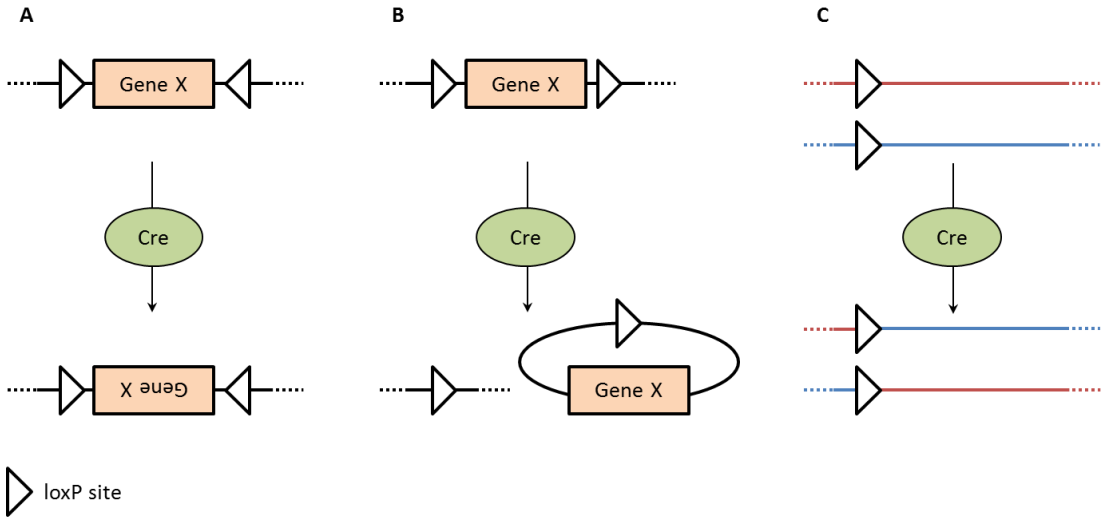

Figure 10. Mechanisms of site-specific Cre recombination.
(A) Inversion of the floxed segment of DNA resulting from the recombination of two loxP sites in opposite directional orientation in a *cis* arrangement.
(B) Excision of the floxed segment of DNA resulting from the recombination of two loxP sites in the same directional orientation in a *cis* arrangement.
(C) Translocation of segments of DNA resulting from the recombination of two loxP sites in a *trans* arrangement.

The specificity of the recombination process mediated by the Cre recombinase is explained by the fact that a random occurrence of a specific 34 bp sequence requires a length of DNA many times higher than the entire mammalian genome. However, it has been shown that mammalian genomes contain pseudo loxP sites which can serve as functional recognition sites for the enzyme, although the affinity of the Cre recombinase for these sites is much lower than for the consensus loxP sites (Thyagarajan et al. 2000). Nevertheless, it has been strikingly demonstrated that the Cre recombinase can be toxic for the cell by attacking the genomic DNA leading to an increased cell death simply because cells are unable to deal with Cre toxicity (reviewed in Schmidt-Supprian and Rajewsky 2007). To increase specificity and stability of the Cre recombination, novel loxP mutants have been developed combining sequences with mutation in the core spacer and/or in the palindromic sequences (Langer et al. 2002 and references therein), and new enzyme variants were generated (Shimshek et al. 2002). The Cre recombinase is a very simple but robust enzyme that functions very efficiently in a variety of organisms, including bacteria, yeast, plants, insects and mammalian. However, the Cre recombinase efficiency can be affected by two factors: (1) mutant loxP sites which differ on the core spacer sequence tend to give a generally lower recombination efficiency compared to the wild-type loxP sites (Lee and Saito 1998); (2) the dynamic of the

recombination process decreases when the length of floxed DNA segment increases (Zheng et al. 2000). Moreover, the ability of the Cre recombinase to access a loxP site placed on a chromosome and then to build site-specific synapsis of DNA may be highly dependent on the surrounding chromatin structure and on the particular location of the loxP site within the genome (Sauer and Henderson 1988).

2.3.2.2 Genomic engineering with Cre-loxP

The key advantage of the Cre-loxP recombination is that additional co-factors or sequences elements are not required for an efficient recombination regardless of the cellular environment, allowing an independent activity for a broad variety of genetic applications. Furthermore, in combination with the advent of mouse embryonic stem cells and homologous recombination-based gene targeting, it has been possible to create any desired modification for any existing gene of the mouse genome. Initially, this system was used in mice to switch-on the expression of specific genes in a given cell population: two distinct transgenic mouse lines were generated separately carrying either a silent transgene (spaced from the promoter by a floxed stop-cassette) or the transgene for the Cre recombinase expression. The mating of the two mouse lines would generate litters with the desired genetic alteration (reviewed in Nagy 2000). Subsequently, a growing number of studies contributed to further develop these genomic engineering strategies to address the function of genes involved in complex networks and their roles in different tissues (reviewed in Kwan 2002). Cre-loxP recombination has proved to be useful also for modeling human conditions, for example chromosomal disorders (Smith et al. 1995). However, even if most of the Cre-transgenic mouse strains seem to normally develop, several problems related to the expression of the Cre-recombinase were observed in a large number of reports, for instance an increased apoptosis in cells expressing high levels of the enzyme or the induction of DNA double strand breaks on cryptic target sites (reviewed in Schmidt-Supprian and Rajewsky 2007).

2.3.2.3 CreER^{T2} mediated recombination

To prevent undesirable side effects of toxicity associated to the expression of the Cre recombinase, it is important to consider the expression levels of the enzyme into the target cell. The Cre recombinase has a nuclear localization signal: after translation, the fully functional enzyme is normally shuttled into the nucleus where it recognizes the loxP sites and catalyzes the recombination of the floxed DNA segment. One widely used strategy to minimize the exposure of the target cell's genomic DNA to the toxicity of Cre recombinase is the employment of systems for the generation of inducible forms of the enzyme. One particularly successful strategy to induce the Cre recombinase activity is the fusion of a mutant of the ligand binding domain of the estrogen receptor (ER) to the C-terminal end of the Cre (Metzger et al. 1995), which enables the localization of the fusion protein in the cytosol via the interaction with the heat shock protein 90 (Hsp90). Different ERs are currently available: the human ER^{T2} was generated by site directed mutagenesis to contain the G400V/M543A/L540A triple mutation (Feil et al. 1997) which prevents the binding of the endogenous estrogen β-estradiol but allows the binding of the synthetic estrogen 4-hydroxytamoxifen (Tamoxifen). The interaction between Tamoxifen and the ER^{T2} leads to the release of the cytosolic Hsp90 and thus permits the shuttling of the fusion protein to the nucleus (Figure 11).

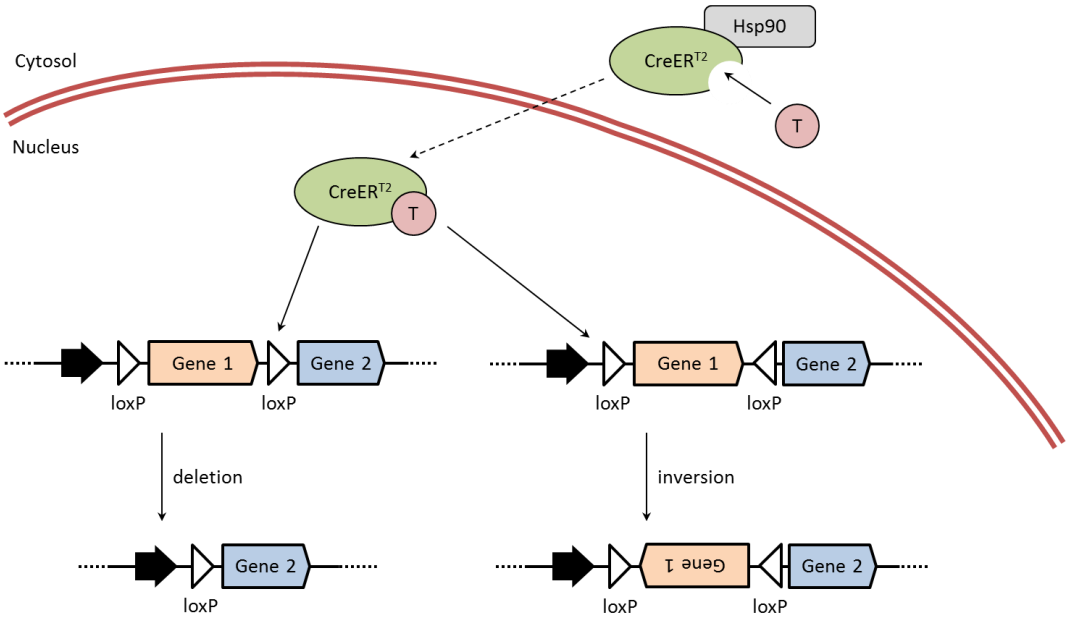

Figure 11. Scheme of the activation of the CreER^{T2} enzyme.
In the absence of the steroid, the CreER^{T2} protein forms a complex with Hsp90 and localizes in the cytoplasm. When the cells are exposed to Tamoxifen (T), the CreER^{T2} is released from the Hsp90 and can translocate to the nucleus where it can recombine the floxed DNA. Here, only two of the three possible recombination events are depicted.

It has been shown that the CreER^{T2} has an enhanced ligand-activated site-specific recombination with an activity approximately ten times more sensitive than the original CreER protein regarding both nuclear translocation and enzymatic activity, thus allowing reducing the amount of Tamoxifen needed for the activation of the recombination process, and consequently minimizing the toxic effects (Indra et al. 1999). To obtain a precise spatial and temporal limitation of the recombination process, the activity of the CreER^{T2} should be strictly dependent to the presence of Tamoxifen; however, the activity of the CreER^{T2} recombinase is leaky, resulting in a basal level of recombination independently from the presence of Tamoxifen (Zhang et al. 1996). Taken together, the inducible CreER^{T2} engineering is a very powerful and effective tool for the elucidation of gene functions and therefore a fundamental approach to study the pathogenesis of human diseases.

2.4 Current models of human cancers

Although there is a continuous increase of the existing knowledges on tumor-specific alterations due to a constant improvement of techniques, such as expression profiling and next generation sequencing (Mwenifumbo and Marra 2013), the research on tumor treatment asks for the understanding of the function that each altered gene harbors in established tumors, with the aim to identify suitable therapeutic targets for precision medicine or personalized therapies (Andre et al. 2014; Eifert and Powers 2012). Therefore, it is important to develop techniques that can help to bridge the gap between the research bench and the bedside to get closer to the patients' condition. The commercially available human cell lines are mainly used to study the function of particular alterations. Although cheap and technically easy to handle, cell lines often present additional mutations which are acquired during the immortalization process, but that are not present in the primary tumors from which they are originated (Domcke et al. 2013), and which might fundamentally change their genetic and/or epigenetic setting (Smiraglia et al. 2001). Furthermore, the establishment of cell lines from acute leukemia primary tumors is rarely successful (Gillet, Varma, and Gottesman 2013), making these derivatives cell lines sometimes doubtful models. On the other hand, working with primary patients' cells *in vitro* is technically almost unfeasible as cells do not reliably grow in culture and the traditional *in vitro* cultures do not reflect the complex environment of patients' tumor. An elegant alternative was provided by the sophisticated genetically engineered mouse models (GEMM) accompanied by syngeneic bone marrow transplantation approaches (Chesler and Weiss 2011; Jacoby, Chien, and Fry 2014) and used in leukemia research for the identification of human tumor-specific alterations. Instead, the patient-derived xenograft (PDX) mouse model of acute leukemia is based on the expansion of human primary samples through serial re-passaging in mice without prior *in vitro* exposure of the cells (Morton and Houghton 2007). Therefore, the PDX mouse model of acute leukemia has the potential advantage to keep the genetic diversity found in patients and therefore it currently provides the best model for the study of alterations in human leukemic cells.

2.4.1 PDX mouse model of acute leukemia

NOD/scid IL2 receptor gamma chain knockout (NSG) mice are severely immunocompromised mice which lack functional T, B, and NK cells, are deficient in multiple cytokine signaling pathways and have many defects in innate immunity (Shultz et al. 2005; Shultz et al. 1995).

For these reasons, tumor cells obtained from patients with acute leukemia are able to engraft and recapitulate the human disease with a highly similar organ distribution when transplanted into NSG mice, enabling the modeling of human acute leukemias (Schmitz et al. 2011). PDX cells are harder in handling for molecular manipulation compared to established cell lines; nevertheless, it is possible to transduce PDX cells with viral vectors to introduce tracers which allow performing preclinical trials at a high level of accuracy and precision, and increase the specificity and complexity of the questions that could be addressed (Terziyska et al. 2012; Vick et al. 2015). A substantial improvement of the PDX mouse model of acute leukemia has been the establishment of the molecular labeling of PDX cells with bioluminescent markers, such as luciferases, in order to monitor the growth of the xenotransplanted tumor cells in the living mice with a sensitive readout (Terziyska et al. 2012; Barrett et al. 2011; Duy et al. 2011; Vick et al. 2015). The bioluminescence *in vivo* imaging allows to perform a variety of preclinical trials and supports the advancement in the understanding of several tumor features, such as the quantification of the leukemic initiating cells when coupled with limiting dilution assays, the evaluation of the tumor distribution and development in the context of the living mouse, and the possibility to monitor the response to drug treatments. Indeed, the PDX mouse model of acute leukemia provides an useful preclinical tool for drug discovery and drug testing with the aim to identify suitable therapeutic targets for precision medicine and personalized therapies (Sausville and Burger 2006). Additionally, the sensitivity of this technique reduces the assay variance with the consequent possibility to minimize the number of animals required for the trials. Furthermore, the labeling of PDX leukemic cells with either fluorescent proteins using the principle of RGB marking (Clappier et al. 2011; Weber et al. 2011) or genetic barcodes (Porter et al. 2014; Zanatta et al. 2014; Cornils et al. 2014) has enabled the investigation of clonal evolution and the detection of the presence of tumor-initiating cells, consequently allowing both the analysis of the expression profiles of clones generated from single cells and the evaluation of the phenotypic behavior in response to drug treatments of the different clones generated from a single patient's sample. Moreover, the expression of other artificial surface antigens for the enrichment of small subpopulations raised the possibility to localize a small number of cells in the context of the bone marrow environment and to develop a minimal residual disease model (Ebinger et al. 2016; Ninomiya et al. 2007).

2.5 Aim of the study

Despite the improvement in the survival rate for childhood ALL and younger adults suffering from AML, infants and adult patients with ALL and the vast majority of AML patients still have a poor prognosis because the current treatments lack valuable options. Novel treatment options are intensively required, at best as targeted therapies directed against decisive elements of the tumor cell. Unfortunately, techniques that allow identifying structures with essential function – which inhibition induces cell death – within individual patient's tumor cells are missing. Those structures might represent therapeutic targets and might exist in the apoptosis signaling pathway.

To bridge the gap, the goal of this present thesis was to establish innovative constitutive and inducible technologies for knockdown in the individualized preclinical PDX mouse model of acute leukemia. Using XIAP and Mcl-1 as examples, we aimed at combining the miR-30 based RNAi technology with $CreER^{T2}$ inducible genetic engineering.

Aim 1. (a) Design and establishment of a system for the constitutive knockdown of XIAP in both cell lines and PDX cells. (b) Validation of XIAP as therapeutic target for ALL patients using the novel constitutive-knockdown system.

Aim 2. (a) Design and establishment of a system for the inducible knockdown of Mcl-1 in cell lines and PDX cells. (b) Validation of the newly established inducible-knockdown system using Mcl-1 in patients' acute leukemia cells expanding in mice.

3. Materials

3.1 Equipment (in alphabetic order)

Equipment	Manufacturer/Brand
Aquintus (water purification station)	MembraPure GmbH
Axiovert 200M Fluorescence/Live cell Imaging Microscope	ZEISS
BD LSRAriaIII (cell sorter)	BD Biosciences
BD LSRFortessa (flow cytometer)	BD Biosciences
Benchtop Calibration Check™ pH-Meter HI 221	HANNA Instrument
BioPhotometer (photometer)	Eppendorf®
Blockthermostat BT 1302	HLC BioTech
Chemical fume hood	Prutscher Laboratory Systems
Compact laboratory balance 440-43N	KERN & SOHN GmbH
EasyPhor Maxi-System chamber	Biozym Scientific GmbH
EasyPhor Mini-System chamber	Biozym Scientific GmbH
Gammacell-40 Atomic Energy of Canada Limited	Chalk River
Gel documentation system Vilber Lourmat E-BOX VX5	PEQLAB Biotechnologie GmbH
Heracell™ 150i CO_2 Incubator (for cell culture)	ThermoFisher Scientific
Heraeus B6060 incubator (for bacteria)	Gemini BV Laboratory
HS12 Hood/Enclosure:Biological Safety Cabinet	Heraeus
Hypercassette RPN11642	Amersham Pharmacia Biotech
Innova® 44 Large-Capacity, Floor-Stackable Incubator Shaker (for bacteria)	Eppendorf®
LightCycler® 480 Instrument II	Roche
Microcentrifuge 5415R	Eppendorf®
Microcentrifuge 5417C	Eppendorf®

Microwave MW 1226 CB	Bomann
Mini-PROTEAN® Tetra Cell device	BIO-RAD
Minishaker MS1 (vortex)	IKA®
NanoDrop ND-1000 Spectrophotometer	PEQLAB Biotechnologie GmbH
Optimax (images develop machine)	Typon - PROTEC
Porcelain mortar and pestle 125 x 60 mm	Finlab Nigeria Limited
PowerPac™ Basic Power Supply	BIO-RAD
Primus 25 advanced® Thermocycler	PEQLAB Biotechnologie GmbH
Rocking platform KS250 Basis	IKA®
Rotanta 460R centrifuge	Hettich Zentrifugen
Sartorius 2001 Mp2 Analytical Balance	Sartorius AG
Tali™ image-based cytometer	Invitrogen, Carlsbad, CA, USA
Telaval 31 Inverted Phase Microscope	ZEISS
Thermo Herasafe HS18 Sterile Hood	ThermoFisher Scientific - Heraeus
Trans-Blot® TurboTM Transfer System	BIO-RAD
Tube Roller Mixer SRT9	Stuart Equipment
UVC/T-M-AR, DNA/RNA UV-cleaner box	Biosan

3.2 Disposable equipment (in alphabetic order)

Disposable equipment	ref#	Manufacturer/Brand
Amersham Hyperfilm ECL (18x24)	28906837	GE Healthcare
Amicon Ultra-15 Centrifugal Filter Unit	UFC910024	Merck Millipore
ColiRoller™ Plating Beats	71013-3	Merck Millipore
Countess® Cell Counting Chamber Slides	LT07-318	ThermoFisher Scientific

EASYSTRAINER 70 µM	542070	Greiner Bio-One
Einmalkanüle 0,60x60 mm (needle for Ficoll)	D-73312	Supra Vivomed GmbH
LightCycler® 480 Multi-well Plate 96-well	04 729 692001	Roche
Mini-PROTEAN® TGX™ Precast Protein Gel 12%	4561046 4561045 4561043	BIO-RAD
Syringe Injekt® Solo	4606205V	Braun
Trans-Blot® TurboTM Midi Nitrocellulose Transfer Packs	1704159	BIO-RAD
Rotilabo®-Spritzenfilter 0,22µm	P668.1	CARL ROTH
50 mL Tube Top Vacuum Filter System, 0.45µm	430314	Corning®
Millex® HV Sterile Syringe Filter, PVDF 0.45 µm	SLHV033RS	Merck Millipore

3.3 Kits (in alphabetic order)

Kit	**ref#**	**Manufacturer/Brand**
CloneJET PCR Cloning Kit	K1231	ThermoFisher Scientific
LightCycler® 480 Probes Master	04707494001	Roche
NucleoBond® Xtra Midi Plus	740412.50	MACHEREY-NAGEL GmbH
NucleoSpin® Gel and PCR Clean-up	740609.240C	MACHEREY-NAGEL GmbH
NucleoSpin® Plasmid EasyPure	740727.250	MACHEREY-NAGEL GmbH
ProFection® Mammalian Transfection System	E1200	Promega
QIAamp DNA Blood Mini Kit	51106	QIAGEN
QIAshredder (50)	79654	QIAGEN
QuantiTect Reverse Transcription Kit	205311	QIAGEN
RNase-Free DNase Set (50)	79254	QIAGEN

RNeasy Mini Kit (50)	74104	QIAGEN

3.4 Chemicals, substances and solutions (in alphabetic order)

Chemical, substance, solution	ref#	Manufacturer/Brand
(Z)-4-Hydroxytamoxifen (4-HT) for cell culture	H7904-25MG	Sigma-Aldrich
2-Propanol (isopropanol)	1096342500	Merck Millipore
4X Laemmly Sample Buffer	1610747	BIO-RAD
Acetic acid glacial	818755.1000	MERCK
Agar-Agar Kobe I (Agar)	5210.3	CARL ROTH
Ampicillin Solution	A2262.100	BIOMOL
Bovine serum albumin (BSA)	A3059-50G	Sigma-Aldrich
Calcium chloride dihydrate – $CaCl_2$	C3306	Sigma-Aldrich
Cell Lysis Buffer 10X	9803S	Cell Signaling Technology
Ciprobay® Breitspektrum-Antibiotikum	8242.05.02	BAYER
Corn oil	C8267-500ML	Sigma-Aldrich
Dimethyl sulfoxide (DMSO)	D2650	Sigma-Aldrich
dNTP Mix (10 mM each)	R0192	ThermoFisher Scientific
Dulbecco's Modified Eagle Medium (DMEM)	21969-035	GIBCO
Ethanol ≥99.8 %, p.a. (EtOH)	9065.1	CARL ROTH
Ethylenediaminetetraacetic acid (EDTA)	E9884	Sigma-Aldrich
Fetal bovine serum Premium (FBS)	P30-1502	PAN Biotech UK Ltd
Ficoll® Paque Plus (Ficoll)	17-1440-03	GE Healthcare – Sigma-Aldrich
GeneRuler DNA Ladder Mix	SM0331	ThermoFisher Scientific
supplied together with 6X DNA Loading Dye	R0611	

Glycerol	G6279-500ML	Sigma-Aldrich
Glycin ≥99 %	3790.3	CARL ROTH
Hefeextrakt (yeast extract)	2363.3	CARL ROTH
HEPES potassium salt	54464	Sigma-Aldrich
Hexadimethrine bromide (polybrene)	H9268-10G	Sigma-Aldrich
Insulin-Transferrin-Selenium (ITS -G)	41400-045	GIBCO
L-Glutamine solution (L-Glu)	25030-024	GIBCO
Manganese Chloride Tetrahydrate – $MnCl_2$	M2190	USBiological
Midori Green Advance MG04	617004	Biozym
Milchpulver (non-fat dry milk)	T145.2	CARL ROTH
MOPS	M1254	Sigma-Aldrich
PageRulerTM Plus Prestained Protein Ladder, 10 to 250 kDa	26619	ThermoFisher Scientific
Penicillin-Streptomycin (10,000 U/mL) (P/S)	15140-122	GIBCO
Phenylmethanesulfonyl Fluoride (PMSF)	8553S	Cell Signaling Technology
Ponceau S solution	P7170	Sigma-Aldrich
Potassium acetate – K-Acetate	P-3542	Sigma-Aldrich
Potassium chloride – KCl	1049361000	Merck Millipore
Potassium dihydrogen phosphate – KH_2PO_4	1048771000	Merck Millipore
Protein Assay Dye Reagent Concentrate	500-0006	BIO-RAD
Puromycin dihydrochloride	P9620-10ML	Sigma-Aldrich
Recombinant Human Flt-3 Ligand Protein (FLT3L)	308-FKN	R&D Systems
Recombinant Human IL-3 (IL-3)	200-03-100	PeproTech
Recombinant Human Stem Cell Factor (SCF)	300-07-100	PeproTech
Recombinant Human TPO (TPO)	300-18-100	PeproTech

Roswell Park Memorial Institute 1640 Medium (RPMI 1640)	21875-034	GIBCO
Select Peptone 140	30392-021	GIBCO
Sodium Chloride – NaCl	3957.2	CARL ROTH
Sodium dihydrogen phosphate dihydrate – Na_2HPO_4	1063421000	Merck Millipore
Sodium dodecyl sulfate (SDS)	L3771	Sigma-Aldrich
Sodium pyruvate solution – Na-Pyruvate	S8636	Sigma-Aldrich
StemPro®-34 SFM Medium supplied together with StemPro®-34 Nutrient Supplement	10640-019 10641-025	GIBCO
SuperSignalTM West Femto Maximum Sensitivity Substrate	34095	ThermoFisher Scientific
SuperSignalTM West Pico Chemiluminescent Substrate	34080	ThermoFisher Scientific
Tamoxifen (4-OHT)	T5648-5G	Sigma-Aldrich
TRIS – Tris base	5429.2	CARL ROTH
TRIS hydrochloride – Tris-HCl	9090.3	CARL ROTH
Trypan Blue solution	T8154	Sigma-Aldrich
Trypsin-EDTA (0.05%), phenol red	25300-054	GIBCO
TurboFect Transfection Reagent	R0531	ThermoFisher Scientific
TWEEN® 20	P7949	Sigma-Aldrich
UltraPure™ Agarose	16500-500	Invitrogen
α-Thioglycerol (α-TG)	M6145-25ML	Sigma-Aldrich
β-mercaptoethanol	444203	Calbiochem

3.5 Homemade buffers and solutions (in alphabetic order)

Buffer, solution	components
ALL Patient Medium (PM)	RPMI 1640
	20% FBS
	1% L-Glu
	1% P/S
	0.6% ITS-G
	1 mM Na-Pyruvate
	50 µM α-TG
AML Patient Medium (DD-Medium)	StemPro®-34 SFM Medium
	2.5% StemPro®-34 Nutrient supplement
	2% FBS
	1% L-Glu
	1% P/S
	10 ng/mL FLT3L
	10 ng/mL SCF
	10 ng/mL TPO
	10 ng/mL IL-3
Annealing buffer	50 mM Hepes pH 7.4
	100 mM NaCl
Blocking buffer 5%	2.5 g non-fat dry milk
	50 mL TBS-T
Chloroquine 100 mM	0,516 g Chloroquine diphosphate
	up to 10 mL with ddH_2O
	filtered to sterile with 0.2 µm filter
Freezing medium for human cells	90% FBS
	10% DMSO
LB Agar	400 mL LB Medium
	6 g Agar
	50 mg/L Ampicillin Solution
Luria-Bertani (LB) broth	8 g Select Peptone 140
	4 g yeast extract
	8 g NaCl
	up to 800 mL with H_2O Milli-Q

	50 mg/L Ampicillin Solution
Phosphate-buffered saline (PBS) 10X	80 g NaCl 2 g KCl 25.6 g Na_2HPO_4 x $7H_2O$ 2 g KH_2PO_4 up to 1 L with ddH_2O
Running Buffer 10X	250 mM Tris-base 1.92 M glycine 1% SDS up to 1 L with ddH_2O adjusted to pH 8.3
Tamoxifen for *in vitro* treatment 5 mM	5 mg 4-HT 2.5 mL 100% EtOH
Tamoxifen for mice treatment 10mg/mL	10 mg 4-OHT 10% EtOH 90% Corn oil
TBS Tween20 (TBS-T)	100 mL TBS 10X 900 mL ddH_2O 0.1% TWEEN® 20
Transformation buffer I (TFB I)	100 nM KCl 10 mM $CaCl_2$ 30 mM K-Acetate 50 mM $MnCl_2$ 15% glycerin 98% up to 400 mL with ddH_2O adjusted to pH 5.8 filtered to sterile
Transformation buffer II (TFB II)	10 mM KCl 75 mM $CaCl_2$ 10 mM MOPS 15% glycerin 98% up to 100 mL with ddH_2O adjusted to pH 7.0 filtered to sterile
Tris-base, acetic acid, EDTA (TAE) buffer 50X	2 M Tris-base

	50 mM EDTA 1 M glacial acetic acid up to 1 L with ddH_2O
Tris-buffered saline (TBS) buffer 10X	200 mM Tris-base 1.5 M NaCl up to 1 L with ddH_2O adjusted to pH 7.6

3.6 Enzymes and buffers

EcoRI-HF™, ref# R3101S (NEW ENGLAND BioLabs)

XhoI, ref# R0146S (NEW ENGLAND BioLabs)

CutSmart® Buffer, ref# B7204S (NEW ENGLAND BioLabs)

All additional restriction enzymes (indicated in the vectors maps in paragraphs 3.9.2 and 3.9.3) and relative buffers required for the cloning of the different plasmids used for this study were ordered at NEW ENGLAND Biolabs.

Pfu DNA Polymerase, recombinant (2.5 U/µL), ref# EP0501 (ThermoFisher Scientific) supplied together with 10X Pfu Buffer with $MgSO_4$

GoTaq® G2 Flexi DNA Polymerase, ref# M7805 (Promega) supplied together with 5X Green GoTaq® Flexi Buffer

T4 DNA LIGASE (1000 U), ref# EL0011 (Thermo Scientific) supplied together with 10X T4 DNA Ligase Buffer

3.7 Oligonucleotides and primers

All 110-mer sequences (Table S1) and primers (Table S2) used in this study were ordered at Eurofins Genomics MWG (http://www.eurofinsgenomics.eu/), resuspended in distilled water to a final concentration of 100 pmol/µL and kept at -20°C.

3.8 Probes for quantitative Real-Time PCR

For the detection and quantification of target cDNA, the LightCycler® 480 PCR Master Probes (Universal ProbeLibrary Set, Human) (Table S3) were used. Probes were used undiluted to a final concentration in the reaction from 0.05 µM to 0.2 µM.

3.9 Plasmids

The pCDH lentiviral backbone was obtained from System Biosciences (Palo Alto, CA, USA). The helper virus pCMV-Gag-Pol (RV-111) and the pCMV-Eco envelope virus (RV-112) were obtained from Cell Biolabs (San Diego, CA, USA).

The coding sequence of mCherry was obtained from Addgene (Cambridge, MA, USA). The coding sequence of eGFP was provided by Stephan Geley (Division of Molecular Pathophysiology – Innsbruck Medical University, Austria). The coding sequence of mtagBFP was provided by Michael Schindler (Helmholtz Zentrum München, Germany). The coding sequence of $CreER^{T2}$ was provided by Marc Schmidt-Supprian (Technische Universität München – Klinikum rechts der Isar, Germany). The sequence of the common miR-30 shRNAmir backbone for the shRNAs expression was provided by Johannes Zuber (Research Institute of Molecular Pathology - IMP, Vienna, Austria). The coding sequence of dsRED which embeds the common miR-30 shRNAmir backbone was obtained from Addgene (Cambridge, MA, USA).

The sequences of all plasmids cloned for this study have been designed using the Clone Manager 7 software, and verified by Sanger sequencing (GATC Biotech AG, Cologne, Germany).

3.9.1 Plasmids for the Reporter Assay

The plasmids used for the Reporter Assay were provided by Johannes Zuber (Research Institute of Molecular Pathology - IMP, Vienna, Austria).

The reporter construct (Figure 12) expresses the dTomato fluorescent protein from a phosphoglycerate kinase (PGK) promoter, and it harbors in its 3’ UTR the target sites of established control shRNAs as well as an array of shRNA target sites to be tested.

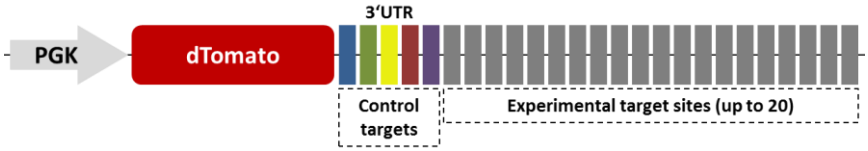

Figure 12. Reporter construct for the generation of a stable reporter line (figure from Thomas Hoffmann, Matthias Muhar, Ines Barbosa and Johannes Zuber - Research Institute of Molecular Pathology - IMP, Vienna, Austria).

The shRNA vector (Figure 13) expresses the GFP reporter from a Tetracycline-dependent TRE promoter, and it harbors in its 3' UTR the miR-30 shRNAmir backbone with embedded the shRNA sequence to be tested.

Figure 13. shRNA expressing vector for the validation of potent single-copy shRNAs (figure from Thomas Hoffmann, Matthias Muhar, Ines Barbosa and Johannes Zuber - Research Institute of Molecular Pathology - IMP, Vienna, Austria).

3.9.2 Plasmids for the constitutive-knockdown system

The construct constitutively encoding for dsRED, which harbors in its 3' UTR the miR-30 shRNAmir cassette, was generated by cloning the dsRED/miR-30 fragment amplified by PCR into the pCDH lentiviral backbone under the control of the viral spleen focus forming virus (SFFV) promoter (Figure 14). The 22-mer shRNA sequences targeting eGFP and Renilla used as control or targeting XIAP were synthetized as part of 110-mer oligonucleotides and cloned into the vector using XhoI and EcoRI.

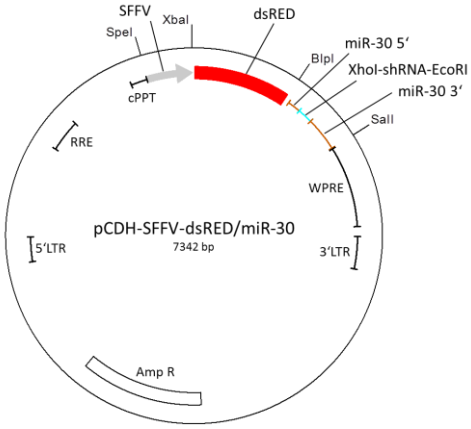

Figure 14. Scheme of the construct used for the constitutive-knockdown system.

The plasmids encoding for the two different fluorescent markers (mtagBFP or eGFP) were generated by cloning the coding sequences of either mtagBFP or eGFP into the pCDH lentiviral backbone under the control of the eukaryotic elongation factor-1 alpha (EF1α) promoter using BamHI and SalI (Figure 15). The two plasmids also contain two different luciferases (Gaussia luciferase (GLuc) or codon optimized enhanced Firefly luciferase (eFFly)).

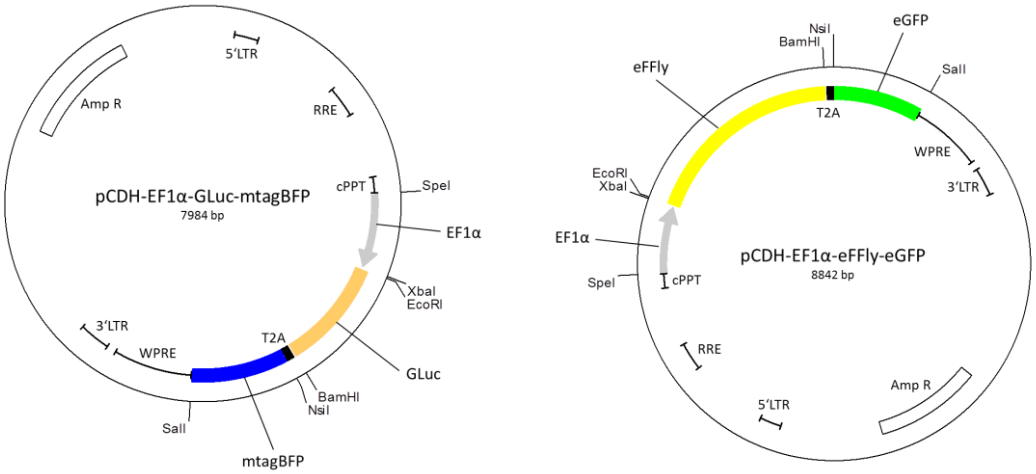

Figure 15. Constructs used for competitive assays with the constitutive-knockdown system: each plasmid expresses a fluorochrome (and a luciferase) under the control of the EF1α promoter.

3.9.3 Plasmids for the inducible-knockdown system

The plasmid constitutively expressing the CreER^{T2} recombinase was generated by cloning into the pCDH lentiviral backbone the coding sequences of the CreER^{T2} and the mCherry fluorescent marker under the control of the viral SFFV promoter using NsiI and SalI (Figure 16). The plasmid harbors also the coding sequence of the GLuc.

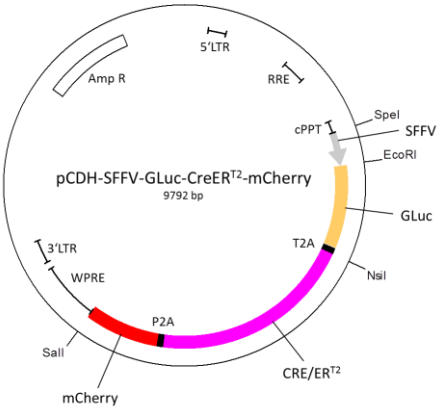

Figure 16. CreER^{T2} expressing construct used for the inducible-knockdown system.

The pCDH lentiviral vector containing the FLIP-cassette was syntetized from GenScript® (Piscataway, NJ, USA). The FLIP-cassette vector expresses the mtagBFP fluorescent marker under the control of the viral SFFV promoter. Two different sets of loxP sites (2272 loxP core's sequence: GGATACCT, and 5171 loxP core's sequence: GTACACAT) were conveniently introduced into the pCDH lentiviral backbone for the specific recombination of the FLIP-cassette. The plasmid presents in antisense direction the coding sequence of the eGFP fluorescent protein, which harbors in its 3' UTR the miR-30 shRNAmir cassette; therefore, they are expressed only upon CreER^{T2} mediated recombination (Figure 17). The 22-mer shRNA sequences targeting Renilla used as control or targeting Mcl-1 were synthetized as part of 110-mer oligonucleotides and cloned into the vector using XhoI and EcoRI.

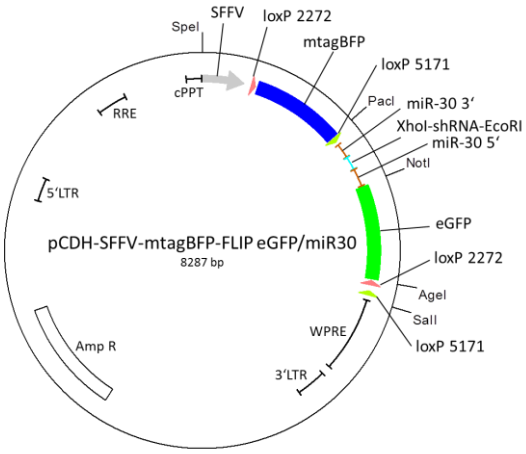

Figure 17. FLIP-cassette vector used for the inducible-knockdown system.

3.9.4 Packaging plasmids

The packaging vectors encoding for Gag, Pol (pMDLg_pRRE) and Rev (pRSV_Rev) were provided by Tim Schroeder (Swiss Federal Institute of Technology ETH Zürich, Basel, Switzerland). The envelope vector encoding for VSV-G (pMD2.G) was obtained from Addgene (Cambridge, MA, USA).

3.10 Antibodies

3.10.1 Primary antibodies for Western blotting

Anti-cIAP1 (D5G9) Rabbit Monoclonal Antibody, ref# 7065S (Cell Signaling Technology), diluted 1:250 in TBS-T.

Anti-cIAP2 (58C7) Rabbit Monoclonal Antibody, ref# 3130S (Cell Signaling Technology), diluted 1:500 in TBS-T.

Anti-GAPDH (6C5) Mouse monoclonal Antibody, ref# CB1001-500UG (Merck Millipore), diluted 1:5000 in blocking buffer 5%.

Anti-αtubulin (DM1A), ref# CP06 (Calbiochem), diluted 1:3000 in blocking buffer 5%.

Anti-Mcl-1 (S-19) Antibody, ref# sc-819 (Santa Cruz Biotechnology), diluted 1:100 in TBS-T.

Anti-XIAP Antibody (clone 48), ref# 610763 (BD Transduction Laboratories™), diluted 1:1000 in blocking buffer 5%.

3.10.2 Secondary antibodies for Western blotting

Anti-mouse IgG, HRP-linked Antibody, ref# 7076S (Cell Signaling Technology), diluted 1:10000 in blocking buffer 5%.

Anti-rabbit IgG, HRP-linked Antibody, ref# 7074S (Cell Signaling Technology), diluted 1:10000 in blocking buffer 5%.

3.11 Cell lines

The HEK-293T, MS-5, ALL and AML cell lines were obtained from DSMZ (Heidelberg, Germany) and kept in culture for a maximum of 3 months. Platinum-A, Platinum-GP and RAg-MEF cell lines were provided by Johannes Zuber (Research Institute of Molecular Pathology - IMP, Vienna, Austria). All cell lines described below and their derivatives were tested for, and found to be free of, mycoplasma infection (MycoAlert™ Mycoplasma Detection Kit, Lonza). The authenticity of all cell lines was verified by DNA fingerprinting using a PCR-single-locus-technology (PowerPlex 21 PCR Kit, Promega) at Eurofins Medigenomix Forensik GmbH (Germany).

3.11.1 ALL cell lines

The NALM-6 cell line (ACC 128, DSMZ, Germany) is a human B cell precursor leukemia line established in 1976 from the peripheral blood of a 19-year-old young man with ALL at relapse. According to the cytoplasmic and surface immunoglobulin characteristics, NALM-6 is considered to be of the pre-B cell phenotype with a peculiar pattern of chromosomal abnormalities in a pseudo-diploid karyotype (Hurwitz et al. 1979).

The REH cell line (ACC 22, DSMZ, Germany) is a human B cell precursor leukemia line established in 1973 from the peripheral blood of a 15-year-old girl with ALL at first relapse. According to morphological and histochemical features, REH is considered to be of the

“common form” (non-T, non-B ALL) of pre-B cell phenotype with pseudo-diploid karyotype and expressing the fusion gene TEL-AML1 (Rosenfeld et al. 1977).

The CCRF-CEM cell line (ACC 240, DSMZ, Germany) is a human T cell leukemia line established in 1964 from the peripheral blood of a 3-year-old girl with ALL at terminal relapse. According to morphological and chromosomal characteristics, CCRF-CEM is considered to be T-ALL cell line with near-diploid karyotype (Foley et al. 1965).

3.11.2 AML cell lines

The MOLM-13 cell line (ACC 554, DSMZ, Germany) is a human myeloid leukemia line established in 1995 from the peripheral blood of a 20-year-old man with AML FAB M5a at relapse. According to morphological and chromosomal features, MOLM-13 is considered to be AML cell line with hyperdiploid karyotype and 4% polyploidy (Matsuo et al. 1997).

The MV4-11 cell line (ACC 102, DSMZ, Germany) is a human myelomonocytic leukemia line established from a 10-year-old boy with acute myeloid leukemia (AML FAB M5) at diagnosis. MV4-11 is considered a B-myeloid leukemia cell line with a hyperdiploid karyotype expressing a typical t(4;11) translocation and related expression of the fusion gene MLL-AFF1, and an FLT3 internal tandem duplication (Lange et al. 1987).

3.11.3 Packaging cell lines

The HEK-293T adherent cell line (ACC 635, DSMZ, Germany) was used for the production of lentiviral particles. HEK-293T is a highly transfectable cell line derivative of a human primary embryonal kidney cell line carrying part of the adenovirus type 5 genome including the temperature sensitive mutant of simian virus 40 large T-antigen (Ahuja, Saenz-Robles, and Pipas 2005).

The Platinum-A adherent cell line (RV-102, Cell Biolabs) is a potent retrovirus packaging cell line based on the 293T cell line and designed for rapid and transient production of high-titer amphotropic retroviruses. Platinum-A were generated using novel packaging construct with an EF1α promoter to ensure longer stability and high-yield retroviral structure protein expression (Gag., Pol., amphotropic Env.) (Morita, Kojima, and Kitamura 2000).

Platinum-GP adherent cell line (RV-103, Cell Biolabs) is a potent retrovirus packaging cell line based on the 293T cell line and designed for rapid and transient production of high-titer retroviruses. Platinum-GP were generated using a novel packaging construct with an EF1α promoter to ensure longer stability and high-yield retroviral structure protein expression (Gag., Pol.). Platinum-GP allows selecting the envelope according to the tropism needed; therefore, the viral Env gene must be co-transfected with the retroviral expression vector (Morita, Kojima, and Kitamura 2000).

3.11.4 Feeder cell line

The MS-5 adherent cell line (ACC 441, DSMZ, Germany) is a murine fibroblastic line growing in monolayers (Itoh et al. 1989). MS-5 cells were used as feeder cell layer for the maintenance in culture of PDX cells.

3.11.5 Reporter Assay cell line

The RAg-MEF cell line is a derivative of murine embryonic fibroblast (MEF) cell line expressing rtTA-M2 and the Puromicine resistance (Fellmann et al. 2011).

4. Methods

4.1 Molecular biology

4.1.1 microRNA backbone and shRNA design

To achieve an efficient knockdown, shRNAs targeting the mRNA of the gene of interest (GOI) have been embedded into the common miR-30 shRNAmir backbone (Fellmann et al. 2013), using XhoI and EcoRI as restriction enzymes. For the de novo design of potent shRNA sequences targeting all the transcript variants of the GOI (NCBI Gene, https://www.ncbi.nlm.nih.gov/gene/), the DSIR algorithm was used (Vert et al. 2006). Subsequently, the DSIR-predicted guide strands were selected according to the criteria described in Fellmann et al. 2011 (Fellmann et al. 2011). A complete list of all the 110-mer miR-30/shRNA sequences used in this study is provided in Table S1.

4.1.2 Annealing of oligonucleotides

To generate the double-stranded DNA fragments coding for the miR-30/shRNAs to be cloned into our vectors, single-stranded complementary DNA oligonucleotides were paired mixing 100 pmol for each DNA oligonucleotide in 18 µL of annealing buffer. For the annealing process with a PCR thermocycler, the following program was used:

90°C	5 min
70°C	10 min
-0.5°C	every 20 sec until 37°C
16°C	20 min
4°C	30 min

Subsequently, the successful annealing was confirmed by electrophoresis on 3% agarose gel as described in paragraph 4.1.5, and annealed oligonucleotides were stored at -20°C.

4.1.3 Polymerase chain reaction

Polymerase chain reaction (PCR) was performed to amplify the coding sequences of mCherry, eGFP, mtagBFP and $CreER^{T2}$ using a Pfu DNA Polymerase. For the PCR reaction, 100 ng of template DNA were used. The master mix contained:

5 µL 10X Pfu Buffer with $MgSO_4$
2 µL dNTP Mix
0.5 pmol forward (FW) primer (0.5 µL of a 1:10 dilution of the stock)
0.5 pmol reverse (RV) primer (0.5 µL of a 1:10 dilution of the stock)
1 µL Pfu DNA Polymerase
up to 50 µL with ddH_2O

For the amplification process with a PCR thermocycler, the following program was used:

95°C	5 min	
95°C	1 min	⎡
53°C*	1 min**	⎢ 35X cycles
72°C	1.5 min	⎣
72°C	10 min	

*The temperature was adapted to the melting temperature (T_m) of the primers used for the amplification.
**The time for the amplification was adapted to the length of the generated amplicon.

The PCR product was checked by electrophoresis on 1% agarose gel as described in paragraph 4.1.5.

4.1.4 Purification of PCR products

PCR products were purified using the NucleoSpin® Gel and PCR Clean-up kit. In short, after adjusting (when necessary) the volume of the PCR reaction mixture with distilled water to a minimum of 100 µL, 2 volumes of NTI buffer were mixed with the PCR reaction mixture and loaded into a column. After centrifugation (11000 g, 30 sec, RT), the column was washed with 700 µL of NT3 buffer (11000 g, 30 sec, RT) and the flow-through was discarded. The silica membrane of the column was dried by centrifugation (11000 g, 1 min, RT) and the residual flow-through was discarded. 25 µL of distilled water were pipetted onto the

membrane and, after incubation (1 min, RT), the DNA fragments were eluted by centrifugation (11000 g, 1 min, RT) into a clean tube. The purity and concentration of the DNA were measured using a spectrophotometer.

4.1.5 Electrophoresis of DNA on agarose gel

The separation of DNA fragments was performed by electrophoresis in a matrix of 1% agarose gel (3% in case of annealed DNA oligonucleotides). Gels contained the appropriate amount of agarose powder for a total volume of 100 mL of 1X TAE buffer and 8 µl of Midori. DNA suspensions were mixed with 1X DNA Loading Dye. Electrophoresis was performed in an electrophoresis chamber with 1X TAE buffer at 90 V. The visualization of the separated DNA fragments was performed under UV light using an agarose gel documentation system.

4.1.6 DNA extraction from agarose gel

To extract and purify the DNA from agarose gels, the NucleoSpin® Gel and PCR Clean-up kit was used. For this purpose, the agarose gel was cut with a clean scalpel around the DNA fragment of interest and the resulting gel slice was completely dissolved in 2 volumes of NTI buffer by incubation at 50°C and seldom vortexing. The mixture was loaded into a column and centrifuged (11000 g, 30 sec, RT). After discarding the flow-through, the column was washed with 700 µL of NT3 buffer (11000 g, 30 sec, RT) and the flow-through was discarded. The silica membrane of the column was dried by centrifugation (11000 g, 1 min, RT) and the residual flow-through was discarded. 25 µL of distilled water were pipetted onto the membrane and, after incubation (1 min, RT), the DNA fragments were eluted by centrifugation (11000 g, 1 min, RT) into a clean tube. The purity and concentration of the DNA were measured using a spectrophotometer.

4.1.7 Restriction digestion of DNA

For the restriction digestion process, 2 µg of plasmid DNA were mixed in distilled water with 1 µL of each restriction enzyme and 1X specific buffer. The mixture was gently mixed and incubated at 37°C for 1 hour. The efficiency of the reaction was controlled by electrophoresis

of the DNA fragments on 1% agarose gel as described in paragraph 4.1.5 and the fragments of interest were conveniently extracted from it as described in paragraph 4.1.6.

4.1.8 Competent bacteria for plasmids amplification

For long-term storage, E. coli DH5α bacteria were maintained in stocks of 50% glycerol at -80°C. To render bacteria competent (passively permeable to DNA), 1 mL out of a 6 mL overnight bacteria starter culture was amplified in 100 mL of LB medium without antibiotics up to an optical density (OD_{600}) between 0.4 and 0.5. The OD_{600} was regularly measured with a photometer and as soon as the desired OD_{600} was reached, the bacteria culture was cooled in ice. The cells were pelleted by centrifugation (4000 g, 5 min, 4°C) and resuspended in 30 mL of TFB I buffer. After incubation (5 min, in ice), bacteria were pelleted by centrifugation (4000 g, 5 min, 4°C) and resuspended in 4 mL of TFB II buffer. 50 µL aliquots of bacteria suspension were prepared in clean tubes and rapidly stored at -80°C.

4.1.9 Ligation of DNA fragments

The plasmids used in this study and described in paragraphs 3.9.2 and 3.9.3 were generated by cloning in our pCDH lentiviral backbone either the coding sequences of recombinant proteins (as PCR products or as products from restriction digestion) or the annealed oligonucleotides for shRNAs expression. For this purpose, 100 ng of restricted and purified vector were mixed in distilled water with the DNA fragment of interest at the usual 1:3 ratio. The correct amount of DNA fragment for a 1:1 ratio was calculated using the following formula:

$$\text{ng of insert (for a ratio 1:1)} = \frac{\text{Kb of insert}}{\text{Kb of plasmid DNA}} \times \text{ng of plasmid DNA}$$

In case of annealed oligonucleotides, 1 µL of annealed oligonucleotides mixture was used instead. Also, to the reaction tube were added 1 µL of T4 DNA Ligase and 1X T4 DNA Ligase buffer. For the ligation process, the reaction tube was incubated at 22°C for 2 hours in a PCR thermocycler to keep a constant temperature. Lastly, the ligation product was either directly transformed into competent bacteria as described in the next paragraph or stored at -20°C before the transformation process.

4.1.10 Heat-shock transformation of plasmid DNA into competent bacteria

50 ng of DNA from the ligation product (5 µL) were added to 50 µL of newly thawed (in ice) competent E. coli DH5α bacteria produced as described in paragraph 4.1.8, gently mixed and incubated in ice for 30 min. For the heat-shock transformation, the mixture was thereafter put at 42°C for 90 sec and then in ice for additional 2 min. Subsequently, the suspension was transferred in 400 µL of LB medium without antibiotics and incubated in shaking at 37°C for 45 min. Then, 250 µL of bacteria culture was plated onto Agar-plates containing Ampicillin for selection and incubated at 37°C overnight.

4.1.11 Colony-PCR

Single colonies were picked from the overnight incubated Agar-plates and inoculated in 2 mL of LB medium containing Ampicillin. These starter cultures were incubated and shaken for 24 hours at RT. To control the ligation process, a colony-PCR was performed on 2 µL of the starter culture. The master mix used for the PCR reaction contained:

4 µL 5X Green GoTaq® Flexi Buffer
0.4 µL dNTP Mix
0.8 pmol FW primer (0.8 µL of a 1:10 dilution of the stock)
0.8 pmol RV primer (0.8 µL of a 1:10 dilution of the stock)
0.125 µL GoTaq® G2 Flexi DNA Polymerase
up to 20 µL with ddH_2O

For the amplification process with a PCR thermocycler, the following program was used:

95°C	2 min	
95°C	1 min	⎡
52°C*	1 min**	⎢ 30X cycles
72°C	3.5 min	⎣
72°C	5 min	

*The temperature was adapted to the T_m of the primers used for the amplification.

**The time for the amplification was adapted to the length of the amplicon generated.

The colony-PCR products were checked by electrophoresis on 1% agarose gel as described in paragraph 4.1.5. The starter cultures containing the specific amplicon were amplified in 6 mL of LB medium added with Ampicillin and incubated in shaking at 37°C overnight.

4.1.12 Plasmid Mini-preparation

For a small-scale preparation of highly pure plasmid DNA, the NucleoSpin® Plasmid EasyPure kit was used. Briefly, the overnight 6 mL bacteria culture produced as described in paragraph 4.1.11 was pelleted (12000 g, 30 sec, RT) and resuspended by pipetting and vortexing in 150 µL of A1 buffer. For the cell lysis, 250 µL of A2 buffer were added, gently mixed and incubated 2 min at RT. The lysis process was blocked by adding 350 µL of A3 neutralization buffer and inverting the tube several times until the mixture had turned from blue to colorless. Then, the mixture was clarified by centrifugation (12000 g, 3 min, RT) and the supernatant was loaded into a column. After centrifugation (1800 g, 30 sec, RT), the flow-through was discarded and the column was washed with 450 µL of AQ buffer (12000 g, 1 min, RT). After discarding the flow-through, the silica membrane of the column was dried by centrifugation (12000 g, 1 min, RT) and the residual flow-through was discarded. 50 µL of distilled water were pipetted onto the membrane and, after incubation (1 min, RT), the plasmid DNA was eluted by centrifugation (12000 g, 1 min, RT) into a clean tube. The purity and concentration of the DNA were measured using a spectrophotometer.

4.1.13 Amplification of plasmid DNA by Midi-preparation

Plasmid DNA Midi-preparation was performed using the NucleoBond® Xtra Midi Plus kit according to manufacturer's instructions. In short, an overnight 100 mL bacteria culture was pelleted (5200 g, 15 min, 4°C) and resuspended by pipetting and vortexing in 8 mL of RES buffer added with RNase A. Cells were lysed adding 8 mL of LYS buffer, gently mixing by inverting the tube and incubated 5 min at RT. Then, 8 mL of NEU neutralization buffer were added and the lysate was gently mixed by inverting the tube several times until the mixture had turned from blue to colorless. The suspension was loaded into a column already equilibrated with 12 mL of EQU buffer and clarified by gravity flow. The filter of the column was washed with 5 mL of EQU buffer by gravity flow and then discarded. The column was washed by gravity flow with 8 mL of WASH buffer and the plasmid DNA was eluted with 5 mL

of ELU buffer by gravity flow into a clean tube. The eluted plasmid DNA was precipitated by adding 3.5 mL of isopropanol, vortexing thoroughly and by centrifugation (15000 g, 30 min, 4°C). After discarding the supernatant, the pellet was washed with 2 mL of 70% EtOH (15000 g, 5 min, RT). Then, the EtOH was carefully removed and the pellet was dried at RT. Finally, plasmid DNA was reconstituted in 100 µL of distilled water and the purity and concentration of the DNA were measured using a spectrophotometer.

4.1.14 Preparation and quantification of protein extracts

Cells were quantified using the Tali™ image-based cytometer and washed once in PBS, pelleted by centrifugation (400 g, 5 min, RT) and lysed by pipetting and vortexing with 1X Cell Lysis Buffer added with 1 mM PMSF (10^6 cells in 50 µL of complete lysis buffer). After incubation (10 min, in ice), cell lysates were centrifuged (12000 g, 10 min, 4°C) and the supernatant was transferred into a pre-chilled clean tube. Protein extracts were quantified using the BIO-RAD protein quantification assay based on the Bradford's method (Bradford 1976). This is a colorimetric assay set up on the absorbance shift of the dye Coomassie Brilliant Blue G-250 from 465 nm to 595 nm when the binding to proteins occurs. Thus, 5 µL of protein extract was diluted in 800 µL of distilled water and mixed with 200 µL of Protein Assay Dye Reagent Concentrate. After incubation (5 min, RT), absorbance was measured at 595 nm with a photometer.

4.1.15 Western blotting

To assess the expression level of specific genes at protein level, 20 µg of protein extract were size fractioned on 12% precast polyacrylamide gel in a mini-gel electrophoresis chamber (constant 35 mA). Then, the proteins were transferred onto a nitrocellulose membrane (0.2 µm) using the BIO-RAD Trans-Blot Turbo Transfer System. To control the quality of the transfer process, the membrane was stained with Ponceau S solution. Then, the membrane was rapidly washed twice with TBS-T to remove the residual Ponceau S solution, incubated and shaken in 5% blocking buffer (30 min, RT) and then incubated overnight in shacking (at 4°C) with the primary antibody. Then, the membrane was washed twice for 8 min with TBS-T and incubated with the horseradish-peroxidase-conjugate secondary antibody for 1 hour at RT. After other 3 washing steps of 8 min each with TBS-T, immune complexes were visualized

using a chemiluminescent reagent and exposure to X-ray films. The expression levels of the proteins of interest were normalized to loading controls and quantified relative to the control using the ImageJ software.

4.1.16 RNA isolation and purification

The quantification of GOI expression at transcription level was performed using the RNeasy Mini Kit, the QIAshredder and the RNase-Free DNase Set on the RNA isolated from cells. Target cells were quantified using the Tali^{TM} image-based cytometer and 1x10^{6} cells was pelleted by centrifugation (400 g, 5 min, RT). The supernatant was completely removed and cells were washed twice with 10 mL of PBS (400 g, 5 min, RT). Cell pellet was loosened by flicking the tube and cells were lysed by pipetting and vortexing with 600 µL of RLT buffer added with 10 µL of β-mercaptoethanol. Then, the lysate was loaded into a QIAshredder column and homogenized by centrifugation (15000 g, 2 min, RT). The flow-through was kept, mixed by pipetting thoroughly with 600 µL of 70% EtOH and loaded into an RNeasy column. After centrifugation (11000 g, 15 sec, RT), the flow-through was discarded and the column was washed with 350 µL of RW1 buffer (11000 g, 15 sec, RT). Subsequently, 80 µL of DNase solution (freshly prepared, composed by 70 µL of RDD buffer and 10 µL of DNase I) was pipetted onto the membrane of the column and, after 15 min of incubation at RT, the membrane was washed with 350 µL of RW1 buffer (11000 g, 15 sec, RT) and the flow-through was discarded. Then, the membrane was washed twice with 500 µL of RPE buffer (11000 g, 15 sec, RT and 11000 g, 2 min, RT). After discarding the flow-through, the membrane was dried by centrifugation (15000 g, 1 min, RT) and the residual flow-through was discarded. 30 µL of RNase-free water was pipetted onto the membrane and the RNA was eluted by centrifugation (11000 g, 1 min, RT) into a clean RNase-free tube. The purity and concentration of the RNA were measured using a spectrophotometer.

4.1.17 Generation of single stranded cDNA by reverse transcription

To generate single stranded cDNA from a template RNA the QuantiTect Reverse Transcription Kit was used according to the manufacturer's instructions. Briefly, a genomic DNA elimination reaction was prepared via mixing 2 µL of 7X gDNA Wipeout buffer, no more than 1 µg of template RNA and up to a total volume of 14 µL with RNase-free water. After

incubation (2 min, 42°C), the reaction was incubated in ice. The master mix used for the reverse transcription of an entire genomic DNA elimination reaction contained:

4 µL 5X Quantiscript RT buffer
1 µL RT Primer mix
1 µL Quantiscript Reverse Transcriptase
14 µL genomic DNA elimination reaction

The suspension was incubated for 15 min at 42°C, then for 3 min at 95°C and finally 80 µL of distilled water were added.

4.1.18 Quantitative real-time PCR and analysis of gene expression level

All quantitative real-time PCR (qPCR) analyses were performed using a LightCycler® 480 Instrument II, and the LightCycler® 480 96-well plates were used for the reactions. All genes to be detected were loaded in duplicates. Two controls were always performed together with each q-PCR: (1) two housekeeping genes were detected, and (2) mRNA was used instead of cDNA.

The cDNA master mix used for one reaction contained:

10 µL 2X LightCycler® 480 Probes Master
1 µL cDNA (prepared as described in paragraph 4.1.17)
up to 15 µL with H_2O PCR-grade

The Primer solution (stored at -20°C and reused several times) used for the reaction contained:

0.2 pmol FW primer (4 µL of the stock)
0.2 pmol RV primer (4 µL of the stock)
up to 100 µL with H_2O PCR-grade

The Primer-Probe mix used for one reaction contained:

1 µL Primer solution (prepared as previously described)
0.2 µL probe from the Universal ProbeLibrary Set
3.8 µL H_2O PCR-grade

The final mix for the reaction was directly loaded into the 96-well plate and contained:

15 µL cDNA master mix (prepared as previously described)

5µL Primer-Probe mix (prepared as previously described)

For the analysis of the result, the fold-change of the GOI was calculated using the following formula:

$$\%\ \text{GOI fold change} = \left(\left(\frac{\text{GOI}\ (2^{-\Delta Cp(\text{mean GOI-mean RG1})})}{\text{RG1}\ (2^{-\Delta Cp(\text{mean GOI-mean RG1})})} + \frac{\text{GOI}\ (2^{-\Delta Cp(\text{mean GOI-mean RG2})})}{\text{RG2}\ (2^{-\Delta Cp(\text{mean GOI-mean RG2})})} \right) \div 2 \right) \times 100$$

Cp = Cp value given by the software of the instrument

RG1/2 = reference gene 1/2

4.2 Cell culture

NALM-6, CCRF-CEM and MV4-11 cell lines were cultured in RPMI 1640 supplemented with 10% of FBS and 1% of L-Glu. REH and MOLM-13 cell lines were cultured in RPMI 1640 supplemented with 20% of FBS and 1% of L-Glu. HEK-293T cell line was cultured in DMEM supplemented with 10% of FBS and 1% of L-Glu. Platinum-A and Platinum-GP cell lines were cultured in DMEM supplemented with 10% of FBS, 1% of P/S and 1% of L-Glu. MS-5 cell line was cultured in alpha-MEM supplemented with 10% of FBS and 1% of L-Glu. RAg-MEF cell line was cultured in DMEM supplemented with 10% of FBS, 1% of P/S, 1% of L-Glu and 4µg/mL of puromycin. All cell lines were kept at 37°C, 5% CO_2 and saturated humidity for a maximum of 3 months.

4.2.1 Freezing and thawing of cell lines

All cell lines were frozen in cryotubes using 1 mL of FBS added with 10% of DMSO. For the thawing, the cryotubes were incubated at 37°C and then the cell suspension was transferred in 9 mL of the appropriate culture medium. After centrifugation (400 g, 5 min, RT) the pellet was resuspended in the same culture medium and transferred into clean culture flask or multi-well plate.

4.2.2 Retroviruses production for the Reporter Assay

The establishment of a stable reporter cell line was performed according to Fellmann et al. 2011. Briefly, retroviral particles carrying the reporter construct (see paragraph 3.9.1) were produced using the Platinum-A adherent packaging cell line. Packaging cells were previously plated in 10 cm^2 culture dish in 9 mL of new culture medium at a density of $10x10^6$ cells per dish and grown to 80% of confluence. Cells in one culture dish were transfected using the ProFection® Mammalian Transfection System; therefore, a DNA solution was prepared diluting 62.5 µL of 2M $CaCl_2$ solution, 10 µg of helper virus (pCMV-Gag-Pol) and 20 µg of reporter construct into sterile distilled water to a final volume of 500 µL. Subsequently, the DNA solution was dropwise-mixed while vortexing to 500 µL of 2X HBS solution and incubated for 15 min at RT. Meanwhile, 2.5 µL of 100 mM chloroquine was added to the packaging cells. At the end of the incubation time, the mixture was resuspended by pipetting and added dropwise onto the packaging cells while mixing gently. Transfected Platinum-A

cells were incubated overnight at 37°C, 5% CO_2 and saturated humidity. After the incubation, the culture medium was replaced with 10 mL of fresh medium and incubated for 2 days at 37°C, 5% CO_2 and saturated humidity. After the incubation, the supernatant was collected, filtered through a 0.45 µm syringe filter and directly applied onto the target RAg-MEF cell line.

The production of retroviral particles for the selection of potent single-copy shRNAs was performed according to Fellmann et al. 2011. Retroviral particles carrying the shRNA expressing vector (see paragraph 3.9.1) were produced using the Platinum-GP adherent packaging cell line. Packaging cells were previously plated in 6-well plates in 4 mL of new culture medium at a density of $1.5x10^6$ cells per well. Cells were transfected using the ProFection® Mammalian Transfection System; therefore, a DNA solution was prepared diluting 15.6 µL of 2M $CaCl_2$ solution, 2.5 µg of envelope vector (pCMV-Eco) and 5 µg of shRNA expressing vector into sterile distilled water to a final volume of 125 µL. Subsequently, the DNA solution was dropwise-mixed while vortexing to 125 µL of 2X HBS solution and incubated for 15 min at RT. Meanwhile, 0.8 µL of 100 mM chloroquine was added to the packaging cells. At the end of the incubation time, the mixture was resuspended by pipetting and added dropwise onto the packaging cells while mixing gently. Transfected Platinum-GP cells were incubated overnight at 37°C, 5% CO_2 and saturated humidity. After the incubation, the culture medium was replaced with 4 mL of fresh medium and incubated at 37°C, 5% CO_2 and saturated humidity. After 2 and 3 days of incubation, the viral supernatant was collected and stored at -80°C.

4.2.3 Reporter Assay for the selection of potent shRNA

The RAg-MEF reporter line (transduced as described in the previous paragraph) was enriched by cell sorting to generate a pure population. The Reporter Assay was performed according to Fellmann et al. 2011; therefore, reporter cells were previously plated in 6-well culture plate in 3 mL of appropriate culture medium at a density of $3x10^5$ cells per well. At the time of infection, the culture medium was discarded and replaced by retroviral supernatant to challenge the cells at a multiplicity of infection (MOI) not greater than 0.2 to ensure single copy integration. Cells were incubated at 37°C, 5% CO_2 and saturated humidity. After 2 days, the transfection efficiency was evaluated by flow cytometry to ensure that it was inferior to 20% and comparable between controls and experimental targets. At 6 days post infection,

the knockdown potential was determined by flow cytometry, using the following gating strategy (Figure 18):

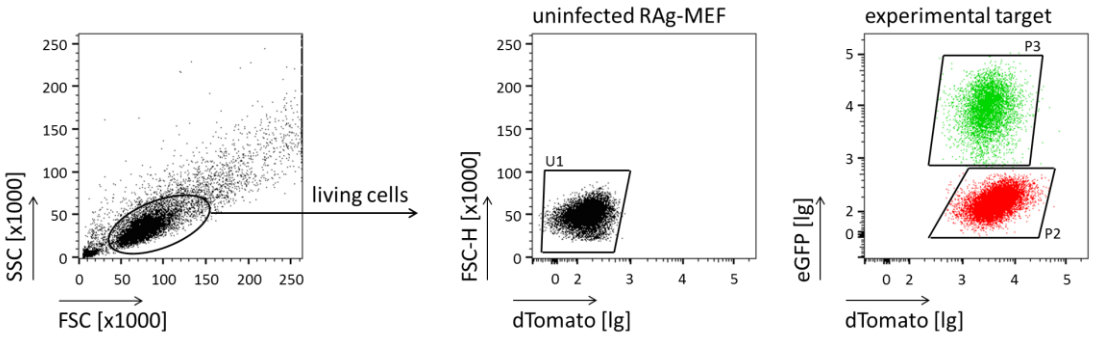

Figure 18. Gating strategy used to calculate the knockdown efficiency.
The living cells population was gated first and subsequently the positivity for dTomato and GFP were used to distinguish the cell population with the knockdown.

Finally, the knockdown efficiency was calculated using the following formula:

$$\% \text{ of knockdown} = 100 - \frac{\text{mean dTomato [P3] - mean dTomato [U1]}}{\text{mean dTomato [P2] - mean dTomato [U1]}} \times 100$$

U1 = completely uninfected RAg-MEF

P2 = RAg-MEF cells infected with the reporter construct only

P3 = RAg-MEF cells infected with both the reporter and shRNA expressing constructs

4.2.4 Lentivirus production for genetic engineering of human cells

The genetic engineering of target cells was performed via transferring transgenes carried by lentiviral vectors. Lentiviral particles were produced using the HEK-293T adherent packaging cell line and a third generation lentiviral system (Dull et al. 1998; Zufferey et al. 1998). Packaging cells were previously plated in 75 cm^2 culture flasks and grown to 80% of confluence. Cells in one culture flask were transfected using the ready-to-use lipid-based TurboFect Transfection Reagent; therefore, a DNA solution was prepared diluting in 1 mL of DMEM medium 5 µg of packaging vector encoding for Gag and Pol, 2.5 µg of packaging vector encoding for Rev, 1.25 µg of envelope vector encoding for VSV-G, 2.5 µg of the desired transfer vector and 24 µL of TurboFect Transfection Reagent. The DNA solution was incubated for 20 min at RT. The exhausted medium of HEK-293T cells was replaced by new complete DMEM medium and the DNA solution was then added dropwise onto the packaging cells while mixing gently. Transfected HEK-293T cells were incubated for 3 days at

37°C, 5% CO_2 and saturated humidity. After the incubation, the supernatant was collected and cleared from floating debris by centrifugation (400 g, 5 min, RT). Subsequently, the supernatant was filtered using a vacuum system with 0.45 µm pore filter and then concentrated by centrifugation (2000 g, 20 min, RT, twice) using Amicon Ultra-15 Centrifugal Filter Unit to a final volume of 200 to 250 µL. Aliquots of concentrated viral particles were stored at -80°C. The titer of the lentiviruses produced were determined by flow cytometry and calculated as follow:

$$\text{titer (TU / mL)} = \frac{F \times N}{V}$$

TU = transducing units

F = % of transduced cells

N = number of cells at infection

V = volume of virus suspension in mL

4.2.5 Lentiviral transduction of cell lines

Prior to transduction, the target cell line was plated in 6-well culture plate in 1 mL of new culture medium at a density of $5x10^6$ cells per mL. Cells were challenged with the lentiviruses at a MOI not inferior to 1. To enhance the transduction efficiency, polybrene was added to the culture at the final concentration of 8 µg/mL (Davis et al. 2004). Cells were incubated at 37°C, 5% CO_2 and saturated humidity. After 24 hours, transduced cells were washed twice with PBS (centrifugation at 400g, 5 min, RT) and re-cultured in new culture medium. Transgene expression was assessed by flow cytometry 5 days after the transduction.

4.2.6 Competitive proliferation assay with cell lines *in vitro*

The target cell line was transduced via two consecutive steps of infection as described in the previous paragraph. For the first round, the plasmid encoding for the fluorescent marker mtagBFP or eGFP (see Figure 15) was used to obtain two distinct populations marked with one of the two fluorescent proteins and enriched to pure population by cell sorting. The second transduction was performed with the knockdown construct (see Figure 14) expressing the miR-30 shRNAmir cassette located in the 3' UTR of the dsRED, in order to link the shRNA expression to the one of the fluorescent marker. The two transfections were

performed such that mtagBFP positive cells expressed the knockdown construct harboring control shRNAs, while eGFP positive cells expressed the knockdown construct harboring the shRNA sequence targeting XIAP. This setting allowed performing competitive proliferation assays in which both cell populations were simultaneously monitored by flow cytometry. Therefore, cell populations prepared as just described were washed once in PBS (400 g, 5 min, RT), quantified using the Tali^{TM} image-based cytometer, mixed at a 1:1 ratio and plated in 6-well culture plate in 3 mL of new culture medium at a density of $5x10^5$ cells per mL. The analyses of the population distribution were performed by flow cytometry twice a week up to 6 weeks or sorted to separate the different populations for further analyses.

4.2.7 Tamoxifen preparation for *in vitro* treatments

The 5 mM Tamoxifen stock solution was prepared by dissolving 5 mg of 4-HT in 2.5 mL of 100% EtOH and mixed by vortexing thoroughly until the solution was clear. Aliquots were stored at -80°C, protected from light, for no longer than 3 months. For the *in vitro* treatment of cells, the appropriate volume of stock solution was diluted in PBS shortly before the application on target cells.

4.2.8 Knockdown induction in cells *in vitro*

The knockdown was induced by treating cells with Tamoxifen. The target cell line was transduced via two consecutive steps of infection as earlier described in paragraph 4.2.5. For the first round, the plasmid encoding for the CreER^{T2} recombinase (see Figure 16) was used and cells were subsequently enriched to pure population by cell sorting. The second transduction was performed with the FLIP-cassette vector (see Figure 17) harboring the shRNA sequence either for a control or targeting Mcl-1. Cells were washed once in PBS (400 g, 5 min, RT), quantified using the Tali^{TM} image-based cytometer, plated in 6-well culture plate in 3 mL of new culture medium at a density of $5x10^5$ cells per mL and added with the appropriate volume of Tamoxifen. Cells were analyzed by flow cytometry at different desired time points or sorted to separate the different populations for further analyses.

4.3 Work with human material and animals

4.3.1 Ethical statements

Written informed consent was obtained from all patients and from parents/guardians. The study was performed in accordance with the ethical standards of the responsible committee on human experimentation (written approval by Ethikkommission des Klinikums der Ludwig-Maximilians-Universität, München, Ethikkommission@med.unimuenchen.de, April 15/2008, number 068-08) and with the Helsinki Declaration of 1975, as revised in 2000.

All animal trials were performed in accordance with the current ethical standards of the official committee on animal experimentation (written approval by Regierung von Oberbayern, poststelle@reg-ob.bayern.de, May 10/2007, number 55.2-1-54-2531-95-10).

4.3.2 Human material

Fresh bone marrow or peripheral blood samples from ALL and AML patients were collected for diagnostic purposes. For ALL-199, primary ALL blasts of second relapse were obtained from a child treated at the Ludwig Maximilians University Children's Hospital (Munich, Germany). ALL-265 was obtained from a child treated for relapsed ALL in Zurich according to the I-BFM study protocol and first cell-engraftment in mice was performed in Zurich (Switzerland). The AML-346 was obtained from an infant treated for relapsed AML in Tübingen (Germany). For the AML-393, primary AML blasts of relapse were obtained from an adult patient treated in Munich (Germany). The clinical data of patients donating ALL and AML cells for xenotransplantation and sample characteristics are summarized in Table S4.

4.3.3 Animals

NSG mice from The Jackson Laboratory (Lund, Sweden) were bred and maintained under specific pathogen-free conditions in the research animal facility of the Hämatologikum institute, at Helmholtz Zentrum München (Deutsches Forschungszentrum für Gesundheit und Umwelt - GmbH). Animals had free access to food and water, and were housed with a 12-hour light-dark cycle and constant temperature.

4.3.4 The individualized xenograft mouse model of acute leukemia

Primary human ALL or AML cells from heparinized peripheral blood or bone marrow aspirates of patients were amplified using the individualized xenograft mouse model as described (Kamel-Reid et al. 1989; Lee, Bachmann, and Lock 2007; Liem et al. 2004; Terziyska et al. 2012; Vick et al. 2015). Blasts were purified by density gradient centrifugation with Ficoll. Cells were washed and resuspended in PBS to a final density of $10x10^6$ cells per a total volume of 100 µl. Cells were then injected into non-irradiated 6 to 16 weeks old male or female mice via tail vein administration. Mice where sacrificed when they showed clinical signs of illness (advanced leukemia stage defined either by the quantification of human blasts in the peripheral blood or the observation of rough fur, hunchback and reduced motility). PDX cells were subsequently isolated from bone marrow or enlarged spleen. Isolated bones (vertebral column, sternum, hip bones, femurs and tibias) were kept in PBS and crushed in a porcelain mortar. The cell suspension was filtered through a 70 µm cell strainer and washed twice with PBS (centrifugation at 400g, 10 min, RT). The spleen was homogenized in PBS and filtered through a 70 µm cell strainer. Mononuclear cells were harvested from the interphase layer after density gradient centrifugation with Ficoll and washed twice with PBS (centrifugation at 400g, 10 min, RT). Cells isolated from either bones or spleen were resuspended either in PM (ALL PDX cells) or DD-Medium (AML PDX cells) and cultured at 37°C, 5% CO_2 and saturated humidity. Accuracy of sample identity was repeatedly verified by fingerprinting of Mitochondrial DNA (Hutter et al. 2004) purified using the QIAamp DNA Blood Mini Kit.

4.3.5 Generation of genetically engineered PDX (GEPDX) acute leukemia cells

For genetic engineering, PDX cells were lentivirally transduced similarly to cell lines as previously described in paragraph 4.2.5. Freshly isolated PDX cells were plated in 6-well culture plate in 1 mL of PM (ALL PDX cells) or DD-Medium (AML PDX cells) at a density of $10x10^6$ cells per mL. Cells were challenged with lentiviruses at a MOI not inferior to 1. To enhance the transduction efficiency, polybrene was added to the culture at the final concentration of 8 µg/mL (Davis et al. 2004). Cells were incubated at 37°C, 5% CO_2 and saturated humidity. After 24 hours of incubation, transduced PDX cells were washed twice with PBS (centrifugation at 300g, 5 min, RT) and co-cultured on previously irradiated MS-5 feeder cells in 3 mL of appropriate culture medium at a density of $5x10^6$ cells per well. Transgene expression was assessed by flow cytometry and positively transduced GEPDX cells

were enriched by cell sorting 5 days after the transduction. Shortly after the enrichment process, GEPDX cells were counted, conveniently resuspended in 100 µL of filtered PBS and injected into NSG mice via tail vein administration.

The MS-5 cell line was used as feeder cells layer for the maintenance in culture of transduced PDX cells for few days; therefore, MS-5 cells were plated in 6-well culture plate in 3 mL of new culture medium at a density of $3x10^5$ cells per well. The day after, feeder cells were γ-irradiated with 70 Gy using a 137-cesium source, washed twice with PBS and directly used for the co-culture.

4.3.6 Freezing and thawing of GEPDX cells

All GEPDX cells were frozen in cryotubes at a density between $10x10^6$ and $50x10^6$ viable cells per mL using 1 mL of FBS added with 10% of DMSO. For the thawing, the cryotubes were incubated at 37°C, then the cell suspension was transferred in 9 mL of PM (ALL PDX cells) or DD-Medium (AML PDX cells) and pelleted by centrifugation (300 g, 5 min, RT). For the re-passaging in NSG mice, the pellet was resuspended in 100 µL of filtered PBS and injected shortly after thawing into mice via tail vein administration. Prior *in vivo* experiments, the pellet was resuspended in the appropriate culture medium to a density of $5x10^6$ viable cells per mL, transferred into clean multi-well plates and kept overnight at 37°C, 5% CO_2 and saturated humidity. Right before the injection into NSG mice, viable cells were counted and conveniently resuspended in 100 µL of filtered PBS.

4.3.7 Competitive proliferation assay with cell lines and GEPDX cells *in vivo*

The PDX samples were transduced as described in paragraph 4.3.5 via two consecutive steps of transfection similarly to cell lines. For the first round, the plasmid encoding either for the fluorescent marker mtagBFP or eGFP (see Figure 15) was used. The second transduction was performed with the knockdown construct (see Figure 14). The two transfections were performed such that mtagBFP positive cells expressed the knockdown construct harboring a control shRNA sequence, while eGFP positive cells expressed the knockdown construct harboring the shRNA sequence targeting XIAP. This setting allowed performing competitive proliferation assays in which both cell populations were expanded in the same living mouse and monitored by post mortem flow cytometry analysis. Cell lines produced as described in

paragraph 4.2.6 were also used to perform competitive proliferation assays *in vivo*. Cells were mixed at a 1:1 ratio for a total amount of 10^5 transduced NALM-6 cells, $3x10^5$ of ALL-199 or ALL-265 GEPDX cells and injected into the tail vain of NSG mice. At different desired time points, cells were isolated from bone marrow and freshly analyzed by flow cytometry or sorted to separate the two populations for further analyses.

4.3.8 Tamoxifen preparation for *in vivo* treatment of mice

For the treatment of mice with Tamoxifen, aliquots were prepared by dissolving 10 mg of 4-OHT in 100 µL of filtered EtOH 100% and 900 µL of filtered corn oil. Subsequently, the suspension was warmed up at 55°C protected from light and frequently mixed by vortexing until the Tamoxifen crystals were completely dissolved. Tamoxifen solutions were stored at -20°C up to 2 weeks and warmed up at 37°C protected from light shortly before administration.

4.3.9 Knockdown induction in GEPDX cells *in vivo*

The PDX samples were transduced as described in paragraph 4.3.5 via two consecutive steps of infection similarly to the cell lines. For the first round, the plasmid encoding for the $CreER^{T2}$ recombinase (see Figure 16) was used and cells were subsequently enriched to pure population by cell sorting. The second transduction was performed with the FLIP-cassette vector (see Figure 17) and then cells were enriched to pure population by cell sorting. A total amount of $3x10^5$ of GEPDX cells were injected into the tail vain of NSG mice. After either 7 days post injection or when more than 15% of human blasts could be detected in the peripheral blood, mice were treated once with 50 mg/kg of Tamoxifen by oral gavage. At the desired time of analysis, cells were isolated from bone marrow and freshly analyzed by flow cytometry or sorted to separate the different populations for further analyses.

4.4 Flow Cytometry

All flow cytometry analyses were performed using a BD LSRFortessa (BD Bioscience). All data produced by flow cytometry were analyzed with FlowJo V10 CL software. All enrichment processes of specific cell populations were performed by Fluorescence-activated cell sorting (FACS) using a BD LSRAriaIII (BD Bioscience). Fluorescent proteins (dsRED, eGFP, mCherry, mtagBFP) were measured using the lasers and filter settings as indicated in Table S5. Transduced cell lines and GEPDX cells populations were considered pure when the expression of the fluorescent protein was greater than 95%.

4.5 Statistical analysis

All statistical analyses were performed using GraphPad Prism 6 software. The measurements are given as mean values with error bars representing the standard error of mean (SEM) of biologically independent replicates (*in vitro* assays) or of all mice analyzed at the indicated time point (*in vivo* assays), unless otherwise indicated. *P* values were calculated using a two-tailed unpaired t test and considered significant when $p < 0,05$.

5. Results

An enormous therapeutic potential relies on the ability to manipulate the fate of a cell. The apoptosis machinery provides core targets which could be more intensively investigated in order to enhance the chance to design valid therapies. Despite the cutting edge technologies already available, further optimization and generation of new tools are indeed required to extend the accuracy of the current knowledge, to develop new therapeutic options and ultimately get closer to the patients' condition. In this regard, the aim of this thesis was to establish innovative constitutive and inducible technologies for knockdown in the individualized preclinical PDX mouse model of acute leukemia.

5.1 Constitutive-knockdown System

Although all the current techniques have greatly improved the level of the research, the technical approaches are unfortunately as yet more focus on the identification of essential alterations rather than the evaluation of the function of potential targets. Therefore, new tools for the precise assessment of specific proteins are intensively required. Here, we aimed at the design and establishment of a novel technique in the PDX *in vivo* model of acute leukemia to prove whether an existing alteration (XIAP overexpression) harbors a targetable function and thus represent a putative therapeutic target.

5.1.1 Expression levels of XIAP in ALL cell lines and PDX samples

High expression of XIAP in cancer cells and its association with aggressiveness and chemoresistance has been demonstrated in a wide variety of human tumors (Schimmer et al. 2006). More recent studies have shown that the inhibition of XIAP sensitized certain solid tumors to conventional chemotherapy (Ehrenschwender et al. 2014; Hu et al. 2003). Nevertheless, its precise role in ALL remains unclear. Therefore, we decided to study XIAP in ALL cell lines and PDX cells. Since high XIAP expression levels have been reported for many different hematological malignancies, we screened XIAP expression levels in three ALL cell lines and two PDX samples. In accordance to published data, we also observed high XIAP expression in our ALL cell lines and PDX samples, conversely to peripheral blood mononuclear cells (PBMCs) from two healthy donors (Figure 19).

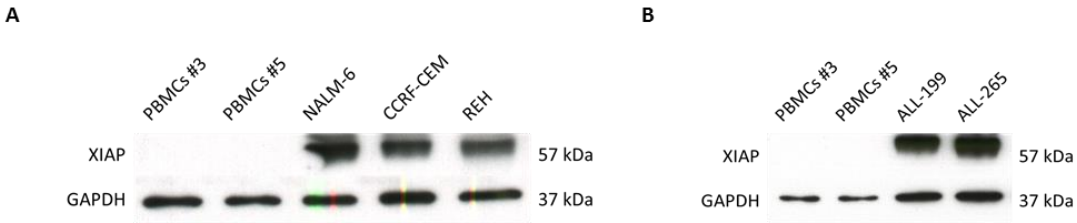

Figure 19. Evaluation of XIAP protein expression level by Western blotting.
(A) Western blotting of XIAP in three established ALL cell lines used in this study in comparison to PBMCs from two healthy donors. GAPDH levels are shown as loading control.
(B) Same as in (A). Two ALL PDX samples used in this study in comparison to PBMCs from two healthy donors were used.

5.1.2 Selection of shRNA sequences targeting XIAP

The first aim was to achieve a strong and stable knockdown of XIAP in ALL cells. As ALL cells are difficult to transfect and it is not easy to obtain stable genomic integration, we decided using lentiviral transduction. In order to elucidate the role of XIAP in ALL cell lines and PDX samples, my colleague Michela Carlet developed a cloning strategy to silence XIAP using shRNA sequences embedded into the miR-30 backbone. To appreciate at a deeper level the importance of specific genes, it is central to use shRNAs able to induce a specific, potent and stable knockdown of the desired target. As described in paragraph 2.3.1.3 of the introduction, the embedment of synthetic shRNA sequences into the context of the miR-30 backbone confers the advantage of triggering potent knockdown of specific targets via entering the natural miRNA biogenesis. The main advantages of this technology are the expression of the shRNAs from pol-II promoters, the possibility to direct monitor the expression of the shRNAs via placing the miR-30 backbone in the 3' UTR of a marker and their limited cell toxicity for not saturating the endogenous RNAi machinery. Therefore, we needed to select suitable 22-mer sequences to be embedded into the miR-30 backbone. For the selection of the shRNA sequences targeting XIAP, we exploited the advantages of the high-throughput assay published by Fellmann et al. in 2011 (Fellmann et al. 2011). The reporter construct (see Figure 12) used for the production of the RAg-MEF reporter cell line (see paragraph 3.11.5) presents the coding sequence for the dTomato fluorescent marker and an array of shRNA target sequences artificially placed in its 3' UTR. Therefore, the transcript derived from the expression of the reporter construct is an mRNA that encodes for the fluorescent protein, but also presents in its 3' UTR region the target sequences of the mRNAs to be tested, and consequently becomes the target of specific desired shRNAs. In our case, the array of shRNA target sequences consisted of control target sequences (for shRNAs

of known knockdown potency), plus seven experimental target sequences originated from the XIAP mRNAs, and designed as complemental sequences of the best 22-mer shRNA sequences generated as described in paragraph 4.1.1 (see Table S1 for all the shRNA sequences targeting XIAP tested and those used as control). The shRNA to be tested was provided with the shRNA expressing vector (see Figure 13) after a second round of transduction of the reporter cell line generated as just described. The artificial presence of shRNA target sequences in the 3' UTR of the dTomato mRNA ensured a direct link between the expression of the fluorescent marker and the strength of knockdown given by the specific shRNA tested, and thus the possibility to monitor and quantify the knockdown via assessing the shift of the dTomato intensity by flow cytometry: strong shRNAs gave a dramatic reduction of dTomato fluorescence; conversely, weak shRNAs induced only a moderate or slight reduction of dTomato intensity. Moreover, the expression of the shRNAs from a single genomic locus ("single copy"), via keeping the transduction efficiency with the shRNA expressing vector below 20%, allowed to quantify and compare the knockdown strength of single shRNAs (Figure 20A – C). Among the seven tested shRNAs targeting XIAP, two potent and one weak shRNAs were selected and each cloned into a lentiviral vector (see Figure 14) for further studies. The different knockdown potency of the three selected shRNAs was re-evaluated by western blotting (Figure 20D), quantified and compared to the results of the Reporter Assay to confirm its accuracy (Figure 20E). Additionally, we observed that the strength of the knockdown given by the best shRNA (sh-XIAP.1) was able to revert almost completely the highly expressed XIAP protein in leukemia cells down to the physiological level of normal PBMCs. Taken together, we could identify and validate strong knockdown of XIAP in ALL cells using lentiviral transduction and expression of suitable shRNA sequences in the miR-30 backbone.

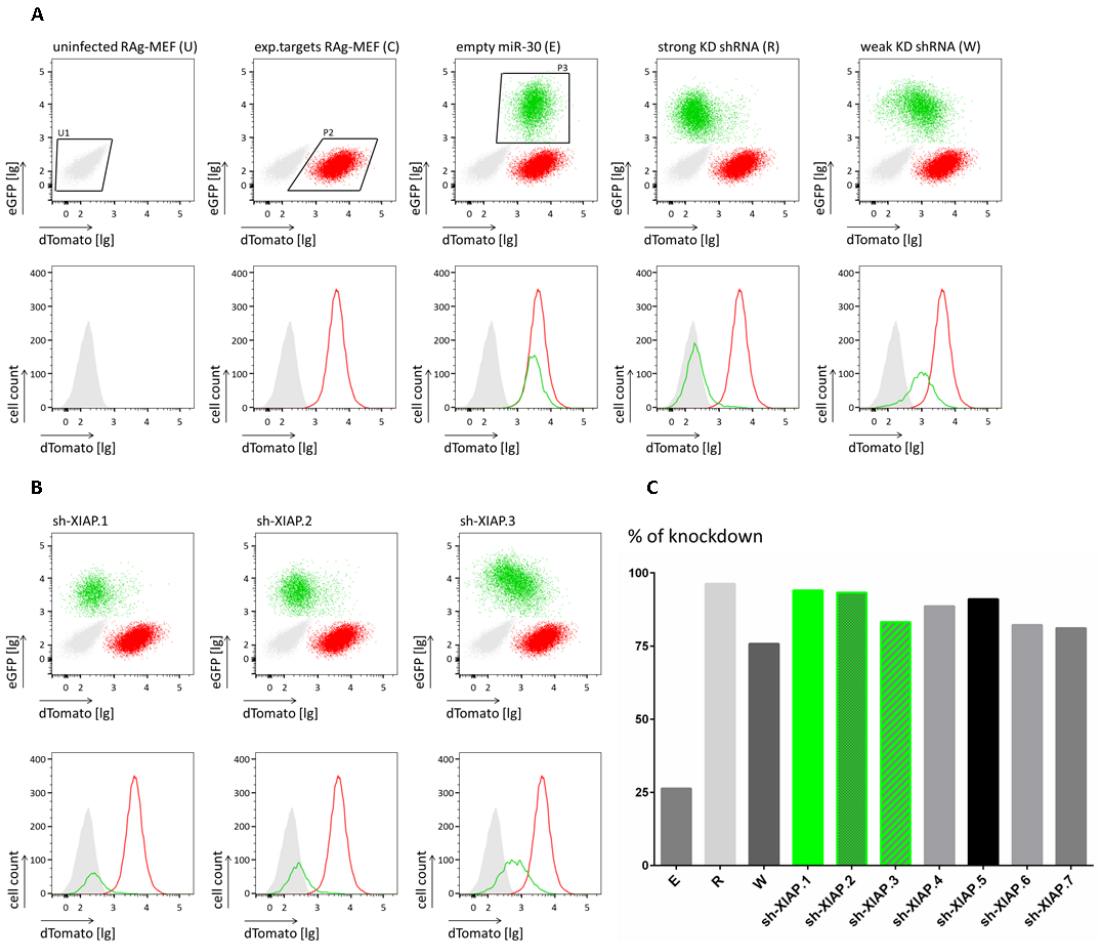

D

E

	% of knockdown	
	Reporter Assay (C)	Western blotting (D)
sh-XIAP.1	94,00	99
sh-XIAP.2	93,31	95
sh-XIAP.3	83,24	67

Figure 20. Reporter Assay for the selection of shRNA sequences targeting XIAP.

(A) Flow cytometry based analysis of the reporter cell lines used for the assay. The graphs show dot plots and histograms of the same populations, and the gating strategy used for the quantification of the knockdown (see paragraph 4.2.3). Here, the dot plots of the controls (U, C, E, R, W) are shown. The mean fluorescent intensity (MFI) of the dTomato of the U and C populations are used to define respectively the minimal and maximal dTomato MFI values of the range of MFI shift knockdown-dependent. E is used to define the dTomato MFI shift using an empty miR-30 backbone. R and W are used as controls of strong and weak knockdown potency respectively. dTomato levels were quantified by flow cytometry 6 days after infection with the shRNA expressing vector.

(B) Same as in (A). The dot plots and histograms of the three selected shRNA sequences targeting XIAP (sh-XIAP.1, sh-XIAP.2, sh-XIAP.3) are shown.

(C) Final readout of the relative reporter knockdown calculated for the shRNA sequences targeting XIAP in comparison to the three included controls (E, R, W) shown in (A). The percentage of knockdown showed here directly correlates with the dTomato MFI shift knockdown-dependent.

(D) Western blotting of XIAP in NALM-6 cells expressing each of the three selected shRNA sequences targeting XIAP (sh-XIAP.1, sh-XIAP.2, sh-XIAP.3) in comparison to NALM-6 cells expressing an

unspecific shRNA sequence used as control (sh-CTRL). XIAP signal intensity was normalized to GAPDH used as loading control, and the knockdown levels (%KD) were quantified relative to the control.
(E) Side-by-side comparison of quantified knockdown potencies of sh-XIAP.1, sh-XIAP.2 and sh-XIAP.3 determined using the Reporter Assay (C) or western blotting (D).

5.1.3 Design of a system for a constitutive knockdown in competitive assays

To enhance the sensitivity of our experiments, we decided to use a competitive setting. Towards this aim, published approaches expressed the miR-30 cassette containing the shRNA sequence in the 3' UTR of different fluorochromes in order to distinguish the different populations (Fellmann et al. 2011). However, the major disadvantage of this tactic is that the equal expression of the knockdown cassettes cannot be evaluated as two different fluorochromes cannot be compared. To overcome this obstacle, we decided to express each shRNA sequence in the 3' UTR of the dsRED fluorescent marker so that their equal expression was measured via assessing the equal expression of the fluorochrome by flow cytometry (see Figure 14). Each lentiviral vector expressing the shRNA sequence was co-transduced with a second lentiviral vector expressing a different fluorescent protein, either mtagBFP or eGFP (see Figure 15). Thus, the dsRED expression indicated the presence of the miR-30 shRNAmir cassette, while the mtagBFP or eGFP expressions were used to distinguish the different cell populations. Cells were generated within two transduction steps as described in paragraph 4.2.6. First, they were molecularly marked to express one of the two different fluorochromes mtagBFP or eGFP for an easy visualization and discrimination of the two populations by flow cytometry even when simultaneously analyzed. The second round of transduction was performed with the lentiviral constructs expressing either the sh-CTRL or the sh-XIAP in the 3' UTR of dsRED, in either mtagBFP or eGFP expressing cells, respectively. After each step of transduction, cells were enriched by cell sorting to have pure populations constitutively expressing the two constructs of the system. This setting allowed competitive assays in which both cell populations were mixed at a 1:1 ratio before been plated *in vitro* or injected in NSG mice and monitored by flow cytometry at the desired time points (Figure 21). Additionally, to achieve a good expression of the shRNAs in the target cells, we used either the viral SFFV promoter or the eukaryotic EF1α promoter.

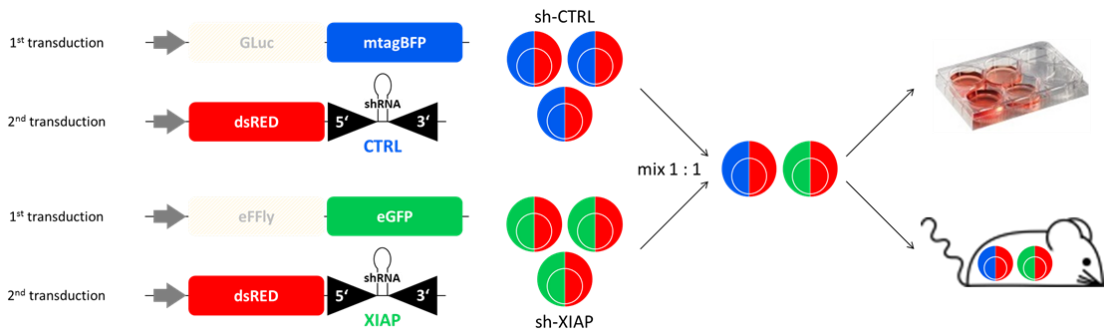

Figure 21. Schemes of the constitutive-knockdown system and experimental settings.
From the left, a scheme of the four plasmids used for the generation of the different cell populations is shown. Vectors harboring the fluorochrome (mtagBFP or eGFP) were transduced first in order to generate cell populations that can be easily distinct by flow cytometry. Subsequently, the constructs expressing the sh-CTRL or the sh-XIAP were transduced either in the blue or green populations respectively. On the right, the scheme of the setting used to perform the experiments: the two cell populations produced as described were mixed at a 1:1 ratio to perform competitive experiments either *in vitro* or *in vivo*.

As all shRNA expressing cells are positive for the expression of the dsRED marker, transduced human cells could be easily distinguished also when the experiments were performed *in vivo*. The other two fluorescent markers allowed visualizing the two subpopulations, and therefore also to precisely quantify the relative changes of the phenotypic behavior of the target population in direct comparison with the control one (Figure 22).

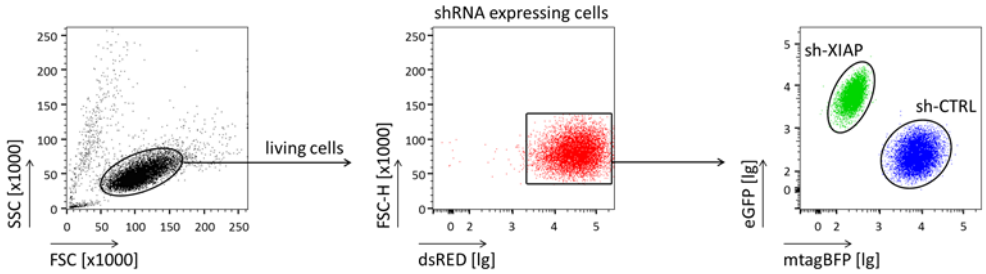

Figure 22. Gating strategy for the analysis of the competitive experiments.
Representative dot plots of the steps of the flow cytometry based analysis used for the quantification of the sh-CTRL and the sh-XIAP populations' distribution. Here, NALM-6 cell line is shown.

5.1.4 Validation of the constitutive-knockdown system

As previously mentioned, the shRNA sequences were expressed in the background of the miR-30 backbone as a single transcript together with the dsRED fluorescent marker. As quality control to make sure that the RNAi pathway could be equally activated among control and target population, for both established cell lines and GEPDX cells transduced with the constitutive-knockdown system, the fluorescence intensity of dsRED protein was compared and confirmed to be equal between the two populations right before the enrichment by cell sorting (Figure 23). If the expression of dsRED was uneven, only the case in which its expression was higher in the control (blue) than in the target (green) population was tolerated, as for example in ALL-265 GEPDX of Figure 23D.

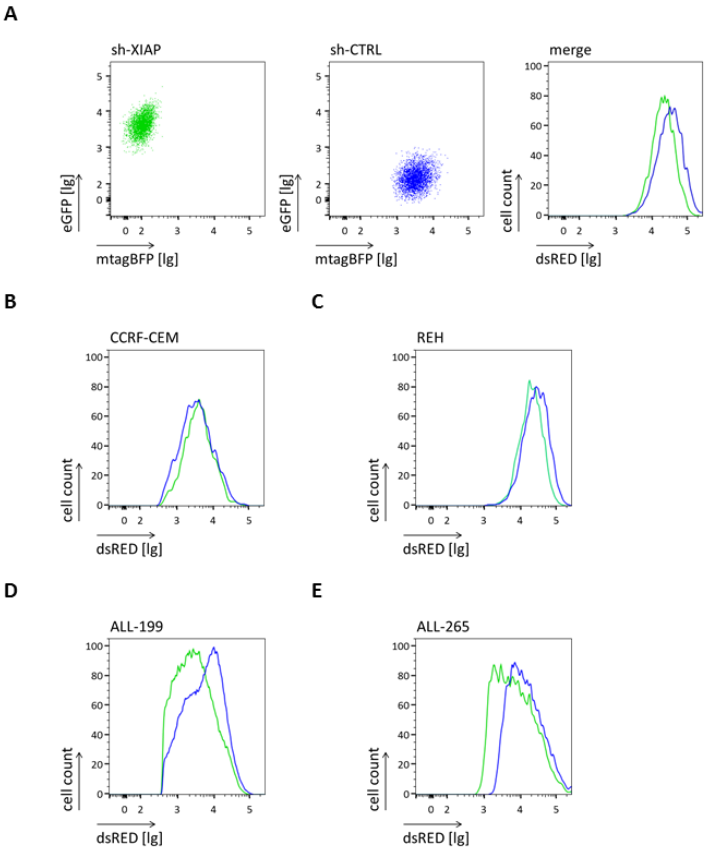

Figure 23. Control of equal dsRED fluorescence intensity in ALL cell lines and GEPDX cells.
(A) Representative dot plots and histograms for the comparison of the dsRED expression. shRNA sequences were expressed in the background of the miR-30 backbone as a single transcript together with the dsRED fluorescent marker. For either established cell lines or GEPDX cells transduced with the constitutive-knockdown system, the intensity of dsRED expression was compared among the sh-CTRL and the sh-XIAP populations (merge) to confirm the equal expression of the corresponding associated shRNA sequence. Here, NALM-6 cell line is shown.
(B – C) Same histograms as in (A). CCRF-CEM (B) and REH (C) cell lines are shown.
(D – E) Same histograms as in (A). ALL-199 (D) and ALL-265 (E) GEPDX cells are shown.

Another important control was to verify that the artificial expression of transgenes and the activation of the RNAi machinery were not affecting the spontaneous behavior of the cells. NALM-6 cells produced after one round of transduction only with the first vector of the competitive system were mixed at a 1:1 ratio and monitored over time by flow cytometry as previously described. Among the total population, 50% of cells belonged to the mtagBFP expressing population and 50% to the eGFP expressing population. This initial proportion did not change until the end of the experiment, confirming that the mere expression of different fluorescent markers did not affect cell proliferation (Figure 24A). The same experiment was performed with NALM-6 cells transduced also with the second construct of the constitutive-knockdown system, and therefore expressing shRNAs. In this case, the same control shRNA sequence (see Table S1) was used to verify that the activation of the RNAi pathway too was not affecting the spontaneous proliferation of the cells. Also in this case, the relative distribution of the two populations remained quite equal until the end of the experiment (Figure 24B). The length of the experiment performed *in vitro* was decided to be of six weeks in order to more precisely compare the results between cell lines and PDX cells expanding in mice.

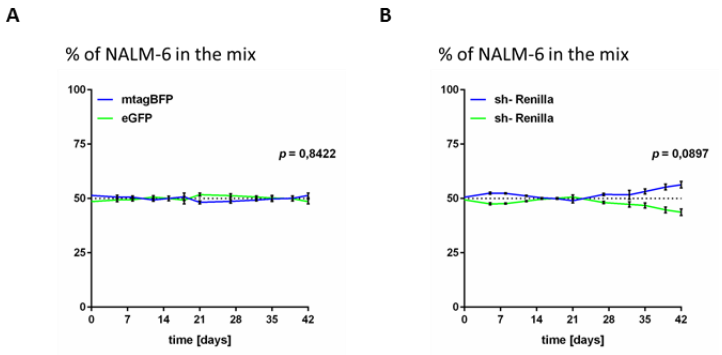

Figure 24. Artificial expression of transgenes and shRNA sequences do not affect the proliferation of NALM-6 cell line *in vitro*.
(A and B) Competitive assay *in vitro* performed to verify the absence of alterations in spontaneous cell proliferation due to the expression of artificial fluorescent markers (A) and on the activation of the RNAi pathway (B). NALM-6 cells transduced either with the first vectors only (A) or both constructs (B) of the constitutive-knockdown system were mixed at a 1:1 ratio and monitored by flow cytometry twice a week up to 6 weeks. Quantification of the sh-CTRL and the sh-XIAP populations' distribution was performed as shown in Figure 22. Error bars represent SEM of biologically independent triplicates.

Thus, the designed competitive system for the constitutive knockdown of specific targets has been validated: our molecular system did not alter the proliferative behavior of cell lines *in vitro*. Additionally, the experimental variance between the control and the target population was minimized and the precision of the readout was maximized, as both shRNAs were expressed in the identical context.

5.1.5 XIAP is essential for the proliferation of ALL cell lines

To investigate the role of XIAP in ALL cells, we performed competitive assays in ALL cell lines *in vitro* expressing the constitutive-knockdown system. NALM-6 cells transduced as previously described were mixed at a 1:1 ratio and analyzed over time by flow cytometry. These cells were analyzed for the XIAP expression both at mRNA (Figure 25B) and protein (Figure 25C) level, to confirm the presence of the knockdown until the end of the experiment. Thus, we could show that XIAP knockdown is very stable, proving the strength of our system. The initially equal relative distribution of the two populations progressively changed and the cells harboring the more potent shRNA targeting XIAP (selected with the Reporter Assay) (sh-XIAP.1) showed a proliferative disadvantage, becoming over time statistically significantly less abundant than the control cells (Figure 25A). For the first time, this experiment showed that XIAP is essential for the proliferation of NALM-6 cell line *in vitro*.

cIAP1 and cIAP2 are two IAP family members that belong to the same class of proteins than XIAP. To exclude their counter regulation as consequence of XIAP knockdown, we assessed the protein level of these other two cell-death mediators in the two populations of NALM-6. The shRNA reduced XIAP level while cIAP1 and cIAP2 remained unchanged (Figure 25D).

To confirm the observation that XIAP knockdown induces a proliferation disadvantage in NALM-6 cell line, we performed the same competitive assay with cells expressing the second strong shRNA sequence targeting XIAP (sh-XIAP.2) (Figure 25E). Also in this case, we could show the change over time of the relative proportion of the two populations in favor of the control one, upon the presence of a stable XIAP knockdown (Figure 25F).

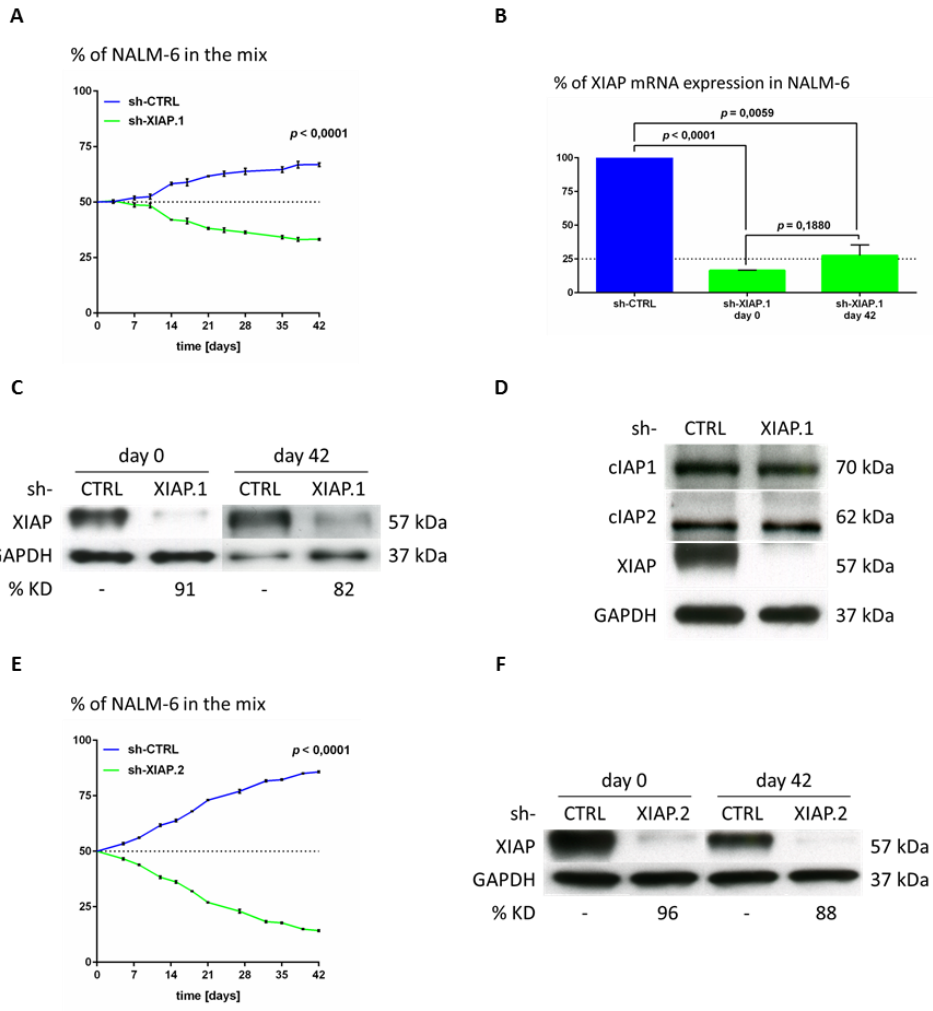

Figure 25. XIAP knockdown impairs the proliferation of ALL NALM-6 cell line *in vitro*.

(A) Competitive assay *in vitro* evaluating the cell populations' distribution of NALM-6 cells expressing the sh-XIAP.1 in comparison to NALM-6 cells expressing the sh-CTRL. NALM-6 cells transduced with the constitutive-knockdown system were mixed at a 1:1 ratio and monitored by flow cytometry twice a week up to 6 weeks. Quantification of the sh-CTRL and the sh-XIAP populations' distribution was performed as shown in Figure 22. Error bars represent SEM of biologically independent triplicates.

(B) qPCR of XIAP mRNA expression levels in NALM-6 cells expressing the sh-XIAP.1 in comparison to NALM-6 cells expressing the sh-CTRL. XIAP levels were detected at the beginning (day 0) and at the end (day 42) of the experiment shown in (A) and relative to HMBS and HPRT1 mRNAs expression levels used as reference genes. Error bars represent SEM of biologically independent triplicates.

(C) Western blotting of XIAP in NALM-6 cells expressing the sh-XIAP.1 in comparison to NALM-6 cells expressing the sh-CTRL. XIAP levels were detected at the beginning (day 0) and at the end (day 42) of the experiment shown in (A) and normalized to GAPDH used as loading control. The XIAP knockdown levels (%KD) were quantified relative to the control.

(D) Western blotting of XIAP, cIAP1 and cIAP2 in NALM-6 cells expressing the sh-XIAP.1 in comparison to NALM-6 cells expressing the sh-CTRL. XIAP, cIAP1 and cIAP2 levels were detected 1 week after infection. GAPDH levels are shown as loading control.

(E) Same as in (A). NALM-6 cells expressing the second selected shRNA sequence targeting XIAP (sh-XIAP.2) in comparison to NALM-6 cells expressing the sh-CTRL are shown.

(F) Same as in (C). NALM-6 cells expressing the sh-XIAP.2 in comparison to NALM-6 cells expressing the sh-CTRL were used.

To further validate our observation, we extended the study to REH and CCRF-CEM cell lines (Figure 26). Both experiments confirmed our hypothesis that XIAP is essential for the proliferation of ALL cells *in vitro*.

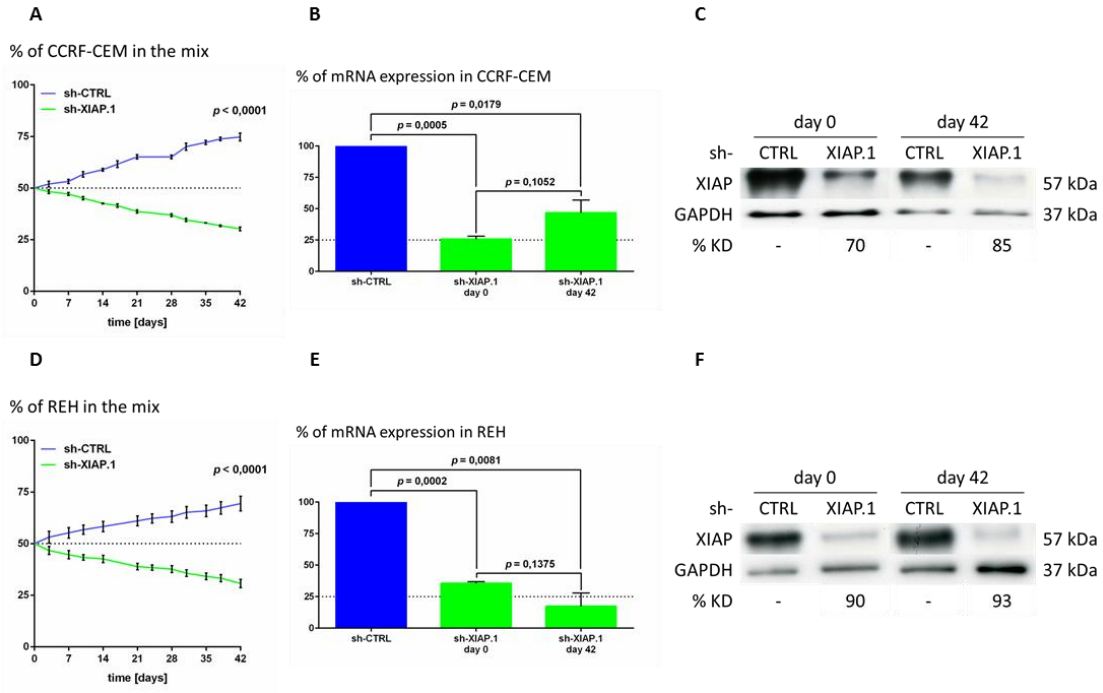

Figure 26. XIAP knockdown impairs the proliferation of ALL cell lines CCRF-CEM and REH *in vitro*.
(A) Competitive assay *in vitro* evaluating the cell populations' distribution of CCRF-CEM cells expressing the sh-XIAP.1 compared with CCRF-CEM cells expressing the sh-CTRL. CCRF-CEM cells transduced with the constitutive-knockdown system were mixed at a 1:1 ratio and monitored by flow cytometry twice a week up to 6 weeks. Quantification of the sh-CTRL and the sh-XIAP populations' distribution was performed as shown in Figure 22. Error bars represent SEM of biologically independent triplicates.
(B) qPCR of XIAP mRNA expression levels in CCRF-CEM cells expressing the sh-XIAP.1 in comparison to CCRF-CEM cells expressing the sh-CTRL. XIAP levels were detected at the beginning (day 0) and at the end (day 42) of the experiment shown in (A) and relative to HMBS and HPRT1 mRNAs expression levels used as reference genes. Error bars represent SEM of biologically independent triplicates.
(C) Western blotting of XIAP in CCRF-CEM cells expressing the sh-XIAP.1 compared with CCRF-CEM cells expressing the sh-CTRL. XIAP levels were detected at the beginning (day 0) and at the end (day 42) of the experiment shown in (A) and normalized to GAPDH used as loading control. The XIAP knockdown levels (%KD) were quantified relative to the control.
(D – F) Same as in (A – C). REH cells were used.

As next step, we evaluated the influence of the *in vivo* environment on cell proliferation. Therefore, NALM-6 cells transduced as previously described were mixed at a 1:1 ratio and injected into NSG mice to perform an *in vivo* competitive assay. NALM-6 cells could engraft in mice and expand to generate full blown mice. At 46 days post injection, mice were

sacrificed and the cells isolated from the bone marrow were analyzed. Indeed, we could observe the unbalanced distribution between the control population and the one expressing the sh-XIAP.1 (Figure 27A). Moreover, cells were tested for XIAP expression level both before injection and after isolation from the mice, revealing a strong and stable knockdown (Figure 27B). This trial showed that the living environment provided by the mouse bone marrow does not alter the phenotypic behavior of cells or the stability of the knockdown, and confirmed the possibility to simultaneously monitor the two different cell populations also when isolated from the bone marrow of the same mouse.

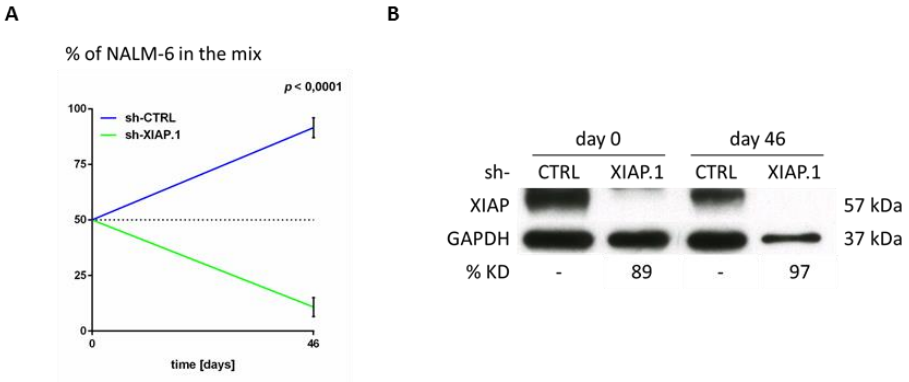

Figure 27. XIAP knockdown impairs the expansion of ALL cell line NALM-6 in mice.
(A) Competitive assay *in vivo* evaluating the cell populations' distribution of NALM-6 cells expressing the sh-XIAP.1 in comparison to NALM-6 cells expressing the sh-CTRL. NALM-6 cells transduced with the constitutive-knockdown system were mixed at a 1:1 ratio and injected into NSG mice (n = 8). At first clinical signs of disease, mice were sacrificed and cells were isolated from bone marrow. The relative proportion of the sh-CTRL and the sh-XIAP populations was quantified by flow cytometry as shown in Figure 22. Error bars represent SEM of all mice analyzed at the indicated time point.
(B) Western blotting of XIAP in NALM-6 cells expressing the sh-XIAP.1 in comparison to NALM-6 cells expressing the sh-CTRL. XIAP levels were detected at the time of injection into mice (day 0) and at the time of isolation (day 46) after the separation of the two populations by cell sorting. The XIAP expression levels were normalized to GAPDH used as loading control. The XIAP knockdown levels (%KD) were quantified relative to the control.

5.1.6 Relationship between knockdown strength and knockdown effects

To investigate whether a dose-relationship exists between knockdown strength and reduction of cell proliferation, we both extended our *in silico* analysis and performed further experiments using either a weak shRNA sequence targeting XIAP or a weak promoter.

First, we examined the cells with high expression of dsRED separately from those with low expression of dsRED in the flow cytometry analysis. In detail, the population of human

shRNA expressing cells was divided to have 50% of the cells in the “low dsRED” gate and the other 50% in the “high dsRED” gate. Since the expression of the dsRED fluorescent marker and the shRNA are linked together, we hypothesized that cells in the “high dsRED” gate should express more protein and therefore also more shRNA targeting XIAP leading to a stronger knockdown; conversely, cells in the “low dsRED” gate should express less protein and also less shRNA. The two resulting subpopulations were analyzed consistently as previously described (Figure 28A). As expected, the flow cytometry analysis of the three ALL cell lines tested (from Figure 25A, Figure 26A and Figure 26D) showed a significantly decreased frequency of the population expressing the shRNA targeting XIAP in the “high dsRED” gate in comparison with the “low dsRED” gate, confirming a dose-response relationship between the shRNA expression and proliferation disadvantage (Figure 28B-D).

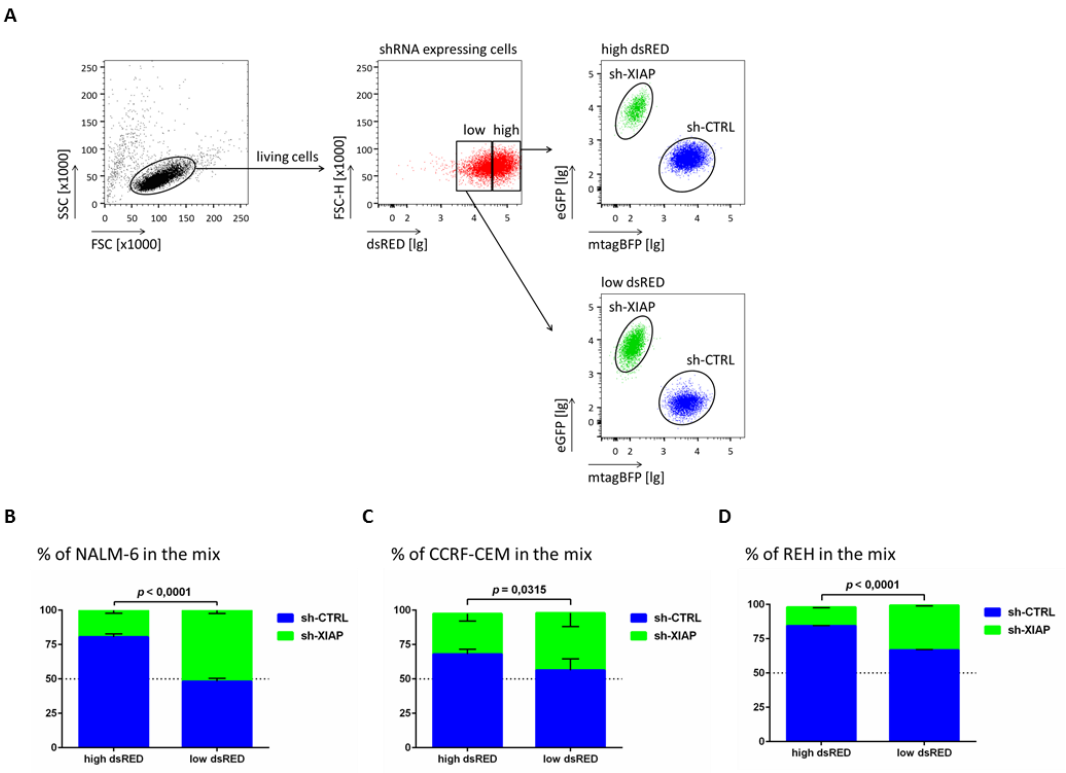

Figure 28. Dose-response relationship between strength of XIAP knockdown and proliferation disadvantage in cell lines *in vitro*.

(A) Representative dot plots of the steps of the flow cytometry based analysis used for the quantification of the dose-response relationship between strength of XIAP knockdown and populations’ distribution. Here, NALM-6 cell line from (B) is shown.

(B) Comparison between the XIAP knockdown effects in NALM-6 cells from Figure 25A at the end (day 42) of the experiments and analyzed as shown in (A). Error bars represent SEM of biologically independent triplicates.

(C – D) Same as in (B). CCRF-CEM cells from Figure 26A (C) and REH cells from Figure 26D (D) are shown.

To further investigate the correlation between the knockdown potency and the effects on proliferation at a biological level, we repeated the competitive experiments using a weak shRNA sequence targeting XIAP (sh-XIAP.3). The experiments performed with the three ALL cell lines tested demonstrated that a partial knockdown of about 70% is not sufficient to reduce cell proliferation, most probably because the remaining amount of XIAP protein is sufficient to maintain its function (Figure 29).

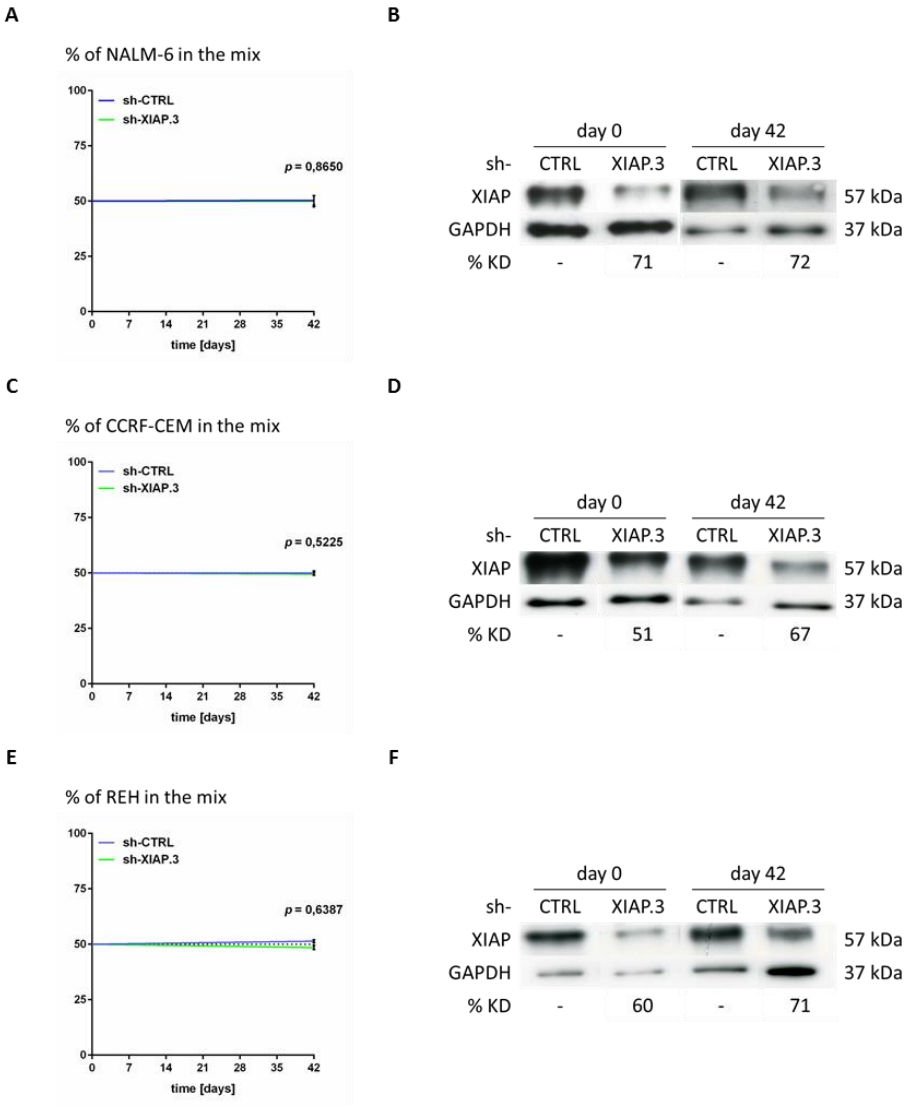

Figure 29. shRNA sequence-dependent dose-response effects of XIAP knockdown in cell lines *in vitro*.

(A) Competitive proliferation assay *in vitro* evaluating the cell populations' distribution of NALM-6 cells expressing the third selected shRNA sequence targeting XIAP (sh-XIAP.3) in comparison to NALM-6 cells expressing the sh-CTRL. NALM-6 cells transduced with the constitutive-knockdown system were mixed at a 1:1 ratio and monitored by flow cytometry twice a week up to 6 weeks. Quantification of the sh-CTRL and the sh-XIAP populations' distribution was performed as shown in Figure 22. Error bars represent SEM of biologically independent triplicates.

(B) Western blotting of XIAP in NALM-6 cells expressing the sh-XIAP.3 in comparison to NALM-6 cells expressing the sh-CTRL. XIAP levels were detected at the beginning (day 0) and at the end (day 42) of

the experiment and normalized to GAPDH used as loading control. The XIAP knockdown levels (%KD) were quantified relative to the control.
(C – F) Same as in (A and B). CCRF-CEM cells (C and D) and REH cells (E and F) were used.

We performed a similar test to confirm the dose-response relationship via using one of our strong sequences targeting XIAP (sh-XIAP.1) under the control of a weaker promoter. The shRNA expressing vectors were modified and the viral SFFV promoter was replaced with the eukaryotic EF1α promoter (Figure 30). Also in this case, the phenotypic effect on the proliferation capability of the cells was either not significant (NALM-6 and REH cell lines) or less prominent (CCRF-CEM cell line) in comparison with the experiments previously shown in Figure 25 and Figure 26.

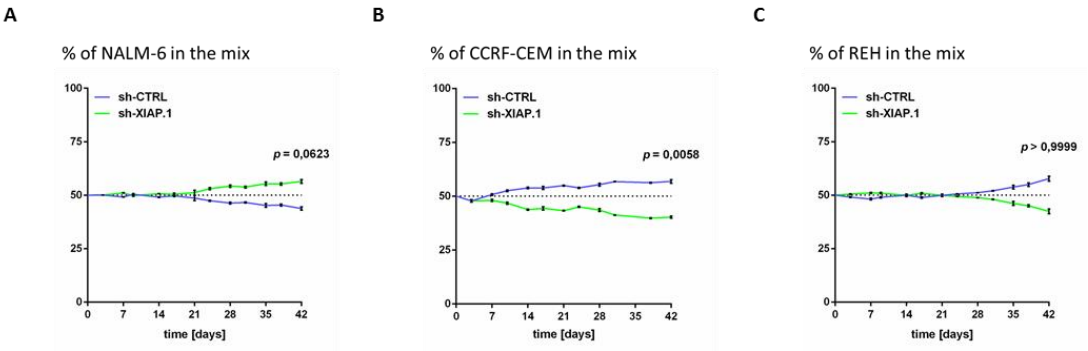

Figure 30. Minor XIAP knockdown hardly impairs proliferation of cell lines *in vitro*.
(A) Competitive assay *in vitro* evaluating the cell populations' distribution of NALM-6 cells expressing the sh-XIAP.1 in comparison to NALM-6 cells expressing the sh-CTRL under the control of the human EF1α pol-II promoter. NALM-6 cells transduced with the constitutive-knockdown system were mixed at a 1:1 ratio and monitored by flow cytometry twice a week up to 6 weeks. Quantification of the sh-CTRL and the sh-XIAP populations' distribution was performed as shown in Figure 22. Error bars represent SEM of biologically independent triplicates.
(B and C) Same as in (A). CCRF-CEM cells (B) and REH cells (C) were used.

The same experiment as above was also performed in an *in vivo* setting. NALM-6 cell lines produced as previously described were used. The flow cytometry analysis of the cells isolated from the bone marrow of mice confirmed the observation previously done with the cell lines *in vitro*: the phenotypic effect of XIAP knockdown is evident only when the knockdown is induced by a stronger promoter (Figure 31).

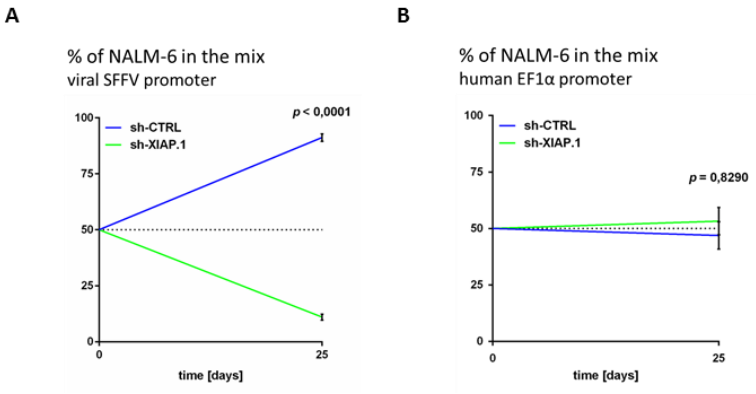

Figure 31. Promoter-dependent dose-response effects of XIAP knockdown in NALM-6 cell line *in vivo*.
(A) Competitive assay *in vivo* evaluating the cell populations' distribution of NALM-6 cells expressing the sh-XIAP.1 in comparison to NALM-6 cells expressing the sh-CTRL. NALM-6 cells transduced with the constitutive-knockdown system were mixed at a 1:1 ratio and injected into NSG mice (n = 3). After 25 days, mice were sacrificed and cells were isolated from bone marrow. The relative proportion of the sh-CTRL and the sh-XIAP populations was quantified by flow cytometry as shown in Figure 22. Error bars represent SEM of all mice analyzed at the indicated time point.
(B) Same as in (A). NALM-6 cells expressing the sh-XIAP.1 compared with NALM-6 cells expressing the sh-CTRL under the control of the human EF1α pol-II promoter were used (n = 7).

Thus, we established a technique that allows performing long-term phenotypic studies both *in vitro* and *in vivo* thanks to a strong and stable knockdown of the desired target. The designed system for competitive assays allows to precisely understand the role of single proteins and their involvement in leukemia growth and development.

5.1.7 Establishment of the constitutive-knockdown system in ALL PDX cells

Currently, the best model to perform molecular and genetic studies on patients' cells is the PDX mouse model of acute leukemia. Therefore, in order to generate a platform that permits further detailed studies, we transferred the system for a constitutive knockdown in PDX cells expanding in mice. The two primary ALL samples obtained from patients with relapsed ALL and previously tested for XIAP expression level (see Figure 19) were transplanted into NSG mice and the re-isolated ALL PDX cells were transduced with the lentiviral vectors of the system. Transduction of PDX cells was performed as described in paragraph 4.3.5 and similarly to cell lines (see Figure 23D-E for the control of dsRED expression) (Figure 32). Based on our previous observation regarding the dose-response relationship between strength of knockdown and impaired proliferation capability, we combined the viral SFFV

promoter and one of the strongest shRNA sequences targeting XIAP (sh-XIAP.1) to perform further studies in PDX cells.

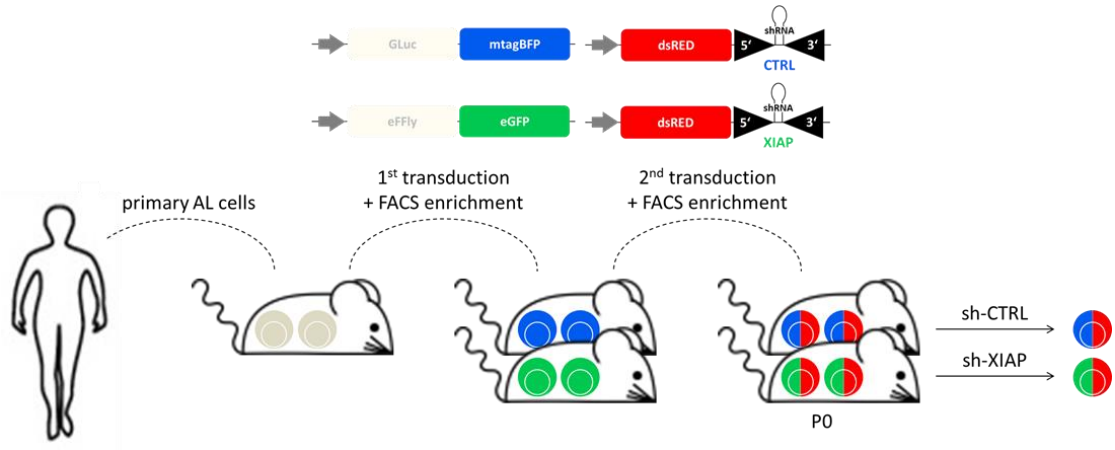

Figure 32. Production of GEPDX transduced with the constitutive-knockdown system.
Scheme showing the constructs used for the generation of the different cell populations and the steps for the production of the ALL GEPDX samples used in this study (see paragraph 4.3.5).

The resulting GEPDX cells (see paragraph 4.3.5) were used first to control whether the artificial expression of transgenes and the activation of the RNAi pathway by control sequences might affect the phenotypic behavior of the cells over re-passaging in mice. ALL-265 GEPDX cells produced as previously described were mixed at a 1:1 ratio and injected into NSG mice. After isolation from the bone marrow of mice, cells were analyzed by flow cytometry. The expression of fluorescent proteins (Figure 33A) and the activation of the RNAi machinery by control sequences (Figure 33B) did not alter the spontaneous expansion of GEPDX cells in mice, although we observed a non-significant difference between the two populations. We further assessed whether the system was stable over re-passaging in mice; therefore, the cells isolated from the bone marrow were subsequently re-injected in recipient mice for three consecutive passages without intermediate manipulations. This control confirmed the stability of the system, including the recombinant expression of both transgenes and shRNAs, without affecting the expansion of the cells *in vivo* (Figure 33C-F).

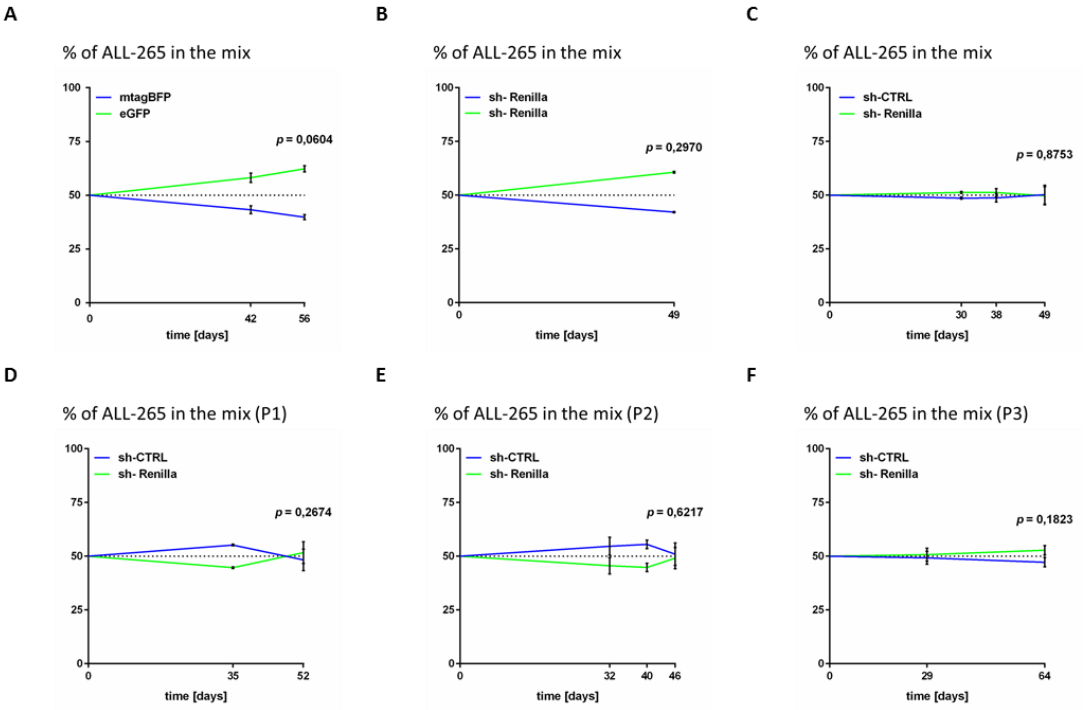

Figure 33. Artificial expression of transgenes and unspecific shRNA sequences is stable and do not affect the expansion of ALL-265 GEPDX cells over re-passaging in mice.

(A and B) Competitive assay *in vivo* to verify the absence of alterations of spontaneous cell proliferation in mice due to the expression of artificial fluorescent markers (A) and the activation of the RNAi pathway (B). ALL-265 GEPDX cells transduced with either the first vectors only of the constitutive-knockdown system (A) or expressing an unspecific shRNA sequence (sh-Renilla) (B) were mixed at a 1:1 ratio and injected into NSG mice (*n* = 8 for each experiment). At different desired time points, mice were sacrificed and cells were isolated from bone marrow. The relative proportion of the sh-CTRL and the sh-XIAP populations was quantified by flow cytometry as shown in Figure 22. Error bars represent SEM of all mice analyzed at the indicated time point.

(C) Same as in (B). ALL-265 GEPDX cells expressing two different unspecific shRNA sequences (sh-CTRL and sh-Renilla) were used (*n* = 9).

(D – F) The mixed populations of ALL-265 GEPDX cells isolated from the bone marrow of mice shown in (C) were re-injected into recipient NSG mice up to three re-passages (*n* = 8 for each passage). Passage one (P1) (D), two (P2) (E) and three (P3) (F) are shown.

Another crucial control for the validation of the system in GEPDX cells expanding in mice was to assess the stability of the knockdown. To perform this important control, ALL-199 GEPDX cells produced as previously described were injected into NSG mice and analyzed for XIAP expression after each passage. The immunoblotting confirmed the stability of XIAP knockdown at protein level over four consecutive passages in mice (Figure 34).

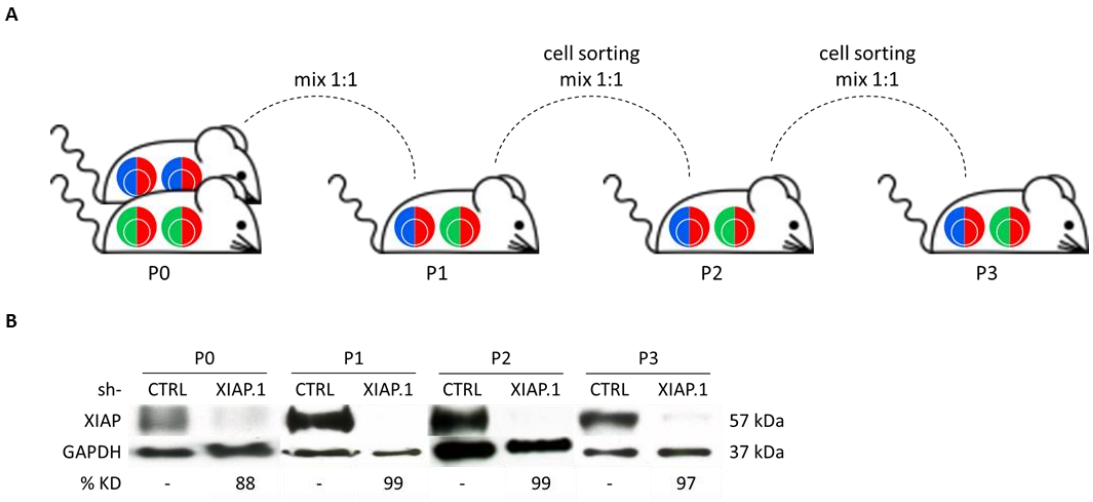

Figure 34. XIAP knockdown is stable in ALL-199 GEPDX cells over re-passaging in mice.
(A) Scheme showing the experimental setting used to verify the stability of the knockdown in ALL-199 GEPDX cells over re-passaging in mice. ALL-199 GEPDX cells produced as shown in Figure 32 (P0) were mixed at a 1:1 ratio and injected into NSG mice (*n* = 7 in P1). At first clinical signs of disease, mice were sacrificed and cells were isolated from bone marrow. After separation by cell sorting, the two populations were mixed again at a 1:1 ratio and re-injected into recipient NSG mice up to three re-passages (*n* = 2 in P2 and P3).
(B) Western blotting of XIAP in ALL-199 GEPDX cells expressing the sh-XIAP.1 in comparison to ALL-199 GEPDX cells expressing the sh-CTRL and separated by cell sorting after each passage. The XIAP expression levels were normalized to GAPDH used as loading control. The XIAP knockdown levels (%KD) were quantified relative to the control.

Taken together our competitive constitutive-knockdown system has been validated for not altering the proliferative behavior of PDX cells expanding in mice and, also in the *in vivo* context, the experimental variance between the control and the target population was minimized and the precision of the readout was maximized.

5.1.8 XIAP is essential for proliferation of ALL PDX cells in mice

To examine the role of XIAP also in ALL PDX cells, we performed competitive assays *in vivo* using GEPDX cells expressing the constitutive-knockdown system. ALL-199 PDX cells transduced as previously described were mixed at a 1:1 ratio and injected into NSG mice. The flow cytometry based analysis of the GEPDX cells isolated from mice bone marrow 40 days after xenotransplantation revealed that the initially equal distribution of the two populations changed over time and the cells with the knockdown of XIAP were statistically significantly less abundant than the control cells (Figure 35A). These cells were analyzed for

the XIAP expression at protein level to confirm the presence of the knockdown until the end of the experiment (Figure 35B). To confirm the observation that the XIAP knockdown induces a proliferation disadvantage in the PDX model, we performed the same competitive assay with ALL-265 GEPDX cells. At the end of the first passage, ALL-265 GEPDX cells were also re-injected in recipient mice without any manipulation to assess if the difference in relative proportion of the two populations could increase upon re-passaging (Figure 35C). Also in the case of the ALL-265 sample, the knockdown of XIAP was stable until the end of the first passage in mice (Figure 35D).

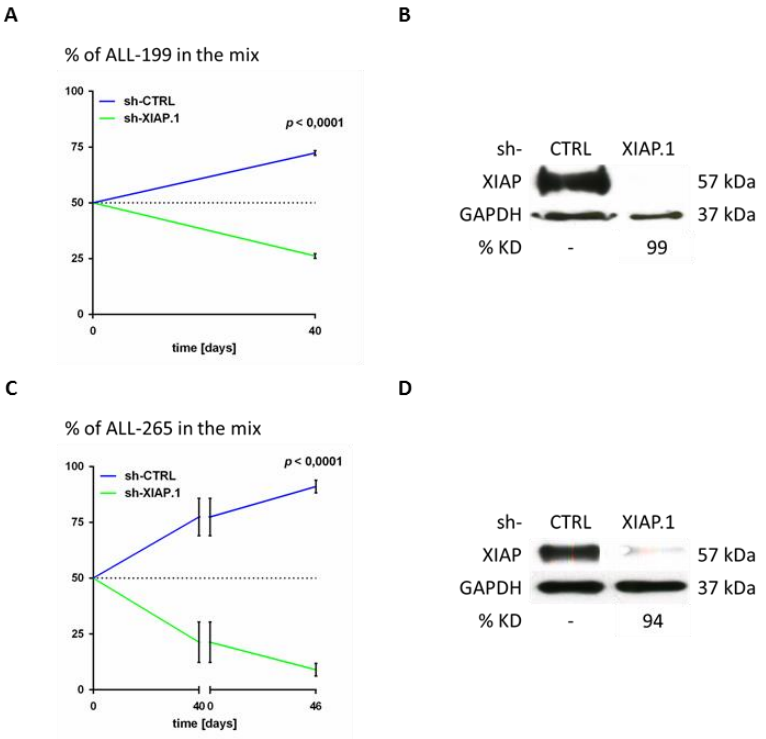

Figure 35. XIAP knockdown impairs the expansion of two different GEPDX cells in mice.
(A) Competitive assay *in vivo* evaluating the cell populations' distribution of ALL-199 GEPDX cells expressing the sh-XIAP.1 in comparison to ALL-199 GEPDX cells expressing the sh-CTRL. ALL-199 GEPDX cells transduced with the constitutive-knockdown system were mixed at a 1:1 ratio and injected into NSG mice (n = 7). At first clinical signs of disease, mice were sacrificed and cells were isolated from bone marrow. The relative proportion of the sh-CTRL and the sh-XIAP populations was quantified by flow cytometry as shown in Figure 22. Error bars represent SEM of all mice analyzed at the indicated time point.
(B) Western blotting of XIAP in ALL-199 GEPDX cells expressing the sh-XIAP.1 in comparison to ALL-199 GEPDX cells expressing the sh-CTRL. XIAP levels were detected at the time of isolation (day 40) after the separation of the two populations by cell sorting (shown also in Figure 34B – P1). The XIAP expression levels were normalized to GAPDH used as loading control. The XIAP knockdown levels (%KD) were quantified relative to the control.
(C and D) Same as in (A and B). ALL-265 GEPDX cells were used. The interrupted x axis indicates that the mixed populations isolated from the bone marrow of mice were re-injected into recipient NSG

mice for one re-passage (*n* = 8 for each passage). The Western blotting of XIAP was performed on the cells at first isolation and after the separation of the two populations by cell sorting.

To find out whether the XIAP expression level could also modulate the proliferation kinetic of GEPDX, we performed the same dose-response analyses and experiments described in paragraph 5.1.6 for cell lines. ALL-199 and ALL-265 GEPDX cells were analyzed as shown in Figure 28A for the expression of the dsRED fluorescent protein. The analysis supported the direct correlation between the strength of XIAP knockdown and the proliferation disadvantage (Figure 36A-B).

Finally, to further confirm that the selection of potent shRNA sequences is necessary to appreciate the precise function of single proteins, ALL-199 PDX cells were transduced with the vector expressing the weak shRNA sequence targeting XIAP (sh-XIAP.3) and used to perform a competitive *in vivo* assay (Figure 36C). Additionally, the immunoblotting analysis performed on the sorted populations at the end of the experiment showed an only minor knockdown of XIAP as expected (Figure 36D). Thus, the analysis of the GEPDX cells isolated from the bone marrow of mice clearly supported once again the hypothesis that XIAP silencing is responsible for the decreased proliferation capability of ALL GEPDX cells. All in all, our newly established system for the constitutive knockdown of XIAP helped to precisely elucidate the role of XIAP as essential gene for the proliferation of ALL cell lines and PDX samples.

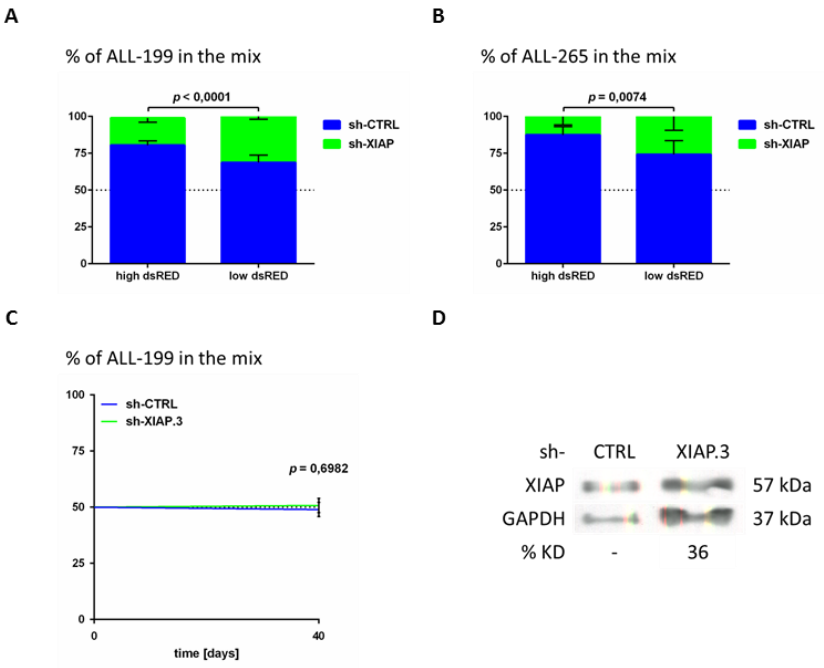

Figure 36. Dose-response relationship between strength of XIAP knockdown and proliferation disadvantage in GEPDX cells in mice.

(A – B) Comparison between the XIAP knockdown effects in ALL-199 GEPDX from Figure 35A (A) and ALL-265 GEPDX from Figure 35C (B) at the end (day 40) of the experiment and analyzed as shown in Figure 28A. Error bars represent SEM of all mice analyzed at the indicated time point.

(C) Competitive assay *in vivo* evaluating the cell populations' distribution of ALL-199 GEPDX expressing the sh-XIAP.3 in comparison to ALL-199 GEPDX expressing the sh-CTRL. ALL-199 GEPDX cells transduced with the constitutive-knockdown system were mixed at a 1:1 ratio and injected into NSG mice (n = 5). At first clinical signs of disease, mice were sacrificed and cells were isolated from bone marrow. The relative proportion of the sh-CTRL and the sh-XIAP populations was quantified by flow cytometry as shown in Figure 22. Error bars represent SEM of all mice analyzed at the indicated time point.

(D) Western blotting of XIAP in ALL-199 GEPDX cells from (C) expressing the sh-XIAP.3 in comparison to ALL-199 GEPDX cells expressing the sh-CTRL. XIAP levels were detected at the time of isolation (day 40) after the separation of the two populations by cell sorting. The XIAP expression levels were normalized to GAPDH used as loading control. The XIAP knockdown levels (%KD) were quantified relative to the control.

5.2 Inducible-knockdown System

The constitutive-knockdown system is an appropriate and attractive tool for a variety of studies on many different targets. However, the loss of some important and vital proteins might lead to dramatic and quick effects, making the constitutive-knockdown system not suitable to study the role of essential genes. At least in the PDX *in vivo* model, the expression of transgenes requires cells expansion and passaging in mice for enrichment to a pure population – an impracticable task in case of "deadly" knockdown. To overcome this limitation, an inducible-knockdown system was highly desired because it would allow the induction of the knockdown via treatment of cells or mice with an inducer drug. After a careful evaluation of published studies, the decision was against a tetracycline-inducible TRE-based expression system, mainly for fearing leakiness of the system which would make once again the production of cell populations with the knockdown of essential genes unfeasible. Instead, my colleague Michela Carlet in collaboration with Marc Schmidt-Supprian decided for a cloning strategy based on a Cre-loxP-based system combined with a miR-30 shRNAmir backbone-based knockdown.

5.2.1 High expression of Mcl-1 in ALL and AML cell lines and PDX samples

Looking for an example target with important role in cell survival to use as positive control for the validation of an inducible-knockdown system in the background of acute leukemia, we selected Mcl-1. Mcl-1 is an anti-apoptotic member of the Bcl-2 family on which cancer cells depend either for survival or resistance to chemotherapy. Additionally, besides of being found to be highly expressed in many human cancers, it is known that its high expression in hematopoietic stem cells promotes malignant transformation (Campbell et al. 2010). Nevertheless, the ability to sensitize tumor cells towards chemotherapy remains a challenge due to the high turnover of the protein and its interaction with a variety of partners. Thus, Mcl-1 might be a striking target for new therapeutic approaches and in combination with conventional chemotherapy. Therefore, three ALL and AML cell lines and four ALL and AML PDX samples were selected for this study and tested for Mcl-1 expression at protein level. According to the literature, Mcl-1 was visible in the ALL and AML cell lines and PDX samples tested, while it was not detectable in PBMCs from a healthy donor (Figure 37).

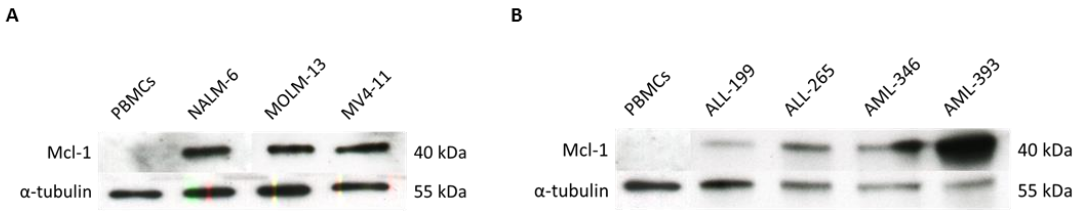

Figure 37. Evaluation of Mcl-1 protein expression level by Western blotting.
(A) Western blotting of Mcl-1 in three established ALL and AML cell lines used in this study in comparison to PBMCs from a healthy donor. α-tubulin levels are shown as loading control.
(B) Same as in (A). Two ALL and two AML PDX samples used in this study in comparison to PBMCs from a healthy donor are shown.

5.2.2 Design of a system for an inducible knockdown

To induce the knockdown of our target Mcl-1, we expressed a shRNA sequence targeting Mcl-1 with the miR-30 backbone placed in the 3' UTR of a fluorochrome, as successfully established for the constitutive-knockdown system. To further develop the model and introduce transgene expression in an inducible manner, we exploited the CreER^{T2} recombinase to specifically induce the knockdown at the desired time. The CreER^{T2} expressing construct (see Figure 16) was transferred into the cells with a first round of transduction. The CreER^{T2} recombinase was constitutively expressed under the control of the viral SFFV promoter together with the mCherry fluorescent marker for an easy identification of the transduced human population by flow cytometry. As described in paragraph 2.3.2.3, the CreER^{T2} interacts via the ER^{T2} with the Hsp90 which enables the localization of the fusion protein in the cytosol and thus preventing the recombinase activity. The nature of the human ER^{T2} insures the specific binding with the synthetic estrogen Tamoxifen which leads to the release of the Hsp90 protein and consequently permits the translocation to the nucleus (see Figure 11). A second round of transduction was performed for the FLIP-cassette expressing vector (see Figure 17). Using two different pairs of loxP sites, Stern et al. developed in 2008 a system for Cre-inducible knockdown cassettes in tissue-specific Cre mouse lines, as loxP-STOP-loxP cassettes used for inducible transgene expression are unable to prevent the transcription of shRNAs (Stern et al. 2008). For the design of our system, we adapted the advantages of the published FLIP vector to our need. In particular, we used the coding sequences of two fluorescent markers (mtagBFP and eGFP) in order to conveniently track and select the transduced cells via flow cytometry, and we incorporated this FLIP-cassette into our pCDH lentiviral backbone under the control of the strong viral SFFV pol-II promoter. The 22-mer shRNA sequence targeting Mcl-1 and the control sequence were

cloned into the FLIP-cassette vector in the background of the miR-30 backbone placed into the 3' UTR of the eGFP fluorescent marker. The eGFP protein was cloned into the FLIP-cassette vector in antisense orientation in order to avoid its spontaneous transcription. Instead and in the absence of Cre activity, the mtagBFP fluorescent marker was expressed under the control of the SFFV promoter and allowed the identification of the transduced cells by flow cytometry (Figure 38A). The FLIP-cassette vector harbors two different sets of loxP sites and their orientation admit one specific stream consisting of two different types of recombination: (1) inversion of the DNA fragment in between the two loxP sites of one set generating two different intermediate constructs that both display the eGFP marker in sense orientation; (2) deletion of the DNA fragment flanked by the two loxP sites of the other set leading to the deletion of the mtagBFP coding sequence and one loxP site per each set. The resulting construct presents only one remaining loxP site per each set making the recombination process irreversible. Thus, the eGFP expression becomes constitutive under the control of the viral SFFV promoter as well as the expression of the shRNA sequence embedded into the miR-30 backbone placed in the 3' UTR of the eGFP coding sequence (Figure 38B), similarly to the lentiviral vector previously used for the constitutive-knockdown system described in paragraph 5.1.3 (see Figure 21). Consequently, we expected an efficient knockdown comparable to the one achieved with the constitutive-knockdown system.

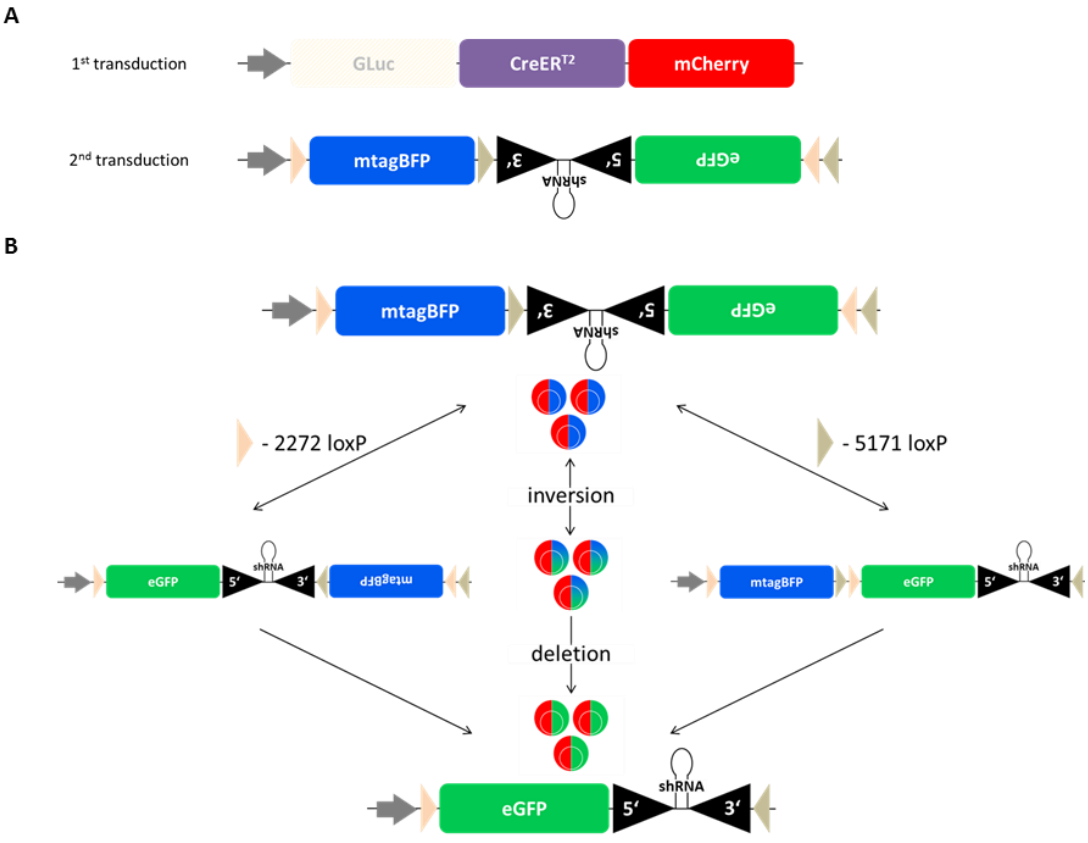

Figure 38. Scheme of the inducible-knockdown system and recombination steps of the FLIP-cassette.
(A) The two plasmids used for the generation of cell populations expressing the inducible-knockdown system are shown. The vector harboring the coding sequence of the $CreER^{T2}$ recombinase and the fluorochrome (mCherry) was transduced first, and the FLIP-cassette construct after.
(B) Diagram showing the steps of the $CreER^{T2}$-regulated RNAi occurring upon treatment with Tamoxifen. The FLIP-cassette expresses the mtagBFP fluorescent marker, while the eGFP and the miR-30 shRNAmir cassette are not expressed because placed in the antisense direction. After recombination, thanks to the two different sets of loxP sites conveniently introduced, the mtagBFP coding sequence is deleted and the eGFP harboring the miR-30 shRNAmir cassette in its 3' UTR is then expressed. In the middle of the scheme, the characteristic colors that allow distinguishing the cell populations at the three different stages of recombination are shown. Adapted figure from Stern et al. 2008 (Stern et al. 2008).

5.2.3 Selection of a strong shRNA sequence targeting Mcl-1

As described in Fellmann et al. 2011 (Fellmann et al. 2011) and previously demonstrated in paragraph 5.1.2, there is a good and reliable correlation between the potency of the shRNA sequence to induce the knockdown of the desired target and the protein expression level detected via immunoblotting. Therefore, seven 22-mer shRNA sequences targeting Mcl-1 were designed (see Table S1 for all the shRNA sequences tested) and cloned into the shRNA expressing lentiviral vector used for the constitutive-knockdown system (see Figure 14). NALM-6 cell line was transduced with each of these constructs with and efficiency such to ensure single copy integration and enriched via cell sorting after 6 days. The expression of Mcl-1 at protein level in the sorted cells was compared to NALM-6 expressing the shRNA sequence used as control (sh-Renilla) and the most potent shRNA sequence targeting Mcl-1 (sh-Mcl-1.1) was selected to perform all future experiments (Figure 39).

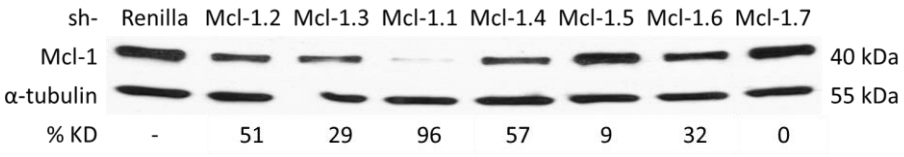

Figure 39. Selection of strong shRNA sequences targeting Mcl-1 by Western blotting.
Western blotting of Mcl-1 in NALM-6 expressing the different shRNA sequences targeting Mcl-1 in comparison to NALM-6 expressing an unspecific shRNA sequence used as control (sh-Renilla). Mcl-1 signal intensity was normalized to α-tubulin used as loading control, and the knockdown levels (%KD) indicated were quantified relative to the control.

5.2.4 Validation of the inducible-knockdown system in cell lines

The strategy that we used to induce an efficient knockdown of our target in the cell population of interest relies on the expression level of the CreER^{T2} enzyme in combination with the one of the FLIP-cassette constructs expressing a specific shRNA sequence. Since either the shRNA targeting the Mcl-1 mRNA or the shRNA used as control (see Table S1 for the shRNA sequence used as control) are located on two different lentiviral vectors, we performed control experiments to check if the expression level of the different shRNAs could be comparable. Therefore, we first evaluated the equal expression of the FLIP-cassette vector among the cell populations harboring either the sh-Mcl-1.1 or the control sequence. Although the expression of the shRNA was not directly linked to the mtagBFP, the comparison was performed to ensure equal initial condition for both cell populations and consequent potentially equal response to the recombination induction upon Tamoxifen treatment. Thus, the fluorescent intensity of the mtagBFP protein was compared among the two populations right before the enrichment by cell sorting for both established cell lines and GEPDX cells transduced with the inducible-knockdown system (Figure 40).

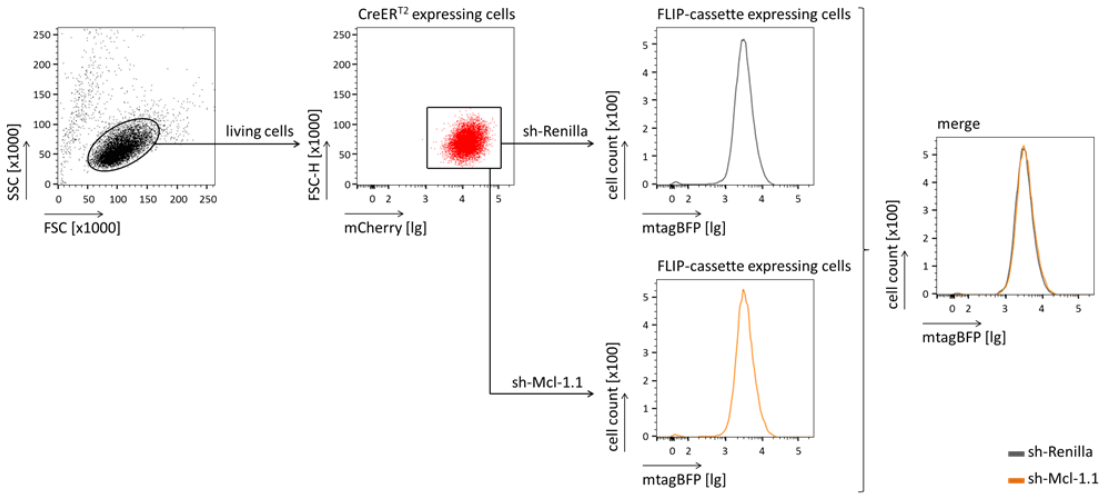

Figure 40. Control of equal mtagBFP fluorescence intensity in NALM-6 cell line.
Representative dot plots and histogram used to assess the equal FLIP-cassette expression. For either established cell lines or GEPDX cells transduced with the inducible-knockdown system, the intensity of mtagBFP was compared among the control and target populations to confirm the equal expression of the FLIP-cassettes (merge). Here, NALM-6 cell line is shown. In the histogram, the control population (sh-Renilla) is depicted in grey and the target population (sh-Mcl-1.1) in orange.

As previously described, cells transduced with the inducible-knockdown system constitutively express the two fluorescent markers mCherry and mtagBFP allowing the selection of the human transduced cells, while the expression of eGFP is induced upon treatment with Tamoxifen and allows the visualization and quantification of the population expressing the shRNA sequence (Figure 41).

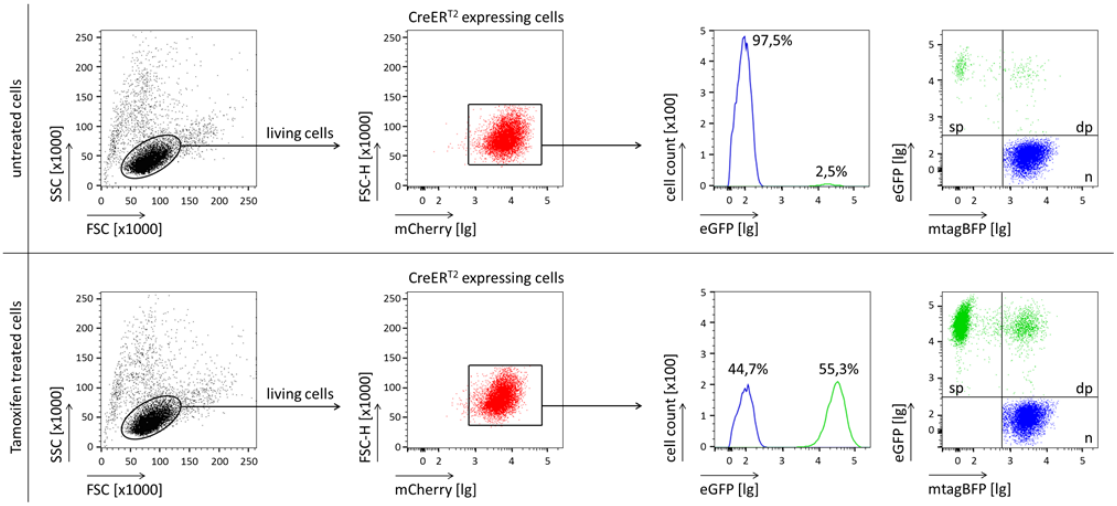

Figure 41. Gating strategy for the analysis of the inducible experiments.
Representative dot plots and histograms of the steps of the flow cytometry based analysis used for the quantification of the populations' distribution. Either untreated established cell lines or untreated GEPDX cells transduced with the inducible-knockdown system constitutively express the fluorochromes mCherry and mtagBFP. The expression of the eGFP fluorescent marker is induced upon treatment with Tamoxifen. Here, NALM-6 expressing the sh-Renilla either untreated or at ca. 3 weeks after treatment are shown. Percentages of the different populations are indicated in the histograms. Abbreviations: sp = eGFP single positive cells; dp = eGFP/mtagBFP double positive cells; n = eGFP negative cells.

Untreated cells showed a small eGFP positive population, which indicates the presence of a minimal basal leakiness of the system. Instead, upon Tamoxifen treatment, the eGFP expressing population was named "flipped" population, indicating those cells in which the CreER^{T2} recombined the FLIP-cassette vectors with consequent expression of the eGFP and the shRNA cloned into the miR-30 placed in its 3' UTR (Figure 42A). Interestingly, we observed that the leakiness of the population carrying the shRNA targeting Mcl-1 was 30 to 50% less than the leakiness of the control population, thus probably already showing the effect of the knockdown of Mcl-1 (Figure 42B). Upon Tamoxifen treatment, the CreER^{T2} activity and the FLIP-cassette recombination could be followed and quantified by flow cytometry via monitoring the progressive expression of the eGFP fluorescent marker and the disappearance of the mtagBFP protein over time. More precisely, cells express the eGFP

fluorescent marker already after 24 hours post-treatment and this population progressively increases for the first three days after treatment (Figure 42C – D). The flipped eGFP positive population can be divided in eGFP single positive cells (sp) and eGFP/mtagBFP double positive cells (dp) as result of the recombination efficacy of the FLIP-cassettes artificially transduced into the cell. When only one vector integrates into the genome, it is likely that the dp population will disappear over time as consequence of the deletion of the mtagBFP coding sequence and degradation of the correspondent protein; on the contrary, when multiple FLIP-cassettes are integrated into the genome, the CreER^{T2} activity might not be sufficient to recombine all FLIP-cassettes, leaving at least one mtagBFP coding sequence undeleted which will keep expressing the correspondent fluorescent marker. Nevertheless, in both instances at least one miR-30 shRNAmir cassette would be in sense orientation allowing the expression of the shRNA (Figure 42E-F).

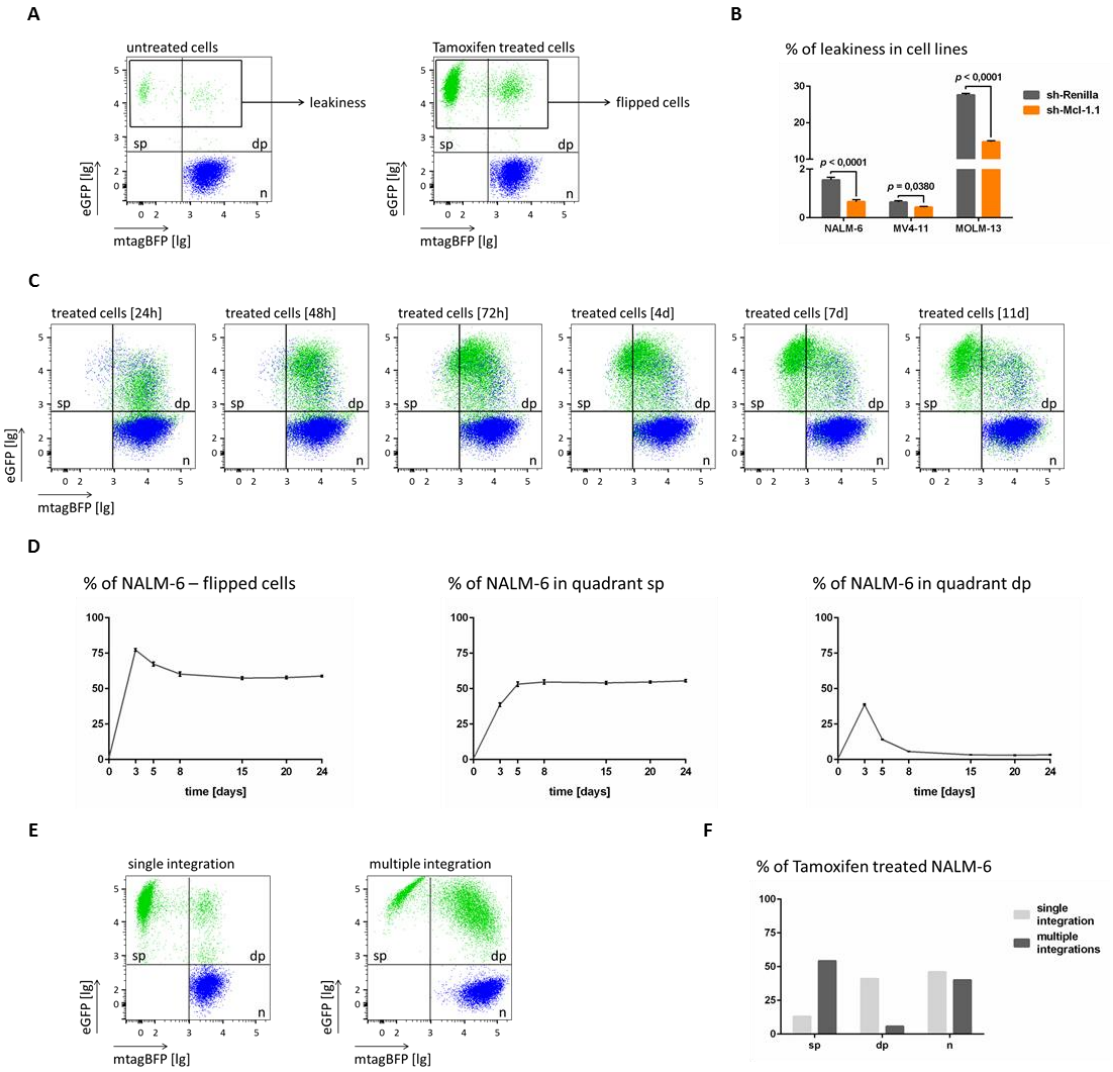

Figure 42. Characterization of the induced eGFP expression.
(A) Representative dot plots showing the different distribution of the cells among the different quadrants before and after Tamoxifen treatment. The expression of eGFP fluorescent marker is induced upon treatment with Tamoxifen (flipped cells) (right panel), while the basal expression of eGFP in untreated cells indicates the leakiness of the system (leakiness) (left panel). Here, NALM-6 cells expressing the sh-Renilla either untreated or at ca. 3 weeks after treatment are shown. Abbreviations: sp = eGFP single positive cells; dp = eGFP/mtagBFP double positive cells; n = eGFP negative cells.
(B) Percentage of leakiness in three cell lines transduced with the inducible-knockdown system at 1 week after the transduction with the FLIP-cassette constructs. The sh-Renilla population is depicted in grey and the sh-Mcl-1.1 population in orange. Error bars represent SEM of biologically independent triplicates.
(C) Representative dot plots showing the eGFP expression over time. Untreated cells (depicted in blue) express the mtagBFP fluorescent marker only. Upon Tamoxifen treatment, the cloud of recombinant cells (depicted in green) shifts to the quadrant of double positive (dp) cells as result of the CreER^{T2} activity and consequent expression of the eGFP fluorescent marker. The cloud of recombinant cells subsequently shifts to the quadrant of single positive (sp) cells as consequence of the deletion of the mtagBFP coding sequence and degradation of the protein. Here, MOLM-13 expressing the sh-Renilla at different time points after treatment with Tamoxifen and analyzed by flow cytometry as shown in Figure 41 are shown.
(D) Final readout of the quantification over time of the flipped cells upon Tamoxifen treatment according to the gating strategy shown in Figure 41. The total amount of flipped cells (left panel) is given by the sum of the amount of cells in the quadrants of eGFP single (middle panel) and double (right panel) positive cells. Here, NALM-6 cells expressing the sh-Renilla are shown. Error bars represent SEM of biologically independent triplicates.
(E) Representative dot plots showing the different distribution of the flipped cells among the quadrants of eGFP single positive (sp) and double positive (dp) cells after treatment with Tamoxifen. Here, NALM-6 cells expressing the sh-Renilla at ca. 3 weeks after treatment with Tamoxifen are shown. NALM-6 cells were transduced with the FLIP-cassette construct at a MOI below (left panel) or greater (right panel) than 0.2 to ensure single or multiple integrations respectively.
(F) Relative amount of cells in the different quadrants of (E).

Although the Cre mediated recombination has become less harmful for the cells after the fusion with the ER^{T2} domain, it is still possible to face toxicity upon treatment with Tamoxifen and consequent translocation of the recombinase into the nucleus. Therefore, we assessed the toxicity given by the Tamoxifen itself and given by the CreER^{T2}-dependent activity. Non-transduced cells did not suffer any toxicity upon Tamoxifen treatment, but cells expressing the CreER^{T2} recombinase showed a transient decreased viability (Figure 43A). Next, we titrated the Tamoxifen evaluating the induced CreER^{T2} activity in cells expressing the FLIP-cassette, and we observed a direct correlation between Tamoxifen concentration and both toxicity and recombination efficiency (Figure 43B-C). Based on these preliminary results and balancing between efficiency and toxicity, we decided to use Tamoxifen at a concentration of 50 nM for further *in vitro* experiments with cell lines.

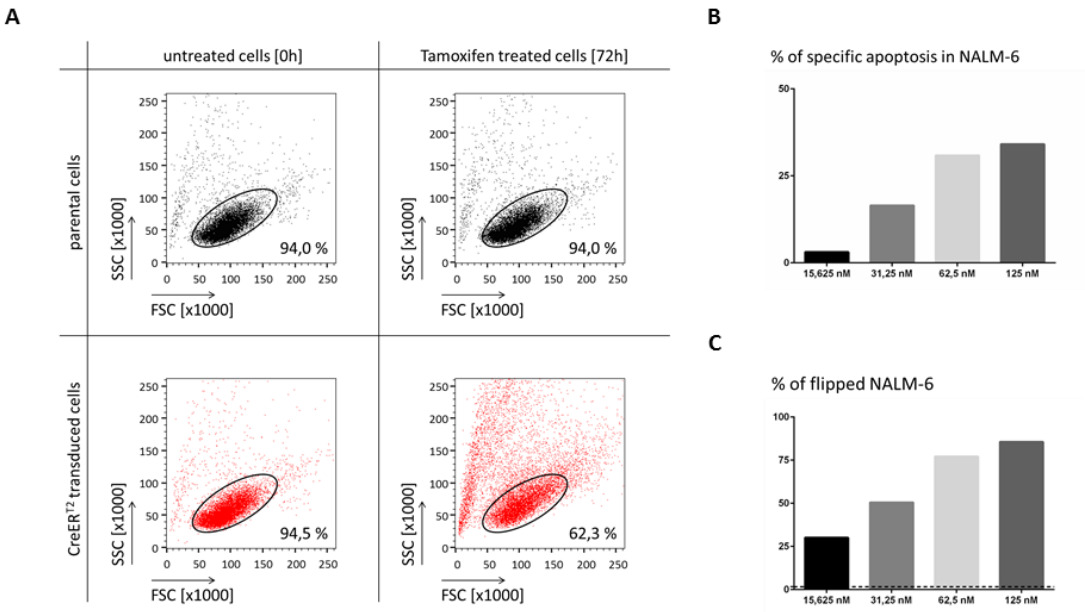

Figure 43. Tamoxifen titration and CreER^{T2} induced toxicity in NALM-6 cell line *in vitro*.
(A) Representative dot plots showing the CreER^{T2} toxicity induced at 72 hours after treatment with 125nM Tamoxifen. Here, not transduced NALM-6 (parental cells) and NALM-6 transduced with the first vector only of the inducible-knockdown system (CreER^{T2} transduced cells) are shown. Percentages of the gated living populations are indicated.
(B) Analysis of the specific apoptosis induced by Tamoxifen treatment and CreER^{T2}-mediated recombination at 72 hours after treatment with four different concentrations of Tamoxifen in NALM-6 cells expressing the sh-Renilla.
(C) Analysis of the efficiency of eGFP expression in NALM-6 cells expressing the sh-Renilla. NALM-6 cells transduced with the inducible-knockdown system were treated with four different concentrations of Tamoxifen and monitored by flow cytometry at 72 hours after treatment. Quantification of the eGFP expression was performed by flow cytometry as shown in Figure 41. The dashed line indicated the percentage of leakiness (1,63%) of untreated NALM-6 cells expressing the sh-Renilla.

Then, to control that the RNAi machinery could be equally activated among control and target population, the induction of eGFP expression was compared up to 72 hours after Tamoxifen treatment and confirmed to be equal between the two populations in all three established cell lines tested (Figure 44).

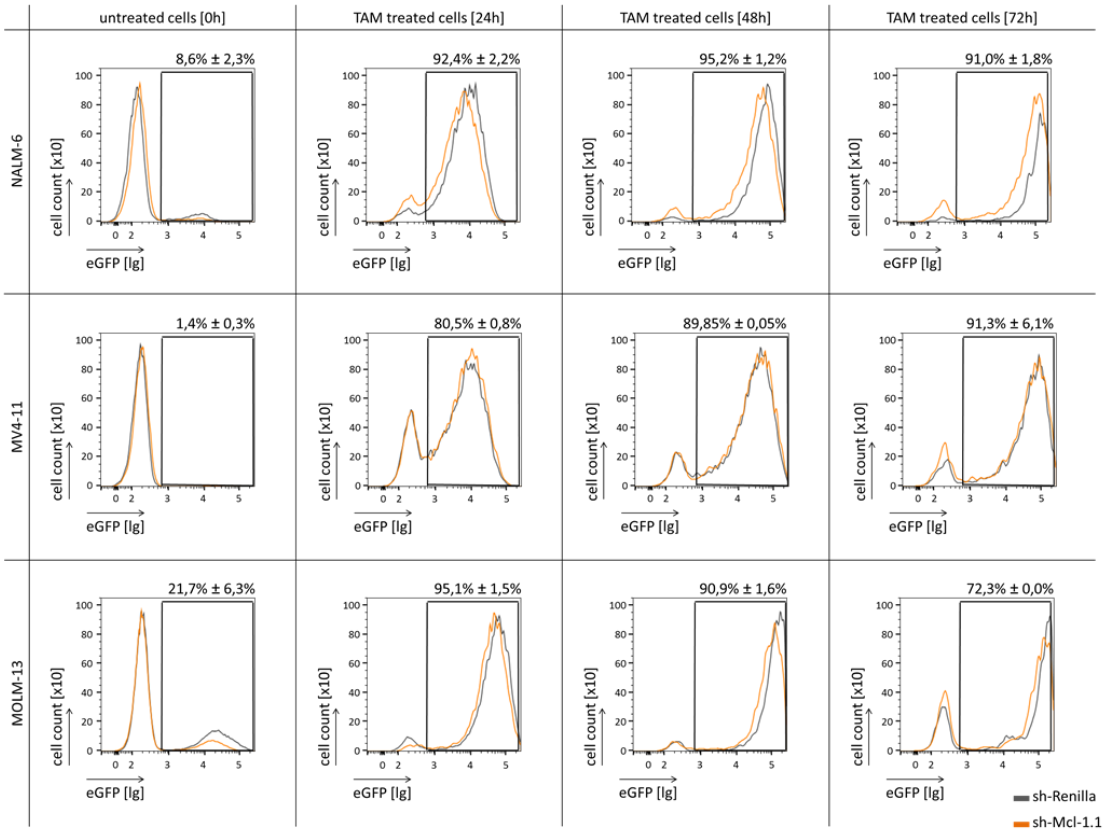

Figure 44. FLIP-cassettes harboring the sh-Renilla or the sh-Mcl-1.1 have similar recombination kinetics in cell lines *in vitro*.

shRNA sequences were expressed after CreER^{T2} induced recombination in the background of the miR-30 backbone as a single transcript together with the eGFP fluorescent marker under the control of the viral SFFV pol-II promoter. The intensity of eGFP was compared among the sh-Renilla and sh-Mcl-1.1 populations to confirm the equal expression of the corresponding associated shRNA sequence. eGFP levels were quantified every 24 hours from the moment of the treatment with Tamoxifen up to 72 hours for both sh-Renilla and sh-Mcl-1.1 expressing cells. Here, NALM-6, MV4-11 and MOLM-13 cell lines are shown. Mean of the percentage of eGFP expressing populations plus minus margin error are indicated above the histograms. The sh-Renilla population is depicted in grey and the sh-Mcl-1.1 population in orange.

All in all, the designed system for the inducible knockdown of specific targets was validated to not alter the basal survival behavior of cell lines *in vitro* up to 72 hours after the knockdown induction via Tamoxifen treatment, and consequently gives the opportunity to easily perform the desired experiments.

5.2.5 Mcl-1 is essential for the survival of ALL and AML cell lines *in vitro*

To elucidate the role of Mcl-1 in ALL and AML cell lines *in vitro*, we induced the knockdown and analyzed the effects over time by flow cytometry. As internal control, we compared the eGFP expression pattern between the control and the target populations at 72 hours after Tamoxifen treatment for each experiment. At this time point, the expression of the fluorochrome usually resulted equal, but it rapidly changed afterwards with a drastic reduction of the population harboring the sh-Mcl-1.1, becoming quickly the statistically significantly less abundant population (Figure 45A). At one week post-treatment, only few eGFP expressing cells were left, indicating a proliferative disadvantage of the cells upon Mcl-1 knockdown and showing an essential role of Mcl-1 for these cells. The surviving eGFP expressing cells were separated by cell sorting and analyzed for the Mcl-1 expression at protein level which confirmed the presence of a strong knockdown (Figure 45B). Since treatment with Tamoxifen was evaluated to be transiently toxic as shown in Figure 43, we calculated the specific apoptosis over time of both control and target population in order to evaluate the apoptosis specifically induced by Mcl-1 knockdown. The analysis performed on the control population clearly showed the transient toxicity of the system up to one week post treatment (also reflected in the quantification of the recombination shown in Figure 45A with the reduction of the eGFP expression from the initial peak to the following plateau). On the contrary, cells expressing the sh-Mcl-1.1 showed a statistically significant higher apoptosis compared to the control cells. The difference in apoptosis did not persist until the end of the experiment because the vast majority of flipped cells were already vanished one week after the treatment (Figure 45C).

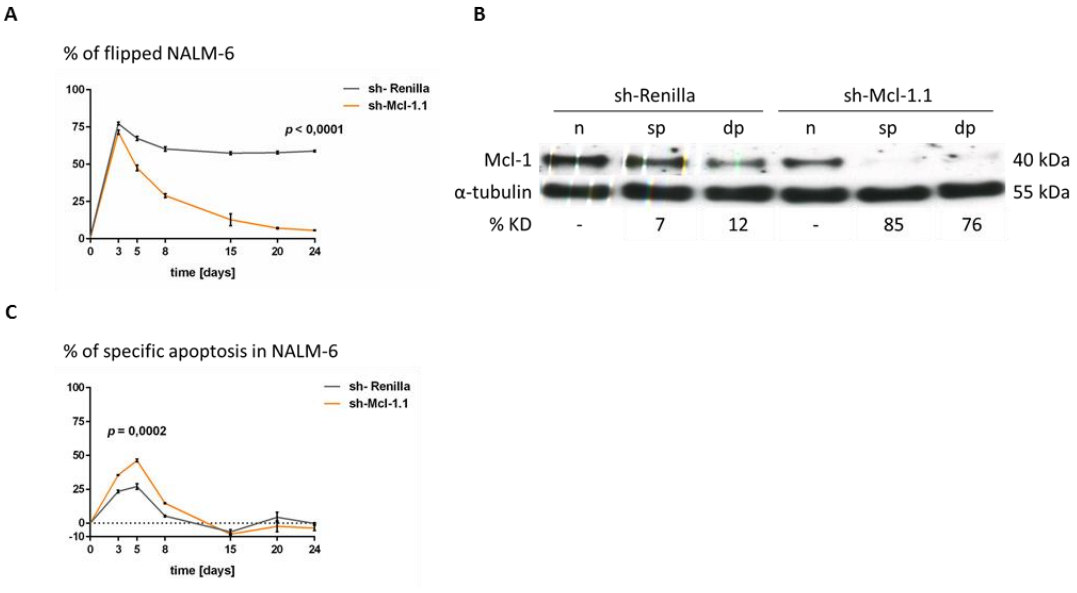

Figure 45. Mcl-1 knockdown induces cell death of ALL NALM-6 cell line *in vitro*.
(A) Inducible knockdown assay *in vitro* evaluating the cell death of NALM-6 cells expressing the sh-Mcl-1.1 in comparison to NALM-6 cells expressing the sh-Renilla. NALM-6 cells transduced with the inducible-knockdown system treated with Tamoxifen (day 0) and monitored by flow cytometry at the desired time points up to ca. 3 weeks. Quantification of the sh-Renilla and the sh-Mcl-1.1 populations' distribution was performed by flow cytometry as shown in Figure 41. Error bars represent SEM of biologically independent triplicates.
(B) Western blotting of Mcl-1 in NALM-6 cells expressing the sh-Mcl-1.1 in comparison to NALM-6 cells expressing the sh-Renilla. 8 days after the treatment with Tamoxifen (day 8 of A), the three populations were separated by cell sorting. Mcl-1 levels were detected and normalized to α-tubulin used as loading control. The Mcl-1 knockdown levels (%KD) were quantified relative to the control.
(C) Specific apoptosis in NALM-6 cells analyzed in (A). NALM-6 cells expressing the sh-Mcl-1.1 in comparison to NALM-6 cells expressing the sh-Renilla are shown. Error bars represent SEM of biologically independent triplicates.

To further validate our observation, we extended the study to two AML cell lines and confirmed our hypothesis. Therefore, we can confirm that Mcl-1 plays an essential role for the survival of ALL and AML cell lines *in vitro* (Figure 46). Of note, the cell sorting of eGFP expressing cells to assess Mcl-1 protein expression level was not possible for the MOLM-13 cell line since all flipped cells disappeared at one week post-treatment.

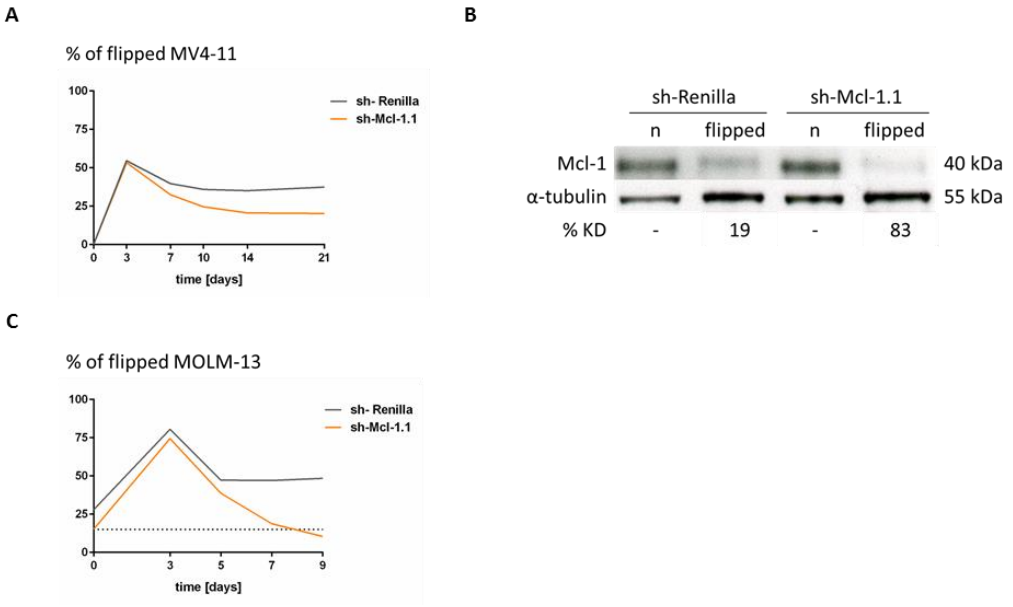

Figure 46. Mcl-1 knockdown induces cell death of two AML cell lines *in vitro*.
(A) Inducible knockdown assay *in vitro* evaluating the cell death of MV4-11 cells expressing the sh-Mcl-1.1 in comparison to MV4-11 cells expressing the sh-Renilla. MV4-11 cells transduced with the inducible-knockdown system treated with Tamoxifen (day 0) and monitored by flow cytometry at the desired time points up to 3 weeks. Quantification of the sh-Renilla and the sh-Mcl-1.1 populations' distribution was performed by flow cytometry as shown in Figure 41.

(B) Western blotting of Mcl-1 in MV4-11 cells expressing the sh-Mcl-1.1 in comparison to MV4-11 cells expressing the sh-Renilla. 7 days after the treatment with Tamoxifen (day 7 of A), the two populations were separated by cell sorting. Mcl-1 levels were detected and normalized to α-tubulin used as loading control. The Mcl-1 knockdown levels (%KD) were quantified relative to the control.
(C) Same as in (A). MOLM-13 cells were used and monitored by flow cytometry at the desired time points up to 9 days.

Taken together, the novel technique that we established allows performing loss-of-function studies of individual genes products *in vitro*, thanks to the strong and inducible knockdown of the desired target.

5.2.6 Establishment of the inducible-knockdown system in ALL and AML PDX cells

As previously mentioned, the current best model that allows molecular and genetic studies on patients' cells is the PDX mouse model of acute leukemia. Therefore, we transferred the inducible-knockdown system from cell lines to the PDX mouse model in order to generate a worldwide innovative *in vivo* platform for loss-of-function studies in PDX cells. As described in paragraph 4.3.5 and similarly to cell lines, primary ALL and AML cells obtained from patients were transplanted into NSG mice; the re-isolated PDX cells were transduced with the lentiviral vectors of the system and enriched to pure population by cell sorting (Figure 47). According to the previous observation concerning knockdown strength and effects, the vectors expressing the more potent shRNA targeting Mcl-1 (sh-Mcl-1.1) under the control of the stronger viral SFFV promoter were used.

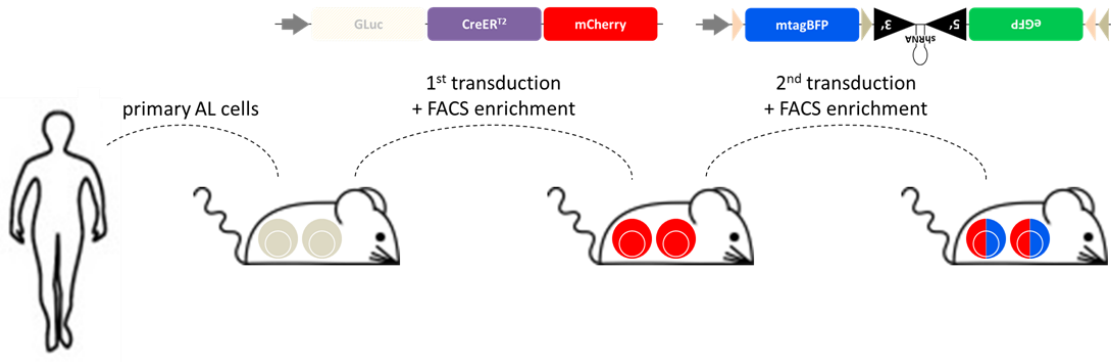

Figure 47. Production of GEPDX transduced with the inducible-knockdown system.
Scheme showing the constructs used for the generation of the GEPDX cell populations and the steps for the production of the ALL and AML GEPDX samples used in this study (see paragraph 4.3.5).

Similarly as for cell lines, the leakiness of the system was visible in GEPDX cells. Again, we interestingly observed that the leakiness of the sh-Mcl-1.1 population was less than in the control suggesting that GEPDX cells expressing the sh-Mcl-1.1 might die and disappear, although the variability of leakiness in GEPDX cells was higher than in cell lines (Figure 48A). In order to validate the recombination efficiency in GEPDX cells, we titrated Tamoxifen on GEPDX cells *in vitro* and could gladly verify that the recombination efficiency was as good as for cell lines and variable among the ALL and AML GEPDX samples tested (Figure 48B-C).

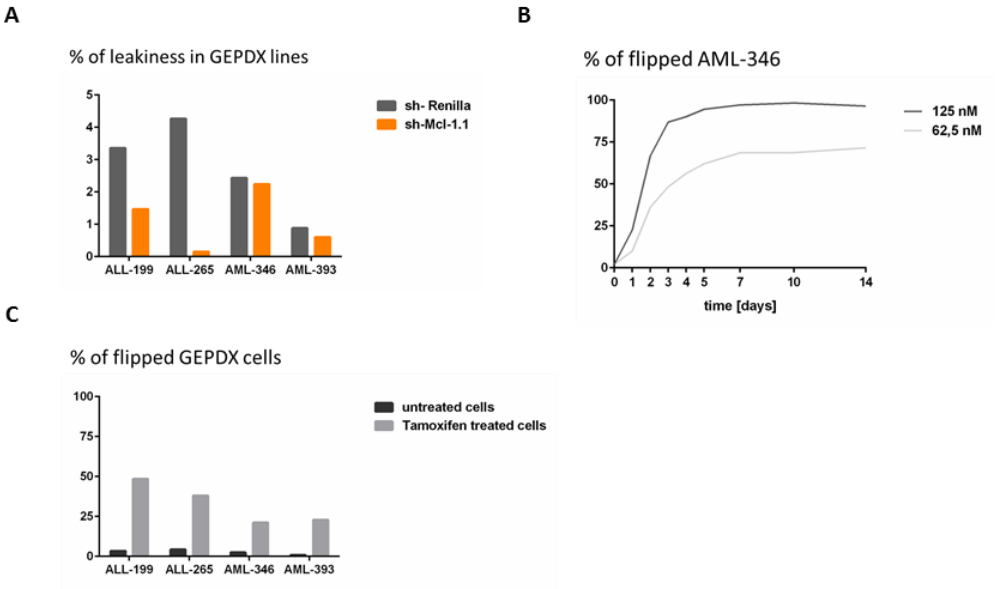

Figure 48. Characterization of the inducible-knockdown system in ALL and AML GEPDX cells *in vitro*.
(A) Percentage of leakiness in two ALL and two AML GEPDX cells transduced with the inducible-knockdown system at 1 week after the transduction with the FLIP-cassette constructs. The sh-Renilla population is depicted in grey and the sh-Mcl-1.1 population in orange.
(B) Analysis of the efficiency of eGFP expression in AML-346 GEPDX cells expressing the sh-Renilla. AML-346 GEPDX cells transduced with the inducible-knockdown system isolated from bone marrow of mice were plated *in vitro*, treated with two different concentrations of Tamoxifen (day 0) and monitored by flow cytometry at the desired time points up to 2 weeks. Quantification of the eGFP expression was performed by flow cytometry as shown in Figure 41.
(C) Analysis of the efficiency of eGFP expression in two ALL and two AML GEPDX cells expressing the sh-Renilla. GEPDX cells transduced with the inducible-knockdown system isolated from bone marrow of mice were plated *in vitro*, treated with Tamoxifen and monitored by flow cytometry at 72 hours after treatment. Quantification of the eGFP expression was performed by flow cytometry as shown in Figure 41.

5.2.7 Mcl-1 is essential for the survival of ALL and AML PDX cells

To extend the study on Mcl-1 in ALL and AML PDX cells, we quantified the knockdown effects in treated GEPDX cells *in vitro*. ALL-265 and AML-346 GEPDX cells transduced with the two-vector inducible-knockdown system were treated with Tamoxifen and analyzed by flow cytometry at different time points. The control and target populations of sample AML-346 showed equal recombination kinetic of the FLIP-cassettes up to one week post treatment. However, the percentage of eGFP positive (thus Mcl-1 negative) cells progressively decreased compared to the control population from one week after the treatment until the end of the experiment, reflecting the Mcl-1-dependent cell death (Figure 49A). The second PDX sample used, the ALL-265, did not show a similar recombination kinetic between the two populations but an increasing difference between the control and the target cells until the end of the experiment, thus reflecting the effects of Mcl-1 knockdown since very early time after the treatment (Figure 49B).

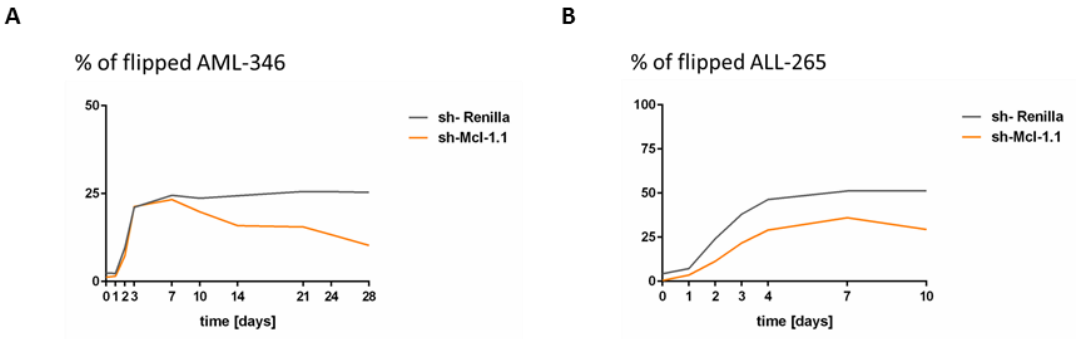

Figure 49. Mcl-1 knockdown induces cell death of ALL and AML GEPDX cells *in vitro*.
(A) Inducible knockdown assay *in vitro* evaluating the cell death of AML-346 GEPDX cells expressing the sh-Mcl-1.1 in comparison to AML-346 GEPDX cells expressing the sh-Renilla. AML-346 GEPDX cells transduced with the inducible-knockdown system isolated from bone marrow of mice were plated *in vitro*, treated with Tamoxifen (day 0) and monitored by flow cytometry at the desired time points up to 4 weeks. Quantification of the sh-Renilla and the sh-Mcl-1.1 populations' distribution was performed by flow cytometry as shown in Figure 41.
(B) Same as in (A). ALL-265 GEPDX cells were used and monitored by flow cytometry at the desired time points up to 10 days.

Although GEPDX cells hardly proliferate *in vitro* and survive only for a short period of time (ALL samples more than AMLs), the results looked promising. Therefore, we decided to perform *in vivo* experiments with ALL and AML GEPDX cells transduced with the inducible-knockdown system. Two different schedules were used for the *in vivo*

experiments: (1) mice were treated with Tamoxifen weeks after cells injection when human blasts could be detected in the peripheral blood, allowing to isolate a high number of GEPDX cells from the bone marrow and facilitating the analysis even shortly after Tamoxifen treatment; (2) treatment with Tamoxifen was done shortly after the engraftment of the cells at one week post injection in order to allow a prolonged period of time before that Tamoxifen-treated mice would succumb to leukemia (Figure 50).

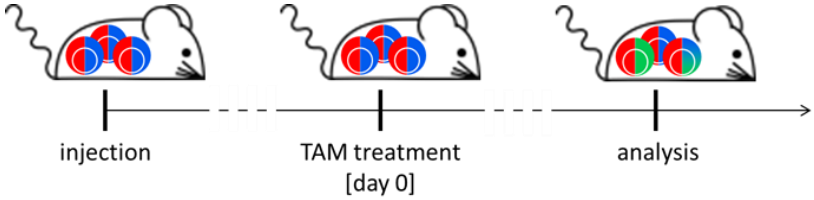

Figure 50. Scheme of the *in vivo* experimental settings with the inducible-knockdown system.
Scheme showing the time line for the *in vivo* inducible knockdown experiments (see paragraph 4.3.9). The treatment with Tamoxifen induces the activity of the CreER^{T2} recombinase; therefore, at the time of isolation of the cells from the bone marrow of mice, the different cell populations can be separated according to the gating strategy shown in Figure 41.

First, we titrated Tamoxifen *in vivo* in order to find a dose able to efficiently induce the recombination but also exerted low toxicity on GEPDX cells. To this aim, mice were injected with either ALL-265 or AML-346 GEPDX cells transduced with the inducible-knockdown system expressing the sh-Renilla and treated with three different doses of Tamoxifen when more than 15% of human blasts could be detected in the peripheral blood. As quality control, the untreated mice were sacrificed to assess the basal leakiness of the system prior the start of the experiment. At 72 hours post treatment, mice were sacrificed and cells were isolated from the bone marrow. An equal volume of cell suspension from all samples was fully analyzed by flow cytometry. The populations' distribution showed that there is a direct correlation between the dose of Tamoxifen used to treat the mice and the eGFP expression. Additionally, the full analysis of a determined volume of cell suspension allowed quantifying the total amount of human cells presents in the bone marrow at the time of isolation, and consequently indirectly assess the toxicity. We could observe again a clear correlation between the total amount of human blasts and Tamoxifen-dependent toxicity (Figure 51).

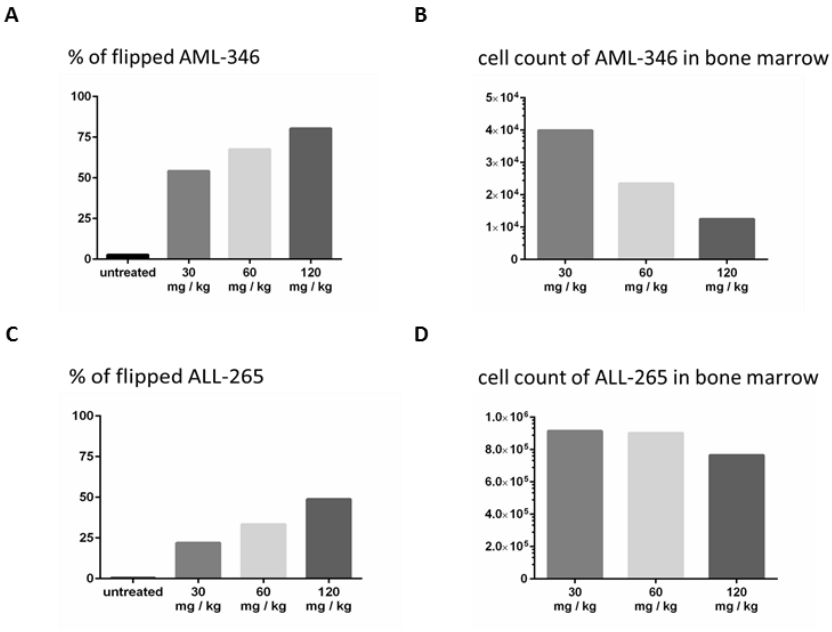

Figure 51. Tamoxifen titration in GEPDX cells expanding in mice.
(A) AML-346 GEPDX cells transduced with the inducible-knockdown system expressing the sh-Renilla were injected into NSG mice (*n* = 8). When more than 15% of human blasts could be detected in the peripheral blood, mice were treated with three different doses of Tamoxifen. Untreated mice were sacrificed prior the start of the experiment, while treated mice were sacrificed at 72 hours after the treatment, and cells were isolated from bone marrow. Quantification of the sh-Renilla and the sh-Mcl-1.1 populations' distribution was performed by flow cytometry as shown in Figure 41. Percentages were quantified relative to the untreated mice.
(B) Total amount of human blasts quantified from samples in (A). One tenth of cell suspension volume after isolation from the bone marrow of mice was fully analyzed by flow cytometry.
(C and D) Same as in (A and B). ALL-265 GEPDX cells were used.

Taking into consideration the previous observations, we selected the application of a single dose of 50 mg/kg of Tamoxifen for all further experiments. We initially screened three of the PDX samples transduced with the inducible-knockdown system. Therefore, several mice were injected with different GEPDX samples and treated with Tamoxifen after one week. Cells were isolated from the bone marrow when mice showed clinical signs of disease and analyzed by flow cytometry to assess the populations' distribution. In all cases, we observed a reduction of the eGFP expressing cells where the shRNA sequence targeting Mcl-1 was expressed. The experiment was repeated for the ALL-265 sample to perform a statistical analysis (Figure 52).

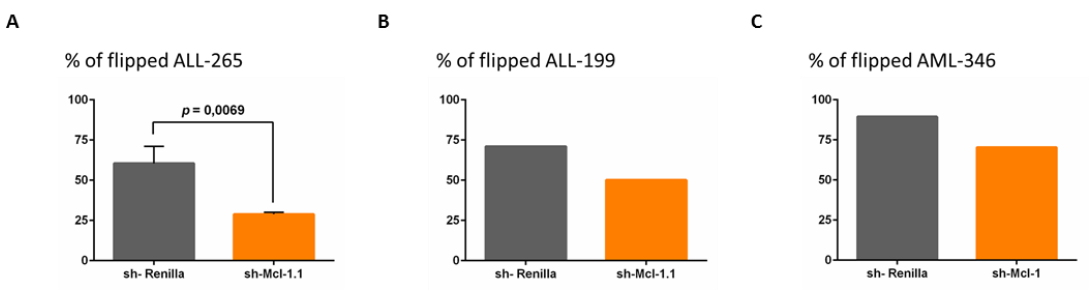

Figure 52. Mcl-1 knockdown induces cell death of ALL and AML GEPDX cells in mice.
(A) Inducible knockdown assay *in vivo* evaluating the cell death of ALL-265 GEPDX cells expressing the sh-Mcl-1.1 compared with ALL-265 GEPDX cells expressing the sh-Renilla. ALL-265 GEPDX cells transduced with the inducible-knockdown system were injected into NSG mice (*n* = 6). 1 week after the injection, mice were treated with Tamoxifen. At first clinical signs of disease, mice were sacrificed and cells were isolated from bone marrow. Quantification of the sh-Renilla and the sh-Mcl-1.1 populations' distribution was performed by flow cytometry as shown in Figure 41. Error bars represent SEM of all mice analyzed at the indicated time point.
(B and C) Same as in (A). ALL-199 (B) and AML-346 (C) GEPDX cells were used (*n* = 4 for each experiment).

Since the ALL-265 sample showed the highest statistically significant sensitivity to Mcl-1 silencing, we used this sample for more detailed analysis to confirm the induction of cell death as consequence of Mcl-1 knockdown. To this aim, mice were injected with cells transduced with the inducible-knockdown system and treated with 50 mg/kg of Tamoxifen when more than 15% of human blast could be detected in the peripheral blood. Cells were isolated from the bone marrow of mice and analyzed by flow cytometry to quantify the populations' distribution every 12 hours post treatment up to 72 hours. This kinetic was performed in order to control and compare the recombination efficiency among the control and target populations. We could show that the two FLIP-cassettes had the same recombination kinetic up to 36 hours post treatment and progressively split until the last time point of analysis, already showing the deathly effect of Mcl-1 knockdown (Figure 53A). To evaluate the effects of Mcl-1 knockdown, a longer experiment was performed. As previously described, mice were injected with transduced ALL-265 PDX cells and treated with Tamoxifen. Twice a week, mice were sacrificed and cells were analyzed by flow cytometry after the isolation from the bone marrow. At three days post treatment, the difference between the two populations was already statistically significant, becoming stronger at the end of the experiment (Figure 53B). At one week post treatment, the eGFP expressing GEPDX cells were enriched via cell sorting after the isolation from the bone marrow. Although the immunoblotting showed a slight knockdown of Mcl-1 in the control population,

probably due to the toxicity still present at this time point, the knockdown was clearly prominent in the target population (Figure 53C). All in all, we could develop a novel system for the inducible knockdown of specific targets in PDX cells expanding in mice, becoming the starting point of a new era of experiments. Additionally, this newly established system suggests the important role of Mcl-1 also in ALL cells.

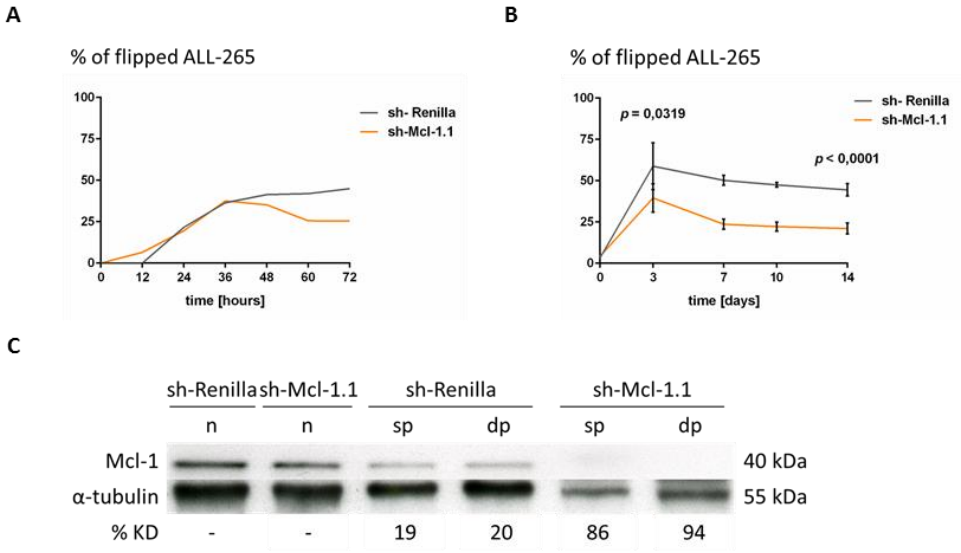

Figure 53. Mcl-1 knockdown induces cell death of GEPDX ALL-265 expanding in mice.
(A) shRNA sequences were expressed after CreER^{T2} induced recombination in the background of the miR-30 backbone as a single transcript together with the eGFP fluorescent marker under the control of the viral SFFV pol-II promoter. ALL-265 GEPDX cells transduced with the inducible-knockdown system were injected into NSG mice (*n* = 14). When more than 15% of human blasts could be detected in the peripheral blood, mice were treated with Tamoxifen (hour 0). Every 12 hours from the moment of the treatment up to 72 hours, mice were sacrificed and cells were isolated from bone marrow. Quantification of the sh-Renilla and the sh-Mcl-1.1 populations' distribution was performed by flow cytometry as shown in Figure 41 to confirm the equal expression of the corresponding associated shRNA sequences.
(B) Inducible knockdown assay *in vivo* evaluating the cell death of ALL-265 GEPDX cells expressing the sh-Mcl-1.1 in comparison to ALL-265 GEPDX cells expressing the sh-Renilla. ALL-265 GEPDX cells transduced with the inducible-knockdown system were injected into NSG mice (*n* = 33). When more than 15% of human blasts could be detected in the peripheral blood, mice were treated with Tamoxifen (day 0). At the desired time point, mice were sacrificed and cells were isolated from bone marrow. Quantification of the sh-Renilla and the sh-Mcl-1.1 populations' distribution was performed by flow cytometry up to 2 weeks after the treatment as shown in Figure 41. Error bars represent SEM of all mice analyzed at the indicated time point.
(C) Western blotting of Mcl-1 in ALL-265 GEPDX cells expressing the sh-Mcl-1.1 in comparison to ALL-265 GEPDX cells expressing the sh-Renilla. 7 days after the treatment with Tamoxifen (day 7 of B), the three populations were separated by cell sorting. Mcl-1 levels were detected and normalized to α-tubulin used as control. The Mcl-1 knockdown levels (%KD) were quantified relative to the control.

6. Discussion

The survival rate for childhood ALL and younger adults suffering of AML has greatly improved during the last decades; however, a subgroup of patients with more aggressive disease still face relapse after the initial chemotherapy because the current front-line treatments are still mainly based on the first drugs developed and thus lack of new valuable options (see Introduction). Therefore, new approaches for the treatment of patients who undergo relapse are intensively needed.

The implementation of profiling techniques in the clinical trial setting is a massive academic reality with an early history in hematological malignancies and which helped identifying actionable targets. However, drug discovery, development and testing remain the major bottlenecks of precision medicine, thus dramatically reducing the possibility of performing both detailed preclinical molecular analyses on the role of specific targets and clinical trials with optimal treatment conditions for the patients (Andre et al. 2014). As wisely suggested by Fellmann and Lowe (Fellmann and Lowe 2014), the current available techniques for studying either specific genetic alterations or patients' (intra-)tumor diversity need to be joined to one another in order to assemble a set of tools able to extend the accuracy of the knowledge and get closer to the patients' condition. Therefore, in this work, we established two versatile tools to silence either non-essential or essential genes in PDX cells expanding in mice. Thus, we are now able to study the role of selected, leukemia-specific target genes in the most suitable cellular context. The selected candidates for this study, XIAP and Mcl-1, are frequently upregulated genes in human cancers, including hematological malignancies and their importance in cell proliferation and survival has been described in previous reports (see Introduction). Hence, we decided to (1) generate an innovative system that give the possibility to elucidate the role of XIAP in human patients' ALL cells expanding in mice, and (2) extend the opportunity to investigate essential genes via creating a system for the inducible knockdown of specific targets in the context of human patients' ALL and AML cells expanding in mice.

6.1 The constitutive-knockdown system

The state of the art technology for understanding the involvement of specific genes in diverse human diseases frequently focuses on intracellular pathways which uses small RNA molecules to modulate the expression level of a gene of interest, thus controlling the amount of the relative protein present in the cells. Until recently, shRNAmir design strategies were mainly based on siRNA data sets without taking in consideration the shRNA processing requirements due to the limited knowledge about the shRNA biogenesis. In 2011, Fellmann et al. have demonstrated that potent single-copy shRNAs share precise sequence features associated with distinct miRNA biogenesis steps, and the most potent shRNAs were also characterized by a striking favoritism for incorporating the guide strand with consequent (1) boost on-target knockdown level, and (2) reduction of passenger-mediated off-target effects (Fellmann et al. 2011). As already described more in detail in the introduction, the use of artificial miR-30 backbones that harbor the sequence for the expression of shRNAs targeting specific proteins has several advantages. One of these advantages is the possibility to backtrack the population of interest which expresses the experimental shRNA via placing the miR-30 shRNAmir cassette in the 3' UTR of a fluorescent marker. In this way, it is possible to quantify the knockdown effects via an easy visualization by flow cytometry of the population of interest at any desired time. Moreover, the presence of a fluorescent marker gives the possibility to select the population of interest without additional manipulations of the cells, as it happens for instance for the selection via antibiotics treatment which might be stressful and armful for the cell.

To select potent shRNA sequences we exploited the DSIR algorithm (Vert et al. 2006) and further optimized the sequences via following the criteria described in Fellmann et al. 2011 (Fellmann et al. 2011). In order to validate the efficiency of the selected shRNA sequences we exploited the Reporter Assay provided by Johannes Zuber (Research Institute of Molecular Pathology - IMP, Vienna, Austria) according to Fellmann et al. 2011 (Fellmann et al. 2011). The Reporter Assay is performed *in vitro* using murine cell lines, thus allowing the study and selection of strong shRNA sequences able to induce highly potent knockdown of the desired target even in the case of very essential genes, which could not be selected otherwise performing the screening in human cell lines. Additionally, all the selected sequences induced a potent reduction of the expression of the protein of interest when tested via Western blotting. All in all, the above described workflow for the selection of potent shRNA sequences turned out to be very successful.

To shuttle the shRNAs into our target cells, the miR-30 cassette expressing the shRNA was placed in the 3' UTR of the dsRED fluorescent marker under the control of a pol-II promoter. This approach directly links the expression of the shRNA to the one of the fluorochrome via the production of a single transcript, in contrast to pol-III promoters. The advantage of this strategy relies in the possibility to control the expression levels of the shRNAs, so that they could be equal in both control and target population, thus facilitating the comparison between the two and making the results more reliable. Furthermore, driving the shRNA expression by the strong viral SFFV promoter had the advantage to induce a strong and stable knockdown over long period of time: remarkably, the knockdown induced by a single copy of the more potent shRNA sequences selected was able to revert almost completely the target overexpression down to the physiological level of normal cells. We believe that the features of our newly designed lentiviral vector used for this study further improved the existing technology.

To fulfill our aim and answer our scientific questions, the system has been designed such that the population of interest could be easily distinct from the control population and therefore allowing competitive assays both *in vitro* and *in vivo*. The possibility to perform competitive assays has several advantages: (1) it minimizes the experimental variance since both populations are in the same context; (2) it allows visualizing small differences because the quantification is direct, simultaneously performed and based only on the ratio between the two populations; and last, but not always less important, (3) it consequently reduces the cost of materials and animals used to perform the experiments. Another technical advantage of this system relies on the fact that it allows the production of frozen stocks of cell populations expressing either the mtagBFP or the eGFP marker color that can be thawed at any time to perform competitive assays for testing any desired target after the simple transduction with the shRNA expressing lentiviral vector, becoming an useful platform for target screening and validation. However, from a technical point of view, the handling of the system needs a good level of precision and manual skills to equally mix the two populations and to perform long-term *in vitro* experiments in order to avoid introducing technical bias in the assays. Moreover, these approaches usually requires several validation steps to be sure that the results of the experiments would not be affected by the intrinsic characteristics of the system itself, such as toxicity due to the ectopic expression of synthetic proteins or the saturation of the RNAi machinery due to the transduction of artificial shRNAs.

As previously mentioned, the PDX mouse model of acute leukemia is the current best model to perform molecular and genetic studies on patients' cells (Morton and Houghton 2007). However, it is important to keep in mind the challenges of PDX cells-based experiments: (1) PDX cells are harder in handling for molecular manipulation compared to established cell lines with consequently an averagely lower efficiency of transduction; to this regard, in order to transduce both cell lines and PDX cells, a third generation lentiviral vector system has been used (Dull et al. 1998; Zufferey et al. 1999). This approach is necessary for the generation of GEPDX because it enables the transduction of non-dividing cells, as for instance xenograft cells which generally do not cycle *in vitro* (Terziyska et al. 2012). Additionally, the viral production was optimized to obtain very high virus titers, thus enhancing the probability of efficient PDX transduction; (2) the lentiviral integration into the genome of the PDX cells might change their properties by causing the modification of the expression of surrounding genes. Nevertheless, until now, we have not detected any alteration of the behavior of the transduced cells that could depend on the lentiviral transduction itself (Terziyska et al. 2012; Vick et al. 2015); and (3) the biological composition of PDX samples is highly more complex in comparison to established cell lines. Nevertheless, although working with PDX samples is more demanding compared to using cell lines and it requires higher technical standards, PDX cells enable the modeling of human acute leukemias because they have the advantage of keeping the typical genetic diversity and therefore they are the best model to get closer to the patients' condition.

The knockdown system described in this thesis has been carefully developed in order to limit and tightly control the above mentioned problems. In summary, we were able to design and validate an efficient and reliable constitutive-knockdown system, which has all the components required to be assessed *in vitro* and *in vivo*, in cell lines as well as in PDX cells. To conclude, our constitutive-knockdown system unlocked a new array of possible functional (and anatomic) studies and could become a platform to study the role of leukemia-specific genes or perform pre-clinical *in vivo* trials and thus helping to gain knowledge in the field of acute leukemias.

6.2 XIAP plays an essential role for the proliferation of human ALL cells

As already described in detail in the introduction, XIAP is the best known member of the IAP family of proteins. Its role is inhibiting both intrinsic and extrinsic pathways of apoptosis via the direct interaction with both initiator and effector caspases (reviewed in Chaudhary et al. 2016; Eckelman, Salvesen, and Scott 2006). The overexpression of XIAP has been demonstrated in a broad variety of human tumors, including hematological malignancies, and it is frequently associated with poor clinical outcome (Schimmer et al. 2006). The therapeutic inhibition of XIAP was reported to be successful in certain solid tumors, especially as sensitizers for chemotherapy (Ehrenschwender et al. 2014; Hu et al. 2003). A second-generation antisense oligonucleotide (ASO) targeting XIAP (AEG35156) entered a phase I/II clinical trial for the treatment of patients with relapsed or refractory AML (Carter et al. 2011); in that study, the knockdown of XIAP on its own was not sufficient to achieve a clinical benefit, while the addition of AEG35156 to the re-induction chemotherapy initially seemed to be well tolerated and associated with a reduction of circulating blasts. However, the first randomized phase II study on AML patients was terminated early as the differences between the study group and the control one were not statistically significant (Katragadda, Carter, and Borthakur 2013). In that case, it could not be excluded that the nature of the ASO's sequence used for the clinical trial might not induce a complete and therefore sufficient knockdown of the XIAP protein in AML blasts. Additionally, yet not enough preclinical studies on ASOs have been performed to exclude that compensatory molecular mechanism and/or off-target effects do not certainly happen.

In my work, I used the newly established system as preclinical platform where the constitutive knockdown of XIAP shall help extending the knowledge about XIAP and uncover its important role also in ALL cells. Thanks to the state of the art technologies concerning the RNAi biogenesis, we were able to design and select shRNAs able to give a strong, specific and stable knockdown of XIAP in ALL cell lines and PDX cells. Although XIAP is well known to be a strong inhibitor of apoptosis, its loss did not result in a drastic reduction of the cell population carrying the XIAP knockdown. Nevertheless, the difference between the control and the target populations was progressively increasing over time. This observation suggests that silencing XIAP is sufficient to generate a proliferative disadvantage. However, further studies are needed to understand the details about the molecular involvement of XIAP in altering the proliferation of ALL cells.

The ALL PDX samples selected for this study were originated from relapsed childhood ALL leukemias and present XIAP overexpression. As already mentioned in the introduction, the relapse is usually associated with sub-optimal re-induction remission rates even if the biological features of the relapse-inducing cells are still unclear. However, the results obtained from the *in vivo* experiments with these two GEPDX samples are promising because they highlighted the dependency of these tumor cells on the alteration of this protein as the mere silencing of XIAP is enough to induce a proliferation disadvantage. Moreover, it would be interesting to repeat the same experiments on samples that do not present XIAP overexpression in order to verify whether the knockdown effects are even more prominent.

Taken together, thanks to the strong and stable knockdown, the newly established competitive system allowed deciphering the dependency of acute leukemias' cells on XIAP in a model which closely mimics the complex environment of individual patients' tumor cells.

6.3 The inducible-knockdown system

The ultimate goal of precision medicine, an attractive novel therapeutic concept, is the design of therapies adapted to the individual characteristic of each patient. A large number of compounds targeting cancer specific genetic alterations have been recently developed and entered clinical trials. Nevertheless, many clinical trials on targeted therapies still failed. In many different cancer fields the search for genes which are essential to sustain the tumor development is required to promote the development of new chemotherapeutic strategies. However, essential genes are, as a matter of fact, more difficult to be studied because their loss-of-function might induce cell death even during the production of the genetically engineered cells, making impossible to perform any sort of further experiment. The possibility to induce the knockdown of the desired target at a specific time circumvents this problem and raises the possibility to potentially study any kind of gene at any given time in the life of the organism of interest.

Based on the positive results collected with the constitutive-knockdown system, we followed the same workflow to select an efficient shRNA sequence and express it using the strong viral SFFV promoter. Moreover, in order to induce an efficient recombination process in our target cells, the expression of the CreER^{T2} enzyme was also driven by the same viral promoter.

As previously described, Stern et al. developed a system for Cre-mediated gene expression (Stern et al. 2008). For the design of our inducible-knockdown system we adapted their technology to our need; in particular, we changed the markers for the selection of the transduced cells with two different fluorochromes and transfer this new FLIP-cassette into our pCDH lentiviral backbone. In this way, we generated a system which combines together (1) the ability to induce potent knockdown via using the rules described by Fellmann et al. in 2011 (Fellmann et al. 2011), (2) the possibility to easily backtrack our population of interest via placing the miR-30 shRNAmir cassette in the 3' UTR of a fluorescent marker, and (3) the capability to induce the knockdown at the desired time thanks to the recombination of the FLIP-cassette by a Tamoxifen-dependent Cre recombinase.

Our preliminary results in PDX cells showed a direct correlation between the CreER^{T2} induced toxicity in the control population and the transduction efficiency with the vector expressing the CreER^{T2}. Therefore, in order to avoid toxicity problems related to the expression of the enzyme and subsequent off-target recombination but still have enough amount of it for an efficient expression of the FLIP-cassette(s), we decided to transduce our target cells with an

efficiency between 20% and 50%. However, since PDX cells cannot be transduced easily, it was challenging to obtain the desired transduction efficiency for two main reasons: (1) the transduction efficiency decreases when the size of the vector increases; (2) sample-specific features that make some sample more difficult to be molecularly manipulated, even when using very high titer viruses. On the contrary, the transduction efficiency with the FLIP-cassette vector was easier because of its smaller size. At the end, those samples not fulfilling the required expression levels of the vectors of the system were simply excluded from the study. After titration of the $CreER^{T2}$ enzyme expression in our cell lines, we could still observe a transient $CreER^{T2}$ induced toxicity up to one week post Tamoxifen treatment, reflected in the reduction of eGFP expression from the initial peak to the following plateau in the control population. In comparison to cell lines, this effect was not visible in GEPDX cells *in vitro*, most probably because of (1) a lower recombination rate with consequent lower toxicity, (2) a slower kinetic in the expression of artificial transgenes after the recombination process, and (3) a higher sensitivity of the cells to the recombination process and consequent quicker death preceding the eGFP expression. However, a similar tendency was visible in the control population of the *in vivo* experiment.

To test and validate our inducible-knockdown system *in vivo*, we decided to target Mcl-1 because of its important role in cell survival and its demonstrated correlation with both cancer cell survival and resistance to chemotherapy (see Introduction). The quantification of the protein expression level of Mcl-1 revealed a potent knockdown after the induction of recombination by Tamoxifen treatment, proving the success of the knockdown strategy. Although silencing Mcl-1 in the AML cell line MV4-11 and in different PDX samples did not result in a complete loss of the target population, the proliferation kinetic was significantly altered.

Taken together, with this novel system for the inducible knockdown of specific targets is now possible to perform a variety of different studies, thus raising the opportunity to greatly extend the knowledge about, in principle, any desired gene in the context of individual patients' tumor cells *in vivo*. However, although the strategy to backtrack the cells of interest, thanks to the expression of fluorochromes visible by flow cytometry, is an advantage for the analysis of the experiments, the quantification of the results was more challenging, especially in the case of PDX cells isolated from mice, because the comparison between control and target population was performed on cells derived from separate contexts. Therefore, the optimization of the system to generate a tool for an inducible knockdown but with the possibility to perform competitive assays would be highly desired.

6.4 Concluding remarks and future perspectives

All in all, this study presents, for the first time, novel integrated techniques for the knockdown of the desired target genes, opening new possibilities to investigate in principle any desired gene both *in vitro* and *in vivo* with a yet unprecedented quality.

One of the most attractive possibilities is the targeting of tumor-specific alterations in order to reduce the side effects on healthy cells, as the targeting of oncogenic translocations. However, this approach restricts the selection of the shRNA sequence to the specific region of the genome where the breakpoint occurs with a higher probability of not being able to generate shRNAs potent enough to induce a strong knockdown. On the other hand, the generation of shRNA sequences for the targeting of tumor-specific translocations would allow circumventing the resistance to therapies given by specific gene mutations, as in the case of BCR-ABL1 positive leukemias not responding to Imatinib treatment due to the T315I mutation.

Another possible use of the two systems presented in this study, is as platforms for drug testing in preclinical trials, with the possibility to follow up the *in vivo* experiments thanks to the expression of luciferases. Currently, there is a high interest in finding new treatment options for patients; therefore, an increasing number of studies focus on the development of drugs combinations that might improve the survival rate. For instance, the silencing of a specific tumor gene might be tested in combination with the commonly used chemotherapeutic drugs to enhance their effects, either in an addictive or synergistic way, thus giving the possibility to reduce the drug dose and therefore limiting its side effects.

Other potential studies stray in the field of stem cells and regenerative medicine therapy. For instance, in hematopoietic research, a lot of attention is directed towards the understanding of the mechanisms behind mobilization and homing of stem cells in the bone marrow; also in this setting, the use of the described tools might help to decipher and interpret the molecular pathways which regulate these two important mechanisms.

Beside the big advantages for the scientific research provided by these newly established knockdown systems, it is already possible to improve them with several new strategies developed in parallel. For example, it has been shown that the single-copy expression of the even more potent sequence results in a relatively low level of mature shRNA, suggesting that the miR-30 backbone could be further optimized (Fellmann et al. 2013). Also, it has been

demonstrated that the enzymatic activity of Cre can be even more tightly controlled via placing two human ER^{T2} on both sides of the enzyme (Zhang et al. 1996).

Over the improvement that can be operated on the systems itself, a variety of conceivable changes are possible in order to create more complex tools. For example, as previously mentioned, a competitive inducible system would enable easier analysis and results interpretation; the concatenation of several miR-30 shRNAmir cassettes could allow targeting the different splice variants of a gene, or even different genes; the combination with other molecular tools for genome editing such as CRISPR/Cas9 and TALEN could be addressed. However, the development of other methods is also highly required in order to make these advanced techniques available also for the clinical use, for instance several clinical trials are currently active for the study of safe viral and non-viral methods for the delivery of small DNA or RNA molecules in a specific tissue or in a whole body.

In conclusion, this work offers both new useful tools for a variety of further studies and also a starting point for the development of even more sophisticated systems able to answer future questions.

7. References

Adams, J. M., and S. Cory. 1998. 'The Bcl-2 protein family: arbiters of cell survival', *Science*, 281: 1322-6.

Adams, J. M., D. C. Huang, H. Puthalakath, P. Bouillet, G. Vairo, K. Moriishi, G. Hausmann, L. O'Reilly, K. Newton, S. Ogilvy, M. L. Bath, C. G. Print, A. W. Harris, A. Strasser, and S. Cory. 1999. 'Control of apoptosis in hematopoietic cells by the Bcl-2 family of proteins', *Cold Spring Harb Symp Quant Biol*, 64: 351-8.

Ahuja, D., M. T. Saenz-Robles, and J. M. Pipas. 2005. 'SV40 large T antigen targets multiple cellular pathways to elicit cellular transformation', *Oncogene*, 24: 7729-45.

Akgul, C., D. A. Moulding, M. R. White, and S. W. Edwards. 2000. 'In vivo localisation and stability of human Mcl-1 using green fluorescent protein (GFP) fusion proteins', *FEBS Lett*, 478: 72-6.

Akgul, C., P. C. Turner, M. R. White, and S. W. Edwards. 2000. 'Functional analysis of the human MCL-1 gene', *Cell Mol Life Sci*, 57: 684-91.

Andre, F., E. Mardis, M. Salm, J. C. Soria, L. L. Siu, and C. Swanton. 2014. 'Prioritizing targets for precision cancer medicine', *Ann Oncol*, 25: 2295-303.

Balduzzi, A., M. G. Valsecchi, C. Uderzo, P. De Lorenzo, T. Klingebiel, C. Peters, J. Stary, M. S. Felice, E. Magyarosy, V. Conter, A. Reiter, C. Messina, H. Gadner, and M. Schrappe. 2005. 'Chemotherapy versus allogeneic transplantation for very-high-risk childhood acute lymphoblastic leukaemia in first complete remission: comparison by genetic randomisation in an international prospective study', *Lancet*, 366: 635-42.

Barrett, D. M., A. E. Seif, C. Carpenito, D. T. Teachey, J. D. Fish, C. H. June, S. A. Grupp, and G. S. Reid. 2011. 'Noninvasive bioluminescent imaging of primary patient acute lymphoblastic leukemia: a strategy for preclinical modeling', *Blood*, 118: e112-7.

Bartel, B., and D. P. Bartel. 2003. 'MicroRNAs: at the root of plant development?', *Plant Physiol*, 132: 709-17.

Bartel, D. P. 2004. 'MicroRNAs: genomics, biogenesis, mechanism, and function', *Cell*, 116: 281-97.

Bassan, R., and D. Hoelzer. 2011. 'Modern therapy of acute lymphoblastic leukemia', *J Clin Oncol*, 29: 532-43.

Belz, K., H. Schoeneberger, S. Wehner, A. Weigert, H. Bonig, T. Klingebiel, I. Fichtner, and S. Fulda. 2014. 'Smac mimetic and glucocorticoids synergize to induce apoptosis in childhood ALL by promoting ripoptosome assembly', *Blood*, 124: 240-50.

Borchert, G. M., W. Lanier, and B. L. Davidson. 2006. 'RNA polymerase III transcribes human microRNAs', *Nat Struct Mol Biol*, 13: 1097-101.

Bradford, M. M. 1976. 'A rapid and sensitive method for the quantitation of microgram quantities of protein utilizing the principle of protein-dye binding', *Anal Biochem*, 72: 248-54.

Breems, D. A., W. L. Van Putten, P. C. Huijgens, G. J. Ossenkoppele, G. E. Verhoef, L. F. Verdonck, E. Vellenga, G. E. De Greef, E. Jacky, J. Van der Lelie, M. A. Boogaerts, and B. Lowenberg. 2005. 'Prognostic index for adult patients with acute myeloid leukemia in first relapse', *J Clin Oncol*, 23: 1969-78.

Campbell, K. J., M. L. Bath, M. L. Turner, C. J. Vandenberg, P. Bouillet, D. Metcalf, C. L. Scott, and S. Cory. 2010. 'Elevated Mcl-1 perturbs lymphopoiesis, promotes transformation of hematopoietic stem/progenitor cells, and enhances drug resistance', *Blood*, 116: 3197-207.

Carter, B. Z., D. H. Mak, S. J. Morris, G. Borthakur, E. Estey, A. L. Byrd, M. Konopleva, H. Kantarjian, and M. Andreeff. 2011. 'XIAP antisense oligonucleotide (AEG35156) achieves target knockdown and induces apoptosis preferentially in CD34+38- cells in a phase 1/2 study of patients with relapsed/refractory AML', *Apoptosis*, 16: 67-74.

Chaudhary, A. K., N. Yadav, T. A. Bhat, J. O'Malley, S. Kumar, and D. Chandra. 2016. 'A potential role of X-linked inhibitor of apoptosis protein in mitochondrial membrane permeabilization and its implication in cancer therapy', *Drug Discov Today*, 21: 38-47.

Chesler, L., and W. A. Weiss. 2011. 'Genetically engineered murine models--contribution to our understanding of the genetics, molecular pathology and therapeutic targeting of neuroblastoma', *Semin Cancer Biol*, 21: 245-55.

Chessells, J. M., P. Veys, H. Kempski, P. Henley, A. Leiper, D. Webb, and I. M. Hann. 2003. 'Long-term follow-up of relapsed childhood acute lymphoblastic leukaemia', *Br J Haematol*, 123: 396-405.

Clappier, E., B. Gerby, F. Sigaux, M. Delord, F. Touzri, L. Hernandez, P. Ballerini, A. Baruchel, F. Pflumio, and J. Soulier. 2011. 'Clonal selection in xenografted human T cell acute lymphoblastic leukemia recapitulates gain of malignancy at relapse', *J Exp Med*, 208: 653-61.

Cornils, K., L. Thielecke, S. Huser, M. Forgber, M. Thomaschewski, N. Kleist, K. Hussein, K. Riecken, T. Volz, S. Gerdes, I. Glauche, A. Dahl, M. Dandri, I. Roeder, and B. Fehse. 2014. 'Multiplexing clonality: combining RGB marking and genetic barcoding', *Nucleic Acids Res*, 42: e56.

Craig, R. W. 2002. 'MCL1 provides a window on the role of the BCL2 family in cell proliferation, differentiation and tumorigenesis', *Leukemia*, 16: 444-54.

Curtin, J. F., and T. G. Cotter. 2003. 'Live and let die: regulatory mechanisms in Fas-mediated apoptosis', *Cell Signal*, 15: 983-92.

Czabotar, P. E., G. Lessene, A. Strasser, and J. M. Adams. 2014. 'Control of apoptosis by the BCL-2 protein family: implications for physiology and therapy', *Nat Rev Mol Cell Biol*, 15: 49-63.

Davis, H. E., M. Rosinski, J. R. Morgan, and M. L. Yarmush. 2004. 'Charged polymers modulate retrovirus transduction via membrane charge neutralization and virus aggregation', *Biophys J*, 86: 1234-42.

Deschler, B., and M. Lubbert. 2006. 'Acute myeloid leukemia: epidemiology and etiology', *Cancer*, 107: 2099-107.

Dombret, H., and C. Gardin. 2016. 'An update of current treatments for adult acute myeloid leukemia', *Blood*, 127: 53-61.

Domcke, S., R. Sinha, D. A. Levine, C. Sander, and N. Schultz. 2013. 'Evaluating cell lines as tumour models by comparison of genomic profiles', *Nat Commun*, 4: 2126.

Dull, T., R. Zufferey, M. Kelly, R. J. Mandel, M. Nguyen, D. Trono, and L. Naldini. 1998. 'A third-generation lentivirus vector with a conditional packaging system', *J Virol*, 72: 8463-71.

Duy, C., C. Hurtz, S. Shojaee, L. Cerchietti, H. Geng, S. Swaminathan, L. Klemm, S. M. Kweon, R. Nahar, M. Braig, E. Park, Y. M. Kim, W. K. Hofmann, S. Herzog, H. Jumaa, H. P. Koeffler, J. J. Yu, N. Heisterkamp, T. G. Graeber, H. Wu, B. H. Ye, A. Melnick, and M. Muschen. 2011. 'BCL6 enables Ph+ acute lymphoblastic leukaemia cells to survive BCR-ABL1 kinase inhibition', *Nature*, 473: 384-8.

Dzhagalov, I., A. St John, and Y. W. He. 2007. 'The antiapoptotic protein Mcl-1 is essential for the survival of neutrophils but not macrophages', *Blood*, 109: 1620-6.

Ebinger, S., E. Z. Ozdemir, C. Ziegenhain, S. Tiedt, C. Castro Alves, M. Grunert, M. Dworzak, C. Lutz, V. A. Turati, T. Enver, H. P. Horny, K. Sotlar, S. Parekh, K. Spiekermann, W. Hiddemann, A. Schepers, B. Polzer, S. Kirsch, M. Hoffmann, B. Knapp, J. Hasenauer, H. Pfeifer, R. Panzer-Grumayer, W. Enard, O. Gires, and I. Jeremias. 2016. 'Characterization of Rare, Dormant, and Therapy-Resistant Cells in Acute Lymphoblastic Leukemia', *Cancer Cell*, 30: 849-62.

Eckelman, B. P., G. S. Salvesen, and F. L. Scott. 2006. 'Human inhibitor of apoptosis proteins: why XIAP is the black sheep of the family', *EMBO Rep*, 7: 988-94.

Ehrenschwender, M., S. Bittner, K. Seibold, and H. Wajant. 2014. 'XIAP-targeting drugs re-sensitize PIK3CA-mutated colorectal cancer cells for death receptor-induced apoptosis', *Cell Death Dis*, 5: e1570.
Eifert, C., and R. S. Powers. 2012. 'From cancer genomes to oncogenic drivers, tumour dependencies and therapeutic targets', *Nat Rev Cancer*, 12: 572-8.
Elbashir, S. M., W. Lendeckel, and T. Tuschl. 2001. 'RNA interference is mediated by 21- and 22-nucleotide RNAs', *Genes Dev*, 15: 188-200.
Elmore, S. 2007. 'Apoptosis: a review of programmed cell death', *Toxicol Pathol*, 35: 495-516.
Esparza, S. D., and K. M. Sakamoto. 2005. 'Topics in pediatric leukemia--acute lymphoblastic leukemia', *MedGenMed*, 7: 23.
Estey, E., and H. Dohner. 2006. 'Acute myeloid leukaemia', *Lancet*, 368: 1894-907.
Estey, E. H. 2014. 'Acute myeloid leukemia: 2014 update on risk-stratification and management', *Am J Hematol*, 89: 1063-81.
Evans, M. K., S. J. Sauer, S. Nath, T. J. Robinson, M. A. Morse, and G. R. Devi. 2016. 'X-linked inhibitor of apoptosis protein mediates tumor cell resistance to antibody-dependent cellular cytotoxicity', *Cell Death Dis*, 7: e2073.
Feil, R., J. Wagner, D. Metzger, and P. Chambon. 1997. 'Regulation of Cre recombinase activity by mutated estrogen receptor ligand-binding domains', *Biochem Biophys Res Commun*, 237: 752-7.
Fellmann, C., T. Hoffmann, V. Sridhar, B. Hopfgartner, M. Muhar, M. Roth, D. Y. Lai, I. A. Barbosa, J. S. Kwon, Y. Guan, N. Sinha, and J. Zuber. 2013. 'An optimized microRNA backbone for effective single-copy RNAi', *Cell Rep*, 5: 1704-13.
Fellmann, C., and S. W. Lowe. 2014. 'Stable RNA interference rules for silencing', *Nat Cell Biol*, 16: 10-8.
Fellmann, C., J. Zuber, K. McJunkin, K. Chang, C. D. Malone, R. A. Dickins, Q. Xu, M. O. Hengartner, S. J. Elledge, G. J. Hannon, and S. W. Lowe. 2011. 'Functional identification of optimized RNAi triggers using a massively parallel sensor assay', *Mol Cell*, 41: 733-46.
Foley, G. E., H. Lazarus, S. Farber, B. G. Uzman, B. A. Boone, and R. E. McCarthy. 1965. 'Continuous Culture of Human Lymphoblasts from Peripheral Blood of a Child with Acute Leukemia', *Cancer*, 18: 522-9.
Fujise, K., D. Zhang, J. Liu, and E. T. Yeh. 2000. 'Regulation of apoptosis and cell cycle progression by MCL1. Differential role of proliferating cell nuclear antigen', *J Biol Chem*, 275: 39458-65.
Fulda, S., and D. Vucic. 2012. 'Targeting IAP proteins for therapeutic intervention in cancer', *Nat Rev Drug Discov*, 11: 109-24.
Galban, S., and C. S. Duckett. 2010. 'XIAP as a ubiquitin ligase in cellular signaling', *Cell Death Differ*, 17: 54-60.
Gillet, J. P., S. Varma, and M. M. Gottesman. 2013. 'The clinical relevance of cancer cell lines', *J Natl Cancer Inst*, 105: 452-8.
Golden, D. E., V. R. Gerbasi, and E. J. Sontheimer. 2008. 'An inside job for siRNAs', *Mol Cell*, 31: 309-12.
Green, D. R. 2005. 'Apoptotic pathways: ten minutes to dead', *Cell*, 121: 671-4.
Hamilton, D. L., and K. Abremski. 1984. 'Site-specific recombination by the bacteriophage P1 lox-Cre system. Cre-mediated synapsis of two lox sites', *J Mol Biol*, 178: 481-6.
Hanahan, D., and R. A. Weinberg. 2000. 'The hallmarks of cancer', *Cell*, 100: 57-70.
———. 2011. 'Hallmarks of cancer: the next generation', *Cell*, 144: 646-74.
Harlin, H., S. B. Reffey, C. S. Duckett, T. Lindsten, and C. B. Thompson. 2001. 'Characterization of XIAP-deficient mice', *Mol Cell Biol*, 21: 3604-8.
Hu, Y., G. Cherton-Horvat, V. Dragowska, S. Baird, R. G. Korneluk, J. P. Durkin, L. D. Mayer, and E. C. LaCasse. 2003. 'Antisense oligonucleotides targeting XIAP induce apoptosis

and enhance chemotherapeutic activity against human lung cancer cells in vitro and in vivo', *Clin Cancer Res*, 9: 2826-36.

Huang, Y., Y. C. Park, R. L. Rich, D. Segal, D. G. Myszka, and H. Wu. 2001. 'Structural basis of caspase inhibition by XIAP: differential roles of the linker versus the BIR domain', *Cell*, 104: 781-90.

Hurwitz, R., J. Hozier, T. LeBien, J. Minowada, K. Gajl-Peczalska, I. Kubonishi, and J. Kersey. 1979. 'Characterization of a leukemic cell line of the pre-B phenotype', *Int J Cancer*, 23: 174-80.

Hutter, G., C. Nickenig, H. Garritsen, F. Hellenkamp, A. Hoerning, W. Hiddemann, and M. Dreyling. 2004. 'Use of polymorphisms in the noncoding region of the human mitochondrial genome to identify potential contamination of human leukemia-lymphoma cell lines', *Hematol J*, 5: 61-8.

Hutvagner, G., and P. D. Zamore. 2002. 'A microRNA in a multiple-turnover RNAi enzyme complex', *Science*, 297: 2056-60.

Igney, F. H., and P. H. Krammer. 2002. 'Death and anti-death: tumour resistance to apoptosis', *Nat Rev Cancer*, 2: 277-88.

Inaba, H., M. Greaves, and C. G. Mullighan. 2013. 'Acute lymphoblastic leukaemia', *Lancet*, 381: 1943-55.

Indra, A. K., X. Warot, J. Brocard, J. M. Bornert, J. H. Xiao, P. Chambon, and D. Metzger. 1999. 'Temporally-controlled site-specific mutagenesis in the basal layer of the epidermis: comparison of the recombinase activity of the tamoxifen-inducible Cre-ER(T) and Cre-ER(T2) recombinases', *Nucleic Acids Res*, 27: 4324-7.

Itoh, K., H. Tezuka, H. Sakoda, M. Konno, K. Nagata, T. Uchiyama, H. Uchino, and K. J. Mori. 1989. 'Reproducible establishment of hemopoietic supportive stromal cell lines from murine bone marrow', *Exp Hematol*, 17: 145-53.

Jacoby, E., C. D. Chien, and T. J. Fry. 2014. 'Murine models of acute leukemia: important tools in current pediatric leukemia research', *Front Oncol*, 4: 95.

Jamil, S., R. Sobouti, P. Hojabrpour, M. Raj, J. Kast, and V. Duronio. 2005. 'A proteolytic fragment of Mcl-1 exhibits nuclear localization and regulates cell growth by interaction with Cdk1', *Biochem J*, 387: 659-67.

Joazeiro, C. A., and A. M. Weissman. 2000. 'RING finger proteins: mediators of ubiquitin ligase activity', *Cell*, 102: 549-52.

Kaelin, W. G., Jr. 2012. 'Molecular biology. Use and abuse of RNAi to study mammalian gene function', *Science*, 337: 421-2.

Kamel-Reid, S., M. Letarte, C. Sirard, M. Doedens, T. Grunberger, G. Fulop, M. H. Freedman, R. A. Phillips, and J. E. Dick. 1989. 'A model of human acute lymphoblastic leukemia in immune-deficient SCID mice', *Science*, 246: 1597-600.

Katragadda, L., B. Z. Carter, and G. Borthakur. 2013. 'XIAP antisense therapy with AEG 35156 in acute myeloid leukemia', *Expert Opin Investig Drugs*, 22: 663-70.

Kerr, J. F., C. M. Winterford, and B. V. Harmon. 1994. 'Apoptosis. Its significance in cancer and cancer therapy', *Cancer*, 73: 2013-26.

Koreth, J., R. Schlenk, K. J. Kopecky, S. Honda, J. Sierra, B. J. Djulbegovic, M. Wadleigh, D. J. DeAngelo, R. M. Stone, H. Sakamaki, F. R. Appelbaum, H. Dohner, J. H. Antin, R. J. Soiffer, and C. Cutler. 2009. 'Allogeneic stem cell transplantation for acute myeloid leukemia in first complete remission: systematic review and meta-analysis of prospective clinical trials', *JAMA*, 301: 2349-61.

Kozopas, K. M., T. Yang, H. L. Buchan, P. Zhou, and R. W. Craig. 1993. 'MCL1, a gene expressed in programmed myeloid cell differentiation, has sequence similarity to BCL2', *Proc Natl Acad Sci U S A*, 90: 3516-20.

Kroemer, G., L. Galluzzi, P. Vandenabeele, J. Abrams, E. S. Alnemri, E. H. Baehrecke, M. V. Blagosklonny, W. S. El-Deiry, P. Golstein, D. R. Green, M. Hengartner, R. A. Knight, S. Kumar, S. A. Lipton, W. Malorni, G. Nunez, M. E. Peter, J. Tschopp, J. Yuan, M.

Piacentini, B. Zhivotovsky, G. Melino, and Death Nomenclature Committee on Cell. 2009. 'Classification of cell death: recommendations of the Nomenclature Committee on Cell Death 2009', *Cell Death Differ*, 16: 3-11.

Kwan, K. M. 2002. 'Conditional alleles in mice: practical considerations for tissue-specific knockouts', *Genesis*, 32: 49-62.

Lange, B., M. Valtieri, D. Santoli, D. Caracciolo, F. Mavilio, I. Gemperlein, C. Griffin, B. Emanuel, J. Finan, P. Nowell, and et al. 1987. 'Growth factor requirements of childhood acute leukemia: establishment of GM-CSF-dependent cell lines', *Blood*, 70: 192-9.

Langer, S. J., A. P. Ghafoori, M. Byrd, and L. Leinwand. 2002. 'A genetic screen identifies novel non-compatible loxP sites', *Nucleic Acids Res*, 30: 3067-77.

Lee, E. M., P. S. Bachmann, and R. B. Lock. 2007. 'Xenograft models for the preclinical evaluation of new therapies in acute leukemia', *Leuk Lymphoma*, 48: 659-68.

Lee, G., and I. Saito. 1998. 'Role of nucleotide sequences of loxP spacer region in Cre-mediated recombination', *Gene*, 216: 55-65.

Lee, R. C., R. L. Feinbaum, and V. Ambros. 1993. 'The C. elegans heterochronic gene lin-4 encodes small RNAs with antisense complementarity to lin-14', *Cell*, 75: 843-54.

Lee, Y., M. Kim, J. Han, K. H. Yeom, S. Lee, S. H. Baek, and V. N. Kim. 2004. 'MicroRNA genes are transcribed by RNA polymerase II', *EMBO J*, 23: 4051-60.

Letai, A., M. C. Bassik, L. D. Walensky, M. D. Sorcinelli, S. Weiler, and S. J. Korsmeyer. 2002. 'Distinct BH3 domains either sensitize or activate mitochondrial apoptosis, serving as prototype cancer therapeutics', *Cancer Cell*, 2: 183-92.

Liem, N. L., R. A. Papa, C. G. Milross, M. A. Schmid, M. Tajbakhsh, S. Choi, C. D. Ramirez, A. M. Rice, M. Haber, M. D. Norris, K. L. MacKenzie, and R. B. Lock. 2004. 'Characterization of childhood acute lymphoblastic leukemia xenograft models for the preclinical evaluation of new therapies', *Blood*, 103: 3905-14.

Lu, M., S. C. Lin, Y. Huang, Y. J. Kang, R. Rich, Y. C. Lo, D. Myszka, J. Han, and H. Wu. 2007. 'XIAP induces NF-kappaB activation via the BIR1/TAB1 interaction and BIR1 dimerization', *Mol Cell*, 26: 689-702.

Matsuo, Y., R. A. MacLeod, C. C. Uphoff, H. G. Drexler, C. Nishizaki, Y. Katayama, G. Kimura, N. Fujii, E. Omoto, M. Harada, and K. Orita. 1997. 'Two acute monocytic leukemia (AML-M5a) cell lines (MOLM-13 and MOLM-14) with interclonal phenotypic heterogeneity showing MLL-AF9 fusion resulting from an occult chromosome insertion, ins(11;9)(q23;p22p23)', *Leukemia*, 11: 1469-77.

Mayer, R. J., R. B. Davis, C. A. Schiffer, D. T. Berg, B. L. Powell, P. Schulman, G. A. Omura, J. O. Moore, O. R. McIntyre, and E. Frei, 3rd. 1994. 'Intensive postremission chemotherapy in adults with acute myeloid leukemia. Cancer and Leukemia Group B', *N Engl J Med*, 331: 896-903.

Metzger, D., J. Clifford, H. Chiba, and P. Chambon. 1995. 'Conditional site-specific recombination in mammalian cells using a ligand-dependent chimeric Cre recombinase', *Proc Natl Acad Sci U S A*, 92: 6991-5.

Mikhailov, V., M. Mikhailova, K. Degenhardt, M. A. Venkatachalam, E. White, and P. Saikumar. 2003. 'Association of Bax and Bak homo-oligomers in mitochondria. Bax requirement for Bak reorganization and cytochrome c release', *J Biol Chem*, 278: 5367-76.

Morita, S., T. Kojima, and T. Kitamura. 2000. 'Plat-E: an efficient and stable system for transient packaging of retroviruses', *Gene Ther*, 7: 1063-6.

Morton, C. L., and P. J. Houghton. 2007. 'Establishment of human tumor xenografts in immunodeficient mice', *Nat Protoc*, 2: 247-50.

Mott, J. L., S. Kobayashi, S. F. Bronk, and G. J. Gores. 2007. 'mir-29 regulates Mcl-1 protein expression and apoptosis', *Oncogene*, 26: 6133-40.

Mwenifumbo, J. C., and M. A. Marra. 2013. 'Cancer genome-sequencing study design', *Nat Rev Genet*, 14: 321-32.

Nagy, A. 2000. 'Cre recombinase: the universal reagent for genome tailoring', *Genesis*, 26: 99-109.

Nijhawan, D., M. Fang, E. Traer, Q. Zhong, W. Gao, F. Du, and X. Wang. 2003. 'Elimination of Mcl-1 is required for the initiation of apoptosis following ultraviolet irradiation', *Genes Dev*, 17: 1475-86.

Ninomiya, M., A. Abe, A. Katsumi, J. Xu, M. Ito, F. Arai, T. Suda, M. Ito, H. Kiyoi, T. Kinoshita, and T. Naoe. 2007. 'Homing, proliferation and survival sites of human leukemia cells in vivo in immunodeficient mice', *Leukemia*, 21: 136-42.

Oltersdorf, T., S. W. Elmore, A. R. Shoemaker, R. C. Armstrong, D. J. Augeri, B. A. Belli, M. Bruncko, T. L. Deckwerth, J. Dinges, P. J. Hajduk, M. K. Joseph, S. Kitada, S. J. Korsmeyer, A. R. Kunzer, A. Letai, C. Li, M. J. Mitten, D. G. Nettesheim, S. Ng, P. M. Nimmer, J. M. O'Connor, A. Oleksijew, A. M. Petros, J. C. Reed, W. Shen, S. K. Tahir, C. B. Thompson, K. J. Tomaselli, B. Wang, M. D. Wendt, H. Zhang, S. W. Fesik, and S. H. Rosenberg. 2005. 'An inhibitor of Bcl-2 family proteins induces regression of solid tumours', *Nature*, 435: 677-81.

Opferman, J. T., H. Iwasaki, C. C. Ong, H. Suh, S. Mizuno, K. Akashi, and S. J. Korsmeyer. 2005. 'Obligate role of anti-apoptotic MCL-1 in the survival of hematopoietic stem cells', *Science*, 307: 1101-4.

Opferman, J. T., A. Letai, C. Beard, M. D. Sorcinelli, C. C. Ong, and S. J. Korsmeyer. 2003. 'Development and maintenance of B and T lymphocytes requires antiapoptotic MCL-1', *Nature*, 426: 671-6.

Porter, S. N., L. C. Baker, D. Mittelman, and M. H. Porteus. 2014. 'Lentiviral and targeted cellular barcoding reveals ongoing clonal dynamics of cell lines in vitro and in vivo', *Genome Biol*, 15: R75.

Pui, C. H., and W. E. Evans. 2013. 'A 50-year journey to cure childhood acute lymphoblastic leukemia', *Semin Hematol*, 50: 185-96.

Pui, C. H., L. L. Robison, and A. T. Look. 2008. 'Acute lymphoblastic leukaemia', *Lancet*, 371: 1030-43.

Ravandi, F., S. O'Brien, D. Thomas, S. Faderl, D. Jones, R. Garris, S. Dara, J. Jorgensen, P. Kebriaei, R. Champlin, G. Borthakur, J. Burger, A. Ferrajoli, G. Garcia-Manero, W. Wierda, J. Cortes, and H. Kantarjian. 2010. 'First report of phase 2 study of dasatinib with hyper-CVAD for the frontline treatment of patients with Philadelphia chromosome-positive (Ph+) acute lymphoblastic leukemia', *Blood*, 116: 2070-7.

Rinkenberger, J. L., S. Horning, B. Klocke, K. Roth, and S. J. Korsmeyer. 2000. 'Mcl-1 deficiency results in peri-implantation embryonic lethality', *Genes Dev*, 14: 23-7.

Rodriguez, A., S. Griffiths-Jones, J. L. Ashurst, and A. Bradley. 2004. 'Identification of mammalian microRNA host genes and transcription units', *Genome Res*, 14: 1902-10.

Rosenfeld, C., A. Goutner, C. Choquet, A. M. Venuat, B. Kayibanda, J. L. Pico, and M. F. Greaves. 1977. 'Phenotypic characterisation of a unique non-T, non-B acute lymphoblastic leukaemia cell line', *Nature*, 267: 841-3.

Saelens, X., N. Festjens, L. Vande Walle, M. van Gurp, G. van Loo, and P. Vandenabeele. 2004. 'Toxic proteins released from mitochondria in cell death', *Oncogene*, 23: 2861-74.

Salvesen, G. S., and C. S. Duckett. 2002. 'IAP proteins: blocking the road to death's door', *Nat Rev Mol Cell Biol*, 3: 401-10.

Sauer, B., and N. Henderson. 1988. 'Site-specific DNA recombination in mammalian cells by the Cre recombinase of bacteriophage P1', *Proc Natl Acad Sci U S A*, 85: 5166-70.

Sausville, E. A., and A. M. Burger. 2006. 'Contributions of human tumor xenografts to anticancer drug development', *Cancer Res*, 66: 3351-4, discussion 54.

Schimmer, A. D., S. Dalili, R. A. Batey, and S. J. Riedl. 2006. 'Targeting XIAP for the treatment of malignancy', *Cell Death Differ*, 13: 179-88.

Schmidt-Supprian, M., and K. Rajewsky. 2007. 'Vagaries of conditional gene targeting', *Nat Immunol*, 8: 665-8.

Schmitz, M., P. Breithaupt, N. Scheidegger, G. Cario, L. Bonapace, B. Meissner, P. Mirkowska, J. Tchinda, F. K. Niggli, M. Stanulla, M. Schrappe, A. Schrauder, B. C. Bornhauser, and J. P. Bourquin. 2011. 'Xenografts of highly resistant leukemia recapitulate the clonal composition of the leukemogenic compartment', *Blood*, 118: 1854-64.

Schultz, K. R., W. P. Bowman, A. Aledo, W. B. Slayton, H. Sather, M. Devidas, C. Wang, S. M. Davies, P. S. Gaynon, M. Trigg, R. Rutledge, L. Burden, D. Jorstad, A. Carroll, N. A. Heerema, N. Winick, M. J. Borowitz, S. P. Hunger, W. L. Carroll, and B. Camitta. 2009. 'Improved early event-free survival with imatinib in Philadelphia chromosome-positive acute lymphoblastic leukemia: a children's oncology group study', *J Clin Oncol*, 27: 5175-81.

Shimshek, D. R., J. Kim, M. R. Hubner, D. J. Spergel, F. Buchholz, E. Casanova, A. F. Stewart, P. H. Seeburg, and R. Sprengel. 2002. 'Codon-improved Cre recombinase (iCre) expression in the mouse', *Genesis*, 32: 19-26.

Shultz, L. D., B. L. Lyons, L. M. Burzenski, B. Gott, X. Chen, S. Chaleff, M. Kotb, S. D. Gillies, M. King, J. Mangada, D. L. Greiner, and R. Handgretinger. 2005. 'Human lymphoid and myeloid cell development in NOD/LtSz-scid IL2R gamma null mice engrafted with mobilized human hemopoietic stem cells', *J Immunol*, 174: 6477-89.

Shultz, L. D., P. A. Schweitzer, S. W. Christianson, B. Gott, I. B. Schweitzer, B. Tennent, S. McKenna, L. Mobraaten, T. V. Rajan, D. L. Greiner, and et al. 1995. 'Multiple defects in innate and adaptive immunologic function in NOD/LtSz-scid mice', *J Immunol*, 154: 180-91.

Smiraglia, D. J., L. J. Rush, M. C. Fruhwald, Z. Dai, W. A. Held, J. F. Costello, J. C. Lang, C. Eng, B. Li, F. A. Wright, M. A. Caligiuri, and C. Plass. 2001. 'Excessive CpG island hypermethylation in cancer cell lines versus primary human malignancies', *Hum Mol Genet*, 10: 1413-9.

Smith, A. J., M. A. De Sousa, B. Kwabi-Addo, A. Heppell-Parton, H. Impey, and P. Rabbitts. 1995. 'A site-directed chromosomal translocation induced in embryonic stem cells by Cre-loxP recombination', *Nat Genet*, 9: 376-85.

Souers, A. J., J. D. Leverson, E. R. Boghaert, S. L. Ackler, N. D. Catron, J. Chen, B. D. Dayton, H. Ding, S. H. Enschede, W. J. Fairbrother, D. C. Huang, S. G. Hymowitz, S. Jin, S. L. Khaw, P. J. Kovar, L. T. Lam, J. Lee, H. L. Maecker, K. C. Marsh, K. D. Mason, M. J. Mitten, P. M. Nimmer, A. Oleksijew, C. H. Park, C. M. Park, D. C. Phillips, A. W. Roberts, D. Sampath, J. F. Seymour, M. L. Smith, G. M. Sullivan, S. K. Tahir, C. Tse, M. D. Wendt, Y. Xiao, J. C. Xue, H. Zhang, R. A. Humerickhouse, S. H. Rosenberg, and S. W. Elmore. 2013. 'ABT-199, a potent and selective BCL-2 inhibitor, achieves antitumor activity while sparing platelets', *Nat Med*, 19: 202-8.

Srinivasula, S. M., R. Hegde, A. Saleh, P. Datta, E. Shiozaki, J. Chai, R. A. Lee, P. D. Robbins, T. Fernandes-Alnemri, Y. Shi, and E. S. Alnemri. 2001. 'A conserved XIAP-interaction motif in caspase-9 and Smac/DIABLO regulates caspase activity and apoptosis', *Nature*, 410: 112-6.

Stehlik, C., R. de Martin, I. Kumabashiri, J. A. Schmid, B. R. Binder, and J. Lipp. 1998. 'Nuclear factor (NF)-kappaB-regulated X-chromosome-linked iap gene expression protects endothelial cells from tumor necrosis factor alpha-induced apoptosis', *J Exp Med*, 188: 211-6.

Steinhart, L., K. Belz, and S. Fulda. 2013. 'Smac mimetic and demethylating agents synergistically trigger cell death in acute myeloid leukemia cells and overcome apoptosis resistance by inducing necroptosis', *Cell Death Dis*, 4: e802.

Stern, P., S. Astrof, S. J. Erkeland, J. Schustak, P. A. Sharp, and R. O. Hynes. 2008. 'A system for Cre-regulated RNA interference in vivo', *Proc Natl Acad Sci U S A*, 105: 13895-900.
Sternberg, N., and D. Hamilton. 1981. 'Bacteriophage P1 site-specific recombination. I. Recombination between loxP sites', *J Mol Biol*, 150: 467-86.
Strasser, A. 2005. 'The role of BH3-only proteins in the immune system', *Nat Rev Immunol*, 5: 189-200.
Subramaniam, D., G. Natarajan, S. Ramalingam, I. Ramachandran, R. May, L. Queimado, C. W. Houchen, and S. Anant. 2008. 'Translation inhibition during cell cycle arrest and apoptosis: Mcl-1 is a novel target for RNA binding protein CUGBP2', *Am J Physiol Gastrointest Liver Physiol*, 294: G1025-32.
Taylor, R. C., S. P. Cullen, and S. J. Martin. 2008. 'Apoptosis: controlled demolition at the cellular level', *Nat Rev Mol Cell Biol*, 9: 231-41.
Terziyska, N., C. Castro Alves, V. Groiss, K. Schneider, K. Farkasova, M. Ogris, E. Wagner, H. Ehrhardt, R. J. Brentjens, U. zur Stadt, M. Horstmann, L. Quintanilla-Martinez, and I. Jeremias. 2012. 'In vivo imaging enables high resolution preclinical trials on patients' leukemia cells growing in mice', *PLoS One*, 7: e52798.
Thomas, L. W., C. Lam, and S. W. Edwards. 2010. 'Mcl-1; the molecular regulation of protein function', *FEBS Lett*, 584: 2981-9.
Thyagarajan, B., M. J. Guimaraes, A. C. Groth, and M. P. Calos. 2000. 'Mammalian genomes contain active recombinase recognition sites', *Gene*, 244: 47-54.
Tse, C., A. R. Shoemaker, J. Adickes, M. G. Anderson, J. Chen, S. Jin, E. F. Johnson, K. C. Marsh, M. J. Mitten, P. Nimmer, L. Roberts, S. K. Tahir, Y. Xiao, X. Yang, H. Zhang, S. Fesik, S. H. Rosenberg, and S. W. Elmore. 2008. 'ABT-263: a potent and orally bioavailable Bcl-2 family inhibitor', *Cancer Res*, 68: 3421-8.
Varfolomeev, E., J. W. Blankenship, S. M. Wayson, A. V. Fedorova, N. Kayagaki, P. Garg, K. Zobel, J. N. Dynek, L. O. Elliott, H. J. Wallweber, J. A. Flygare, W. J. Fairbrother, K. Deshayes, V. M. Dixit, and D. Vucic. 2007. 'IAP antagonists induce autoubiquitination of c-IAPs, NF-kappaB activation, and TNFalpha-dependent apoptosis', *Cell*, 131: 669-81.
Vert, J. P., N. Foveau, C. Lajaunie, and Y. Vandenbrouck. 2006. 'An accurate and interpretable model for siRNA efficacy prediction', *BMC Bioinformatics*, 7: 520.
Vick, B., M. Rothenberg, N. Sandhofer, M. Carlet, C. Finkenzeller, C. Krupka, M. Grunert, A. Trumpp, S. Corbacioglu, M. Ebinger, M. C. Andre, W. Hiddemann, S. Schneider, M. Subklewe, K. H. Metzeler, K. Spiekermann, and I. Jeremias. 2015. 'An advanced preclinical mouse model for acute myeloid leukemia using patients' cells of various genetic subgroups and in vivo bioluminescence imaging', *PLoS One*, 10: e0120925.
Voziyanov, Y., S. Pathania, and M. Jayaram. 1999. 'A general model for site-specific recombination by the integrase family recombinases', *Nucleic Acids Res*, 27: 930-41.
Vucic, D., V. M. Dixit, and I. E. Wertz. 2011. 'Ubiquitylation in apoptosis: a post-translational modification at the edge of life and death', *Nat Rev Mol Cell Biol*, 12: 439-52.
Weber, K., M. Thomaschewski, M. Warlich, T. Volz, K. Cornils, B. Niebuhr, M. Tager, M. Lutgehetmann, J. M. Pollok, C. Stocking, M. Dandri, D. Benten, and B. Fehse. 2011. 'RGB marking facilitates multicolor clonal cell tracking', *Nat Med*, 17: 504-9.
Weisberg, E., A. L. Kung, R. D. Wright, D. Moreno, L. Catley, A. Ray, L. Zawel, M. Tran, J. Cools, G. Gilliland, C. Mitsiades, D. W. McMillin, J. Jiang, E. Hall-Meyers, and J. D. Griffin. 2007. 'Potentiation of antileukemic therapies by Smac mimetic, LBW242: effects on mutant FLT3-expressing cells', *Mol Cancer Ther*, 6: 1951-61.
Wyllie, A. H., J. F. Kerr, and A. R. Currie. 1980. 'Cell death: the significance of apoptosis', *Int Rev Cytol*, 68: 251-306.
Yang, T., K. M. Kozopas, and R. W. Craig. 1995. 'The intracellular distribution and pattern of expression of Mcl-1 overlap with, but are not identical to, those of Bcl-2', *J Cell Biol*, 128: 1173-84.

Youle, R. J., and A. Strasser. 2008. 'The BCL-2 protein family: opposing activities that mediate cell death', *Nat Rev Mol Cell Biol*, 9: 47-59.

Zanatta, D. B., M. Tsujita, P. Borelli, R. B. Aguiar, D. G. Ferrari, and B. E. Strauss. 2014. 'Genetic barcode sequencing for screening altered population dynamics of hematopoietic stem cells transduced with lentivirus', *Mol Ther Methods Clin Dev*, 1: 14052.

Zeng, Y., E. J. Wagner, and B. R. Cullen. 2002. 'Both natural and designed micro RNAs can inhibit the expression of cognate mRNAs when expressed in human cells', *Mol Cell*, 9: 1327-33.

Zhang, Y., C. Riesterer, A. M. Ayrall, F. Sablitzky, T. D. Littlewood, and M. Reth. 1996. 'Inducible site-directed recombination in mouse embryonic stem cells', *Nucleic Acids Res*, 24: 543-8.

Zheng, B., M. Sage, E. A. Sheppeard, V. Jurecic, and A. Bradley. 2000. 'Engineering mouse chromosomes with Cre-loxP: range, efficiency, and somatic applications', *Mol Cell Biol*, 20: 648-55.

Zufferey, R., J. E. Donello, D. Trono, and T. J. Hope. 1999. 'Woodchuck hepatitis virus posttranscriptional regulatory element enhances expression of transgenes delivered by retroviral vectors', *J Virol*, 73: 2886-92.

Zufferey, R., T. Dull, R. J. Mandel, A. Bukovsky, D. Quiroz, L. Naldini, and D. Trono. 1998. 'Self-inactivating lentivirus vector for safe and efficient in vivo gene delivery', *J Virol*, 72: 9873-80.

8. Supplemental tables

Table S1. 110-mer sequences of all miR-30/shRNAs used in this study

XhoI (TCGAG) and EcoRI (G) restriction sites are depicted in red, 5' and 3' miRNA contexts and loop are in black, the sense-passenger strand is in blue, the antisense-guide strand is in green.

eGFP.442 (enhanced GFP, control, sh-CTRL)

TCGAGAAGGTATATTGCTGTTGACAGTGAGCGCCAGCCACAACGTCTATATCATTAGTGAAGCCACA
GATGTAATGATATAGACGTTGTGGCTGTTGCCTACTGCCTCGG

MCL-1.1231 (human, NM_021960.4, NM_182763.2, NM_001197320.1, sh-Mcl-1.2)

TCGAGAAGGTATATTGCTGTTGACAGTGAGCGCCAGCTTGTAAATGTATTTGTATAGTGAAGCCACA
GATGTATACAAATACATTTACAAGCTGTTGCCTACTGCCTCGG

MCL-1.3284 (human, NM_021960.4, NM_182763.2, NM_001197320.1, sh-Mcl-1.3)

TCGAGAAGGTATATTGCTGTTGACAGTGAGCGAAAGGGTTAGGACCAACTACAATAGTGAAGCCAC
AGATGTATTGTAGTTGGTCCTAACCCTTCTGCCTACTGCCTCGG

MCL-1.1421 (human, NM_021960.4, NM_182763.2, NM_001197320.1, sh-Mcl-1.1)

TCGAGAAGGTATATTGCTGTTGACAGTGAGCGCACAGAACGAATTGATGTGTAATAGTGAAGCCACA
GATGTATTACACATCAATTCGTTCTGTATGCCTACTGCCTCGG

MCL-1.767 (human, NM_021960.4, NM_182763.2, NM_001197320.1, sh-Mcl-1.4)

TCGAGAAGGTATATTGCTGTTGACAGTGAGCGCAAGAAGCAAAGTTCAGTTTCATAGTGAAGCCACA
GATGTATGAAACTGAACTTTGCTTCTTTTGCCTACTGCCTCGG

MCL-1.2515 (human, NM_021960.4, NM_182763.2, NM_001197320.1, sh-Mcl-1.5)

TCGAGAAGGTATATTGCTGTTGACAGTGAGCGCAACCTCAGAGTTTAAAAGCTATAGTGAAGCCACA
GATGTATAGCTTTTAAACTCTGAGGTTTTGCCTACTGCCTCGG

MCL-1.901 (human, NM_021960.4, NM_182763.2, NM_001197320.1, sh-Mcl-1.6)

TCGAGAAGGTATATTGCTGTTGACAGTGAGCGACAGGCAAGTCATAGAATTGATTAGTGAAGCCACA
GATGTAATCAATTCTATGACTTGCCTGGTGCCTACTGCCTCGG

MCL-1.1153 (human, NM_021960.4, NM_182763.2, NM_001197320.1, sh-Mcl-1.7)

TCGAGAAGGTATATTGCTGTTGACAGTGAGCGCAGCCTAGTTTATCACCAATAATAGTGAAGCCACA
GATGTATTATTGGTGATAAACTAGGCTATGCCTACTGCCTCGG

Renilla (Renilla Luciferase, control, sh-Renilla)

TCGAGAAGGTATATTGCTGTTGACAGTGAGCGCAGGAATTATAATGCTTATCTATAGTGAAGCCACA
GATGTATAGATAAGCATTATAATTCCTATGCCTACTGCCTCGG

XIAP.1331 (human, NM_001167.3, NM_001204401.1, sh-XIAP.4)

TCGAGAAGGTATATTGCTGTTGACAGTGAGCGCCAGAAAGAGATTAGTACTGAATAGTGAAGCCAC
AGATGTATTCAGTACTAATCTCTTTCTGTTGCCTACTGCCTCGG

XIAP.1774 (human, NM_001167.3, NM_001204401.1, sh-XIAP.1)

TCGAGAAGGTATATTGCTGTTGACAGTGAGCGAAAGCATCATACTATAACTGAATAGTGAAGCCACA
GATGTATTCAGTTATAGTATGATGCTTCTGCCTACTGCCTCGG

XIAP.2006 (human, NM_001167.3, NM_001204401.1, sh-XIAP.2)

TCGAGAAGGTATATTGCTGTTGACAGTGAGCGCGAGGTTGGTTGTTGTGTTTTATAGTGAAGCCACA
GATGTATAAAACACAACAACCAACCTCTTGCCTACTGCCTCGG

XIAP.2155 (human, NM_001167.3, NM_001204401.1, sh-XIAP.5)

TCGAGAAGGTATATTGCTGTTGACAGTGAGCGAAAAGATGTCAAAGATATGTTATAGTGAAGCCACA
GATGTATAACATATCTTTGACATCTTTCTGCCTACTGCCTCGG

XIAP.4783 (human, NM_001167.3, NM_001204401.1, sh-XIAP.3)

TCGAGAAGGTATATTGCTGTTGACAGTGAGCGACAGCATTAGTTTCACATGATATAGTGAAGCCACA
GATGTATATCATGTGAAACTAATGCTGGTGCCTACTGCCTCGG

XIAP.6475 (human, NM_001167.3, NM_001204401.1, sh-XIAP.6)

TCGAGAAGGTATATTGCTGTTGACAGTGAGCGCTAGGACAATCATCAATGCATATAGTGAAGCCACA
GATGTATATGCATTGATGATTGTCCTATTGCCTACTGCCTCGG

XIAP.5334 (human, NM_001167.3, NM_001204401.1, sh-XIAP.7)

TCGAGAAGGTATATTGCTGTTGACAGTGAGCGCTACAAGGTTGCAAGAGCTCAATAGTGAAGCCACA
GATGTATTGAGCTCTTGCAACCTTGTAATGCCTACTGCCTCGG

Table S2. Primers sequences

sequence	T_m [°C]	amplicon [bp]	application
CACAAATTTTGTAATCCAGAGGTTG	53	-	shRNAs sequencing (related to Figure 14)
GATCACATGGTCCTGCTG	53.1	-	shRNAs sequencing (related to Figure 17)
FW1: TTTGCCTGACCCTGCTTG FW2: AGTGCAGGGGAAAGAAT RV: CACAAATTTTGTAATCCAGAGGTTG	55.8 50.8 53	(1) 1307 (2) 1637	Colony-PCR (related to Figure 14 either with the EF1α (FW1) or SFFV (FW2) promoter)
FW: AGTGCAGGGGAAAGAAT RV: CACAAATTTTGTAATCCAGAGGTTG	50.8 53	2482	Colony-PCR (related to Figure 17)
FW: CCAATGCATATGAGCGAGCTGATTAAGGAGAAC RV: ACGCGTCGACTTAATTAAGCTTGTGCCCCAGTTTGC	61.7 66.8	713	cloning of mtagBFP (related to Figure 15)
FW: CCAATGCATATGGTGAGCAAGGCGGAG RV: ACGCGTCGACTTACTTGTACAGCTCGTCCATGC	63.5 66.5	732	cloning of eGFP (related to Figure 15)
FW: CGCGGATCCATGGTGAGCAAGGGCGAG RV: CTAGCTAAGCTTACTTGTACAGCTCGTCCATGC	68.3 62.5	721	cloning of mCherry (related to Figure 16)
FW1: GGACTAGTGATCAAGGGCGGGTACATG FW2 : CCATCGATGATCAAGGGCGGGTACATG RV1: CTAGTCTAGAGAGTGAGGGGTTGTGAGC RV2: CGGAATTCGAGTGAGGGGTTGTGAGC	62.1 62.7 60.8 63.1	~ 328	cloning of SFFV promoter (related either to Figure 14 (FW1-RV1) or to Figure 16 (FW1-RV2) or to Figure 17 (FW2-RV1))
FW: CGGCCCAATTGGCCACCATGGTGAGCAAGGGCGAG RV: CGGGATCCGCCACCATGGCCTCCTCCGAGAAC	72.6 71.5	1179	cloning of dsRED/miR-30 (related to Figure 14)
FW: CCAATGCATATGTCCAATTTACTGACCGTACACCAAAATTTGCC RV:	64.7 75.1	1975	cloning of $CreER^{T2}$ (related to Figure 16)

CCAATGCATGCCACGAAGCAAGCAGGAGA TGTTGAAGAAAACCCCGGGCCTCCCGGGG ACTGTGGCAGGGAAACCCTCTG			
FW: TTTTGGGACATGGATATACTCAGTT RV: AGCACTTTACTTTATCACCTTCACC	54 55.1	89	qPCR of XIAP
FW: GAGACTCTGCTTCGCTGCAT RV: AGTTGCCCATCCTTCATAGC	57.5 54.9	104	qPCR of HMBS
FW: TGATAGATCCATTCCTATGACTGTAGA RV: CAAGACATTCTTTCCAGTTAAAGTTG	54.4 52.9	127	qPCR of HPRT1

Table S3. LightCycler® 480 Probes Master

gene	NM	probe #
XIAP	NM_001167.3 NM_001204401.1	68
HMBS	NM_000190.3 NM_001024382.1	75
HPRT1	NM_000194	22

Table S4. Clinical data of patients donating ALL and AML cells for xenotransplantation and sample characteristics

sample	type	sex	age [years]	stage	cytogenetics	Time of passaging through mice [days]
199	pre-B ALL	female	8	relapse	somatic trisomy 21; leukemic homozygous deletion 9p	ca. 42
265	pre-B ALL	female	5,5	relapse	hyperploidy with additional 6, 13, 14, 17, 18, 21, X	ca. 43
346	AML	female	1	relapse	c-Kit-Mutation	ca. 40
393	AML	female	47	relapse	karyotype aberrant, MLL-AF10 translocation	ca. 38

Table S5. Filter settings for flow cytometry and cell sorting

laser [nm]	bandpass filter	fluorochromes detected
405	450/50	mtagBFP
488	510/20	GFP, eGFP
561	610/20	mCherry
	585/42	dTomato, dsRED

9. Acknowledgements

Thanks to Prof. Dr. Irmela Jeremias, who gave me the possibility to work on these incredibly interesting projects, her guide and support through my work, her suggestions and useful discussions.

Huge, immense and sincere thanks to Dr. Michela Carlet, for her irreplaceable presence as mentor and friend, for sharing her projects with me, her excellent practical advices through all these years, her essential moral support, time, coffee and good mood.

Great thanks to Prof. Dr. Marc Schmidt-Supprian, who kindly supervised my work and progresses during all these years, as head of my Thesis Committee and for the collaboration in the design of the cloning strategy of the FLIP-cassette construct.

I am thankful to the Thesis Committee members Prof. Dr. Arnd Kieser and Prof. Dr. Olivier Gires, for the constructive discussions and good ideas.

Thanks to our collaborators Dr. Johannes Zuber, Dr. Thomas Hoffmann and Dr. Mareike Roth, who provided the common miR-30 shRNAmir backbone and the Reporter Assay.

I am indebted to Annette Frank, Maike Fritschle, Volker Groiß, Miriam Krekel and Liliana Mura, for their technical assistance and time spent for the care of the mice. Thanks also to Fabian Klein, who performed all the cells enrichments by cell sorting.

I express my gratitude to all the staff members of the research animal facility of the Hämatologikum institute, for the constant care of all the mice.

Many thanks to all my colleagues, officemates and friends Dr. Wen-Hsin Liu, Dr. Erbey Özdemir, Dr. Cornelia Finkenzeller, Dr. Sarah Ebinger, for help, moral support and big fun; and to all the other group members.

Perhaps, I will not have enough words to express my gratitude to my big family, far but always in my heart, for their invisible but indispensable presence.

Big thanks to my journey fellows Raffo and Raffino, Elvira and Giulia, who made me feel at home.

Warm thanks to all my old friends from all over the World: Rugg and Ale, for the best long distance friendship; Lauretta, Fio, Guiduz, Zorro and Vitto, who were always there for me; special thanks to Tripodi, for the brotherly friendship and for the best holiday break ever.

Last but definitely not least, I am thankful to Vikas, who put the right spice in my "after Ph.D." life.